

# Dissertation

Development of solid acid catalysts  
with a novel zeolite framework and  
their catalytic properties

(新規ゼオライト骨格を有する固体酸  
触媒の開発とその触媒特性)

Graduate School of Engineering Science  
Yokohama National University

Qing LIU

劉 青

09 2021

# ***Abstract***

Light olefins are extremely essential raw materials in petrochemicals because they are building blocks for various end products, such as polyethylene and polypropylene. Recently, market analysis showed that the demand for light olefins is desperate and the current supply cannot match the demand. Considering energy savings and flexibility of operation, fluid catalytic cracking (FCC) process is expected to maximize the production of light olefins. Hexane cracking reaction has always been considered as a model reaction to produce light olefins. Except for that, with the increasing demand for olefins, dimethyl ether (DME)-to-olefins (DTO) process as a non-petroleum route to make olefins has also attracted considerable attention. It is of great significance to develop a new catalyst that has high chemical stability as well as high catalytic activity and selectivity to light olefins. YNU-5 is a large-pore zeolite recently discovered in Yokohama National University, containing a distinguishable three-dimensional channel system: 2-dimensional 12-ring ( $0.78\text{ nm} \times 0.59\text{ nm}$ ; large micropore) with channel intersection connected with 8-ring channel ( $0.44\text{ nm} \times 0.34\text{ nm}$ ; small micropore), thus forming a large space around  $7.97\text{ \AA}$  that are accessible through 12-ring windows. Besides, there is an isolated 8-ring channel ( $0.40\text{ nm} \times 0.29\text{ nm}$ ; small micropore) in the framework. The application of YNU-5 zeolites has not been well studied so far. With the aim of investigating the catalytic performance, YNU-5 zeolite was used as solid catalyst over DTO reaction and cracking reaction after successful framework stabilization. However, the rapid deactivation of YNU-5 zeolites limited its application. To enhance the catalytic ability, I also intended to prepare hierarchical zeolites. The hierarchical structure was successfully introduced to the YNU-5 structure by appropriate treatments to form mesopores. Compared to conventional YNU-5 zeolites confronting with severe mass transfer constraints of reactants or products due to the intrinsic micropores, hierarchical materials successfully showed higher catalytic activity and selectivity. In addition, shape-selectivity of the YNU-5 was examined and scientifically useful information was obtained.

The doctoral thesis will consist of 6 chapters, focusing on (I) the introduction, (II) synthetic investigation of YNU-5 zeolite, (III) hexane cracking reaction over YNU-5 zeolite catalyst, (IV) preparation of hierarchical YNU-5 zeolite and effect of hierarchy on the catalytic performance of YNU-5 zeolite, (V) shape-selective alkylation of naphthalene over YNU-5 zeolite, and (VI) summary of all results and conclusions.

## Chapter 1: Introduction

Chapter 1 introduces the background of YNU-5 zeolite. Synthetic aspects including the history and an overview of hierarchical zeolites concerning the recent

achievements in preparing strategies and the advantages of hierarchy in enhancing their catalytic performance. The purpose and significance of this research were also discussed.

## Chapter 2: Synthetic investigation of YNU-5 zeolite

Chapter 2 represents the hydrothermal syntheses of YNU-5 crystals by utilizing the method starting from concentrated silicate solution and using FAU-type zeolite as a precursor. During the synthesis investigation, it was found that a very slight amount of an impurity phase tended to contaminate the desired product YNU-5. The phase-selection was sensitive to the levels of water in the synthesis mixture, such that a pure phase could be produced but it was also possible to intentionally form specific trace impurities. Dealuminated pure YNU-5 exhibited rapid deactivation due to coking at time on stream (TOS) values exceeding 5 min. Surprisingly, this deactivation was greatly suppressed when the material contained a trace amount of ZSM-5 consisting of nano-sized particles. The formation of ZSM-5 nanoparticles evidently improved the performance of the catalytic system during the dimethyl ether-to-olefin (DTO) reaction. The product distributions obtained from this reaction using highly dealuminated and very pure YNU-5 resembled those generated by 12-ring rather than 8-ring zeolite catalysts. The high selectivity for desirable C3 and C4 olefins during the DTO reaction over YNU-5 is beneficial. When the synthesis was performed using YNU-5 zeolite as crystal seeds instead of FAU zeolite, MFI-type zeolite was turned to be the final product.

## Chapter 3: Hexane cracking reaction over YNU-5 zeolite

This chapter describes the results of hexane-cracking using the YNU-5 zeolite as a catalyst. The effect of dealumination and temperature on the catalytic performance was investigated. Dealuminated YNU-5 zeolites with various Si/Al ratios were prepared by acid treatment using HNO<sub>3</sub> aqueous solutions with different concentrations. The proton form of YNU-5 without dealumination having Si/Al ratio around 9 deactivated rapidly during the reaction due to heavy coke formation, whereas properly dealuminated YNU-5 with lower Al content exhibited high catalytic selectivity of propylene and resistance to coke formation for hexane cracking at the reaction temperatures of 550 to 650°C. By decreasing Al content, the selectivity to propylene increased while the selectivity of ethylene decreased mainly due to less content of strong Brønsted acid sites. Part of this fact as well as the removal of acid sites on the external surface could have caused the suppression of sequential reactions producing coke precursors.

Chapter 4: Preparation of hierarchical YNU-5 zeolite and the effect of hierarchy on the catalytic performance of YNU-5 zeolite

Secondary porosity (mesoporosity in this work) was successfully introduced into the framework of YNU-5 zeolite through base treatment using NaOH aqueous solution. This chapter describes the influence of time and temperature of the base treatment on the desilication for tuning the formation of mesoporosity. Textural properties were analyzed based on sorption isotherms. YNU-5 zeolites with various Al content prepared by HNO<sub>3</sub> treatments were used as parent samples for desilication by base treatment. It was found that Al atoms in the framework plays an important role during desilication process, which avoids excessive desilication that leads to collapse of the framework structure. As a result of the negatively charged  $[\text{AlO}_4]^-$  tetrahedra, excessive hydrolysis of the Si–O–Al bond in the presence of OH<sup>−</sup> was avoided compared with the relatively easy cleavage of the Si–O–Si bond in the absence of neighboring Al. Apart from that, the effect of mesoporosity has been studied over hexane cracking reaction. Comparing to a standard YNU-5 zeolite with a similar Si/Al ratio and acid sites, an increase in activity of YNU-5 zeolite was successfully observed.

Chapter 5: Shape-selective alkylation of naphthalene over YNU-5 zeolite

Shape-selective alkylation of naphthalene over conventional large-pore (12-ring) zeolites such as mordenite, beta and USY was first investigated prior to the catalytic use of YNU-5. YNU-5 zeolite is undoubtedly the candidate of the similar application because it has 12-ring channels. The shape-selective catalysis in the isopropylation of naphthalene (NP) over YNU-5 zeolites was discussed. In both cases of parent YNU-5 (H<sup>+</sup>-form) and dealuminated YNU-5 zeolite, 1-isopropylnaphthalene (1-IPN) and 2-isopropylnaphthalene (2-IPN) were the principal products. As for the dialkylated naphthalene isomers, the selectivity to β,β-diisopropylnaphthalene (β,β-DIPN) was enhanced after dealumination, accompanying the decrease in the catalytic activity. Aluminum atoms on the external surface and near the pore-mouth of the 12–12–8-ring channel were preferentially removed by dealumination treatment with aqueous nitric acid, and the remaining internal acid sites played the important roles during the reaction. The high β,β-selectivity is attributed to restrict transition state mechanism inside the 12-ring channels. The reactant molecules are too bulky to access the acid sites inside 8-ring channel. This fact is consistent with the low conversion of naphthalene.

Chapter 6: Conclusion

The results of this study and prospects are described as a summary.

# Contents

Abstract .....	1
Chapter one .....	7
Introduction.....	7
1.1 Zeolites .....	7
1.2 Synthesis of Zeolites.....	8
1.2.1. Hydrothermal synthesis of zeolite .....	8
1.2.2. Dry-gel conversion (DGC) synthetic route.....	13
1.3 YNU-5 zeolite.....	13
1.4 Application as solid acid catalyst .....	14
1.4.1 Acidity of zeolite.....	14
1.4.2 Shape selectivity of zeolite .....	16
1.4.3 Catalytic application .....	17
1.4.3.1 Methanol-to-olefins(MTO) reaction .....	17
1.4.3.2 Fluid Catalytic Cracking (FCC).....	18
1.4.3.3 Limitation of zeolites as solid acid catalyst.....	18
1.5 Hierarchical zeolites .....	20
1.5.1 Design of Hierarchical Zeolites .....	20
1.5.2 Catalytic applications of Hierarchical Zeolites.....	22
1.5.2.1 Fluid Catalytic Cracking (FCC).....	22
1.5.2.2 Methanol-to-hydrocarbon reaction (MTH).....	22
1.6 Aims of research .....	22
1.7 References.....	23
Chapter Two .....	28
The Synthesis of YNU-5 Zeolite and Its Application to the Catalysis in the Dimethyl Ether-to-Olefin Reaction.....	28
2.1 Introduction.....	28
2.2 Experimental .....	30
2.2.1. Measurements .....	30
2.2.2. Typical YNU-5 Synthesis Procedure .....	31
2.2.3. Preparation of MFI-Type Zeolite Nanocrystals .....	32
2.2.4. Post-Synthesis Modification .....	32
2.2.5. Procedure for the DTO Reaction .....	33
2.3. Results and Discussion .....	33
2.3.1. Synthetic Investigations of YNU-5.....	33
2.3.2. Effects of a Trace of MFI on the Physicochemical Properties of YFI Samples .....	37
2.3.3. DTO Reaction over the YFI Catalyst.....	41
2.4. Conclusions.....	46
2.5 References.....	47
Chapter Three.....	49

Hexane cracking reaction over YNU-5 zeolite .....	49
3.1 Introduction.....	49
3.2 Experimental.....	50
3.2.1. Measurements .....	50
3.2.2. Typical synthesis of YNU-5 zeolite .....	51
3.2.3. Post-synthesis treatments of YNU-5 zeolites .....	51
3.2.3.1 Ion-exchange of calcined YNU-5 to $\text{NH}_4^+$ form .....	51
3.2.3.2 Typical procedure of dealumination .....	51
3.2.3 Catalytic reaction .....	52
3.3 Results and Discussion .....	53
3.3.1 Dealumination of YNU-5 zeolites .....	53
3.3.1.1 $\text{NH}_3$ TPD profiles.....	53
3.3.1.2 $^{27}\text{Al}$ MAS NMR.....	55
3.3.1.3 $\text{N}_2$ adsorption .....	55
3.3.2 Hexane cracking reaction .....	57
3.3.2.1 Hexane cracking over MFI and BEA catalysts.....	57
3.3.2.2 Hexane cracking over dealuminated YNU-5 zeolites.....	58
3.4 Conclusions and outlook.....	60
3.5 References.....	60
Chapter Four .....	62
Introduction of hierarchical structure into YNU-5 zeolite and its enhanced catalytic performance for cracking of hexane .....	62
4.1 Introduction.....	62
4.2 Experimental .....	63
4.2.1 Materials .....	63
4.2.2 Measurements .....	63
4.2.3. Typical synthesis of YNU-5 zeolite .....	64
4.2.4. Preparation of Hierarchical YNU-5 zeolite .....	64
4.2.5. Post-synthesis treatments of YNU-5 zeolites.....	64
4.2.5.1 Ion-exchange of calcined YNU-5 to $\text{NH}_4^+$ form.....	64
4.2.5.2 Typical procedure of dealumination .....	65
4.2.5.3 Typical procedure of dealumination .....	65
4.3. Catalytic reaction .....	66
4.4. Results and Discussion .....	66
4.4.1. Preparation of hierarchical YNU-5 zeolite .....	66
4.4.2. Dealumination of hierarchical YNU-5 zeolite .....	73
4.5 Physiochemical properties of treated samples .....	76
4.5.1 Textural properties of treated samples .....	76
4.5.2 Acidity of treated samples.....	78
4.6 Catalytic test.....	79
4.7 Conclusions.....	82
4.8 References.....	83

Chapter Five.....	85
Shape-selective alkylation of naphthalene over YNU-5 zeolite .....	85
5.1 Introduction.....	85
5.2 Synthesis of YNU-5 zeolite .....	87
5.3 Ion-exchange of YNU-5 zeolite.....	88
5.4 Dealumination of YNU-5 zeolite.....	88
5.5 Characterization .....	88
5.6 Isopropylation of naphthalene .....	89
5.6.1 Experiment procedures .....	89
5.6.2 GC analysis .....	89
5.7 Results and Discussion .....	92
5.8 Conclusions.....	96
5.9 References.....	96
Chapter six .....	97
Conclusions.....	97
Acknowledgment .....	99

# Chapter one

## Introduction

### 1.1 Zeolites

In 1756, the Swedish mineralogist A. F. Cronstedt firstly found the natural zeolite. Since then, there are increasingly intensive investigations on the field of zeolite. Zeolites are generally defined as microporous, crystalline aluminosilicates with a three-dimensional framework and uniformly ordered pores of molecular dimension.<sup>1,2</sup> Basic building unit of zeolite is  $\text{TO}_4$  tetrahedra (T = tetrahedral atom, e.g., Si, Al); and each apical oxygen atom is shared between two adjacent tetrahedra<sup>2</sup> (Figure 1.1). The Loewenstein rule,<sup>3</sup> indeed postulates that two  $\text{AlO}_4$  members cannot be located in direct vicinity in the zeolite framework, thus suggesting that zeolites must have a Si/Al ratio higher than 1 to infinity. Except for Si, Al, the introduction of heteroatoms, such as, Ge, P, B, Fe, Ga, Ti or Zn in the zeolite framework produce the so-called “zeotypes”.<sup>4</sup> Zeolitic tetrahedra have a characteristic negative charge in their structure, which is generated when  $\text{Al}^{3+}$  is isomorphically substituted for  $\text{Si}^{4+}$  in the lattice. Negative charges can be neutralized by the cations, like  $\text{K}^+$ ,  $\text{Na}^+$ ,  $\text{Ca}^{2+}$ ,  $\text{Mg}^{2+}$ , and water molecules accommodated in zeolites.<sup>1</sup> This characteristic provides zeolite the ion-exchange properties due to these “balancing species” being loosely bonded to the framework mainly by electrostatic interactions. This exchange capacity can also be used to create catalytic sites inside the pores, leading to active site confinement.<sup>5</sup> Different from amorphous aluminosilicate, zeolites have a particular periodic structure and a well-

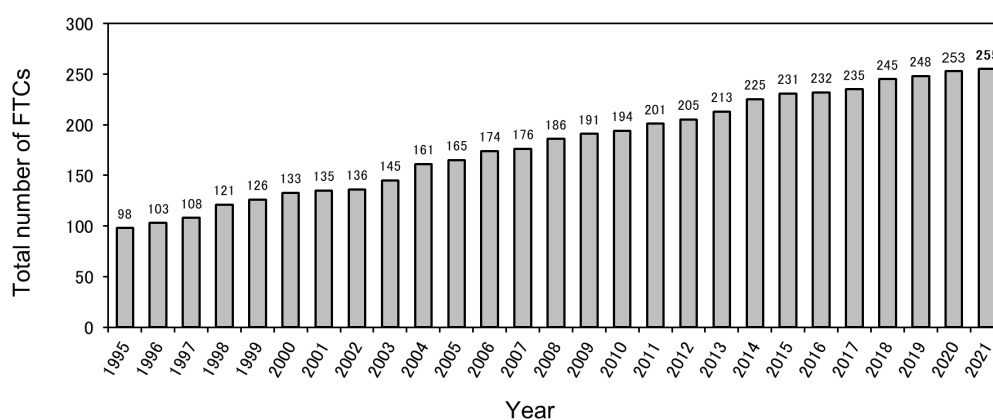


**Figure 1.1.** Number of zeolite skeletal cords

defined microporous channel system.<sup>6</sup> Generally, zeolites are classified into small-,



medium-, large-, and extra-large-pore zeolites according to their topologies and the size of pores. Typically, small-pore zeolites have pore sizes in the range of 0.30–0.45 nm (8-ring), while medium-pore zeolite openings range from 0.45–0.60 nm (10-ring) and large pore materials have their largest pores in the range from 0.60–0.80 nm (12-ring).<sup>7</sup> The first two-dimensional (14- and 12-ring) channel germanium-containing zeolite (IM-12) with extra-large pores was reported in 2004.<sup>8</sup> Extra-pore zeolites have pore size larger than 0.80 nm (14-ring). Their particular properties make zeolite applicable in industry. For example, ion-exchange and sorption properties are respectively exploited in laundry detergent powders and adsorbents/desiccants. Catalytic acidity is employed in hydrocarbon (petrochemistry, refining) and environmental technology.<sup>9</sup>

The Structure Commission of the International Zeolite Association (IZA-SC) is the organization responsible for assigning the framework type codes (FTC) for the proper nomenclature of the zeolite frameworks. The codes are also accepted by IUPAC. The nomenclature code is based on three Roman capital letters and only defines the T atom network topology, independent of the chemical composition or symmetry.<sup>10</sup> Currently, the diversity of existing crystalline molecular sieve topologies is documented in 253 frameworks by IZA-SC.<sup>11</sup> Figure 1.2 displays the increase of the number of FTC from 1995 to 2020.

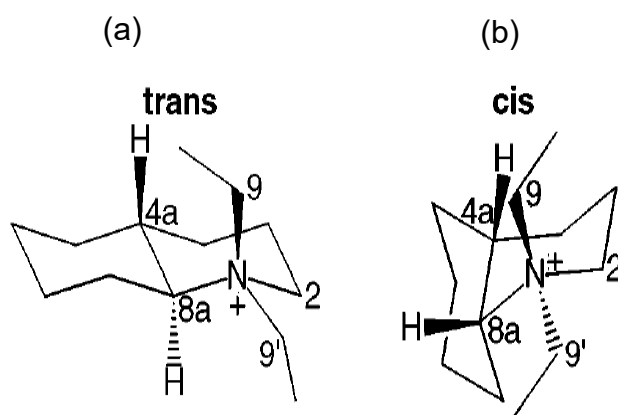


**Figure 1.2.** Differences in trans (a) and cis (left) configurations of decahydroquinoline derivatives <sup>37</sup>

## 1.2 Synthesis of Zeolites

### 1.2.1. Hydrothermal synthesis of zeolite

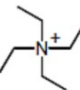
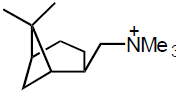
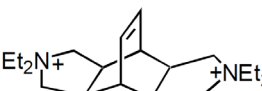
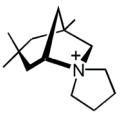
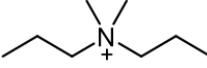
Since the pioneering work by Barrer and Milton in 1940s, there has been much progress during the last 60 years in synthesizing zeolites. Intense research activity in zeolite synthesis is shown by a handful of articles including review and books.<sup>2, 12–17</sup> Hydrothermal synthesis is the most used route to make zeolites, occurring under the high-temperature (> 100°C) and high-pressure (<1 bar) condition in alkaline aqueous

solution in a closed system. Nowadays, the concept of hydrothermal synthesis covers the entire region above room temperature and 1 bar.<sup>16,17</sup> A large number of variables affects the nucleation and crystallization of a specific zeolite phase, such as gel composition of the starting material,<sup>18</sup> the T (Si, or Al) source,<sup>19–23</sup> the alkalinity, water content, temperature, organic structure directing agents (OSDA), etc. Thus, many parameters need to be controlled, which renders the understanding of the zeolite growth mechanisms relatively challenging.<sup>24</sup>

For example, zeolites A(LTA), X(FAU), Y(FAU), B(ANA), and HS(SOD) are possible to be obtained in the same  $\text{Na}_2\text{O} - \text{Al}_2\text{O}_3 - \text{SiO}_2 - \text{H}_2\text{O}$  system by altering the region.<sup>18</sup> This work identifies how gel composition in starting material affected the formation of zeolites. With respect to T sources, sodium silicate, colloidal silica solution, fumed silica, tetramethylorthosilicate (TMOS), and tetraethylorthosilicate (TEOS) are commonly used as Si sources in the synthesis of zeolite. The solubility, reactivity, and surface area of Si sources have direct influence on the nucleation and crystallization of the product. During the synthesis of LTA, it was reported that the crystallization rate, and crystal size have relationship with the surface areas of Si sources.<sup>25</sup> Typical Al sources are sodium aluminate, pseudo-boehmite, aluminum hydroxide, aluminum isopropoxide, and aluminum sulfate.

The mineralizing agent plays the role of the crystallization catalyst. Movement of element T from the gel to the crystal via the solution is ensured by the so-called mineralizing agents  $\text{OH}^-$  and  $\text{F}^-$ .<sup>26</sup>  $\text{OH}^-$  leads to the dissolution of Si and Al sources to

**Table 1.1.** OSDAs and Zeolites

Materials	FTC	OSDA	Channel system	Reference
Beta	*BEA		12-12-12R	30
CIT-1	CON		12-12-10R	31
MCM-68	MSE		12-10-10R	32
ITQ-7	ISV		12-12-12R	32
YNU-5	YFI		12-12-8R	34

the solution to form Si–O–Al linkages. In other words, alkalinity also influence the crystallization process by accelerating the dissolution rate of T sources, simultaneously, suppressing the polymerization degree of silicate anions while accelerating the polymerization of polysilicate and aluminate anions. Therefore, the pH value of the solution plays a huge role during the hydrothermal synthesis by shorting the induction and nucleation period and speeding up the crystallization.<sup>10, 27, 28</sup> The presence of F<sup>−</sup> make it possible to obtain zeolite in a neutral or acidic system.<sup>29</sup>

OSDA acts as a central role in the discovery of high-silica zeolites ( $\text{SiO}_2/\text{Al}_2\text{O}_3 > 12$ ) with novel framework topologies and compositions. Several typically used OSDAs in yielding zeolites (12-ring) syntheses are listed in Table 1.1.<sup>31–34</sup>

In 1996, Kubota et al. clarified the correlation between the relative hydrophobicity and rigidity of organic cations and the phase selectivity of high silica zeolite and they concluded that rigid, bulky and relatively short ( $< 10 \text{ \AA}$  for the longest axis) molecules with moderate hydrophobicity are the best candidates for the structure-direction of new high-silica molecular sieves.<sup>35</sup> Except for the hydrophobicity, the size and shape of OSDA molecules also have effect on the phase of final product.<sup>36–40</sup> For example, the *cis*-isomers and *trans*-isomers of decahydroquinoline derivatives leads to totally deferent products. The former (Figure 1.2a) is selective for SSZ-48 (SFE) in borosilicate gels for  $\text{Si/B} = 25$  while the pure *trans*-deviates (Figure 1.2b) of leads to kenyaite (a layered silicate).<sup>35</sup> This fact identifies that there is a high correlation for the space-filling details of the guest organocations and the type of crystalline host lattice developed in the synthesis.<sup>35</sup>

The mechanisms of zeolite formation are still elusive due to complex chemical reactions, equilibria, and solubility variations occurring throughout the crystallization process.<sup>2</sup> The two proposed mechanism of zeolite synthesis are (i) solid-phase transformation mechanism and (ii) liquid-mediate transport mechanism. The solid-phase transformation mechanism was first proposed by D. W. Breck and E. M. Flanigen in 1968, standing for the direct transformation of zeolite crystal from the amorphous gel phase. Figure 1.3 displays the rough process scheme of solid-phase transformation mechanism.<sup>41</sup> Depolymerization of gel structure firstly occurs with the presence of OH<sup>−</sup> ions and then aluminosilicates and silicate anions in the gel rearranged around the hydrated cation species, forming the basic polyhedral units. By periodically linkage, crystalline zeolite is formed.

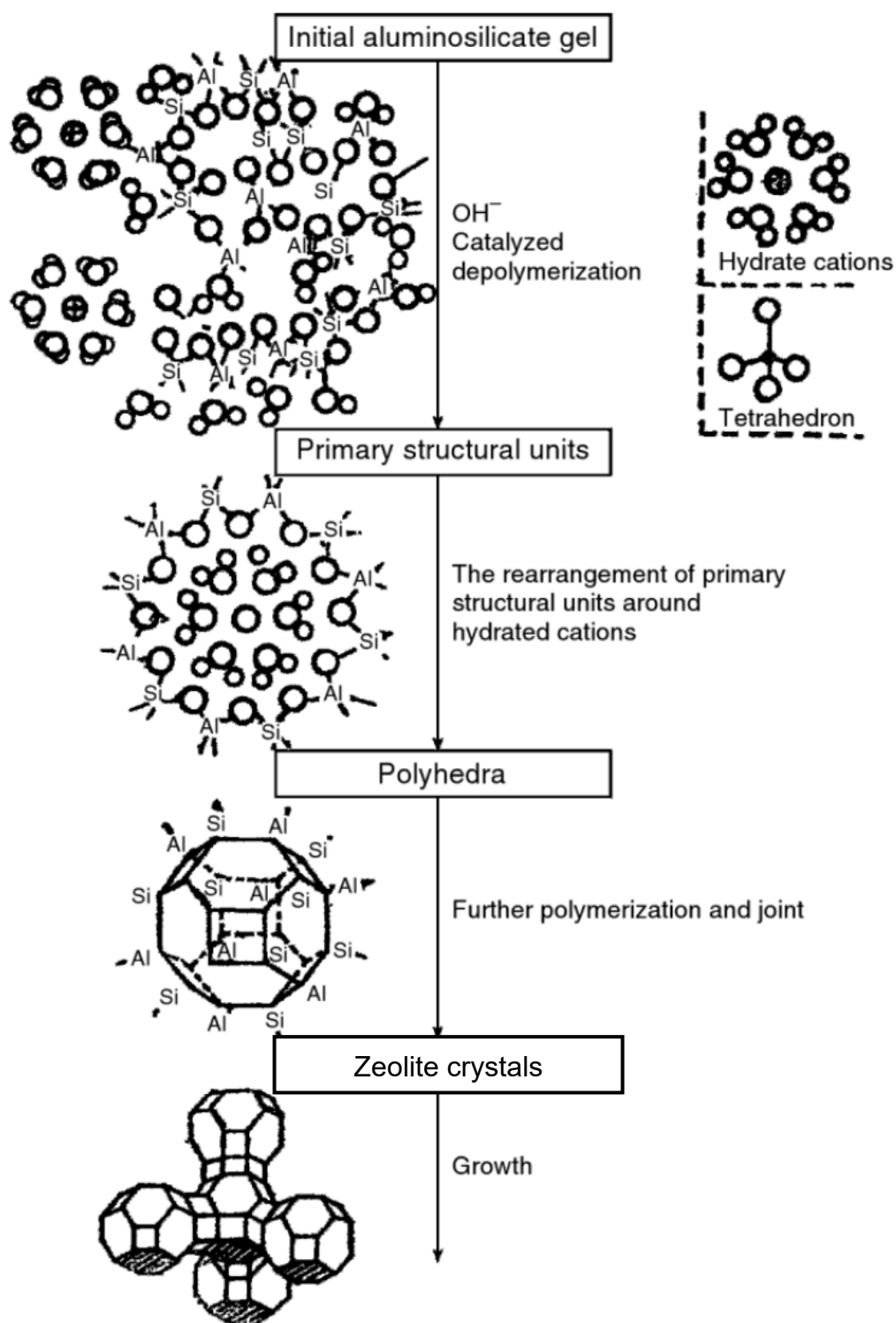
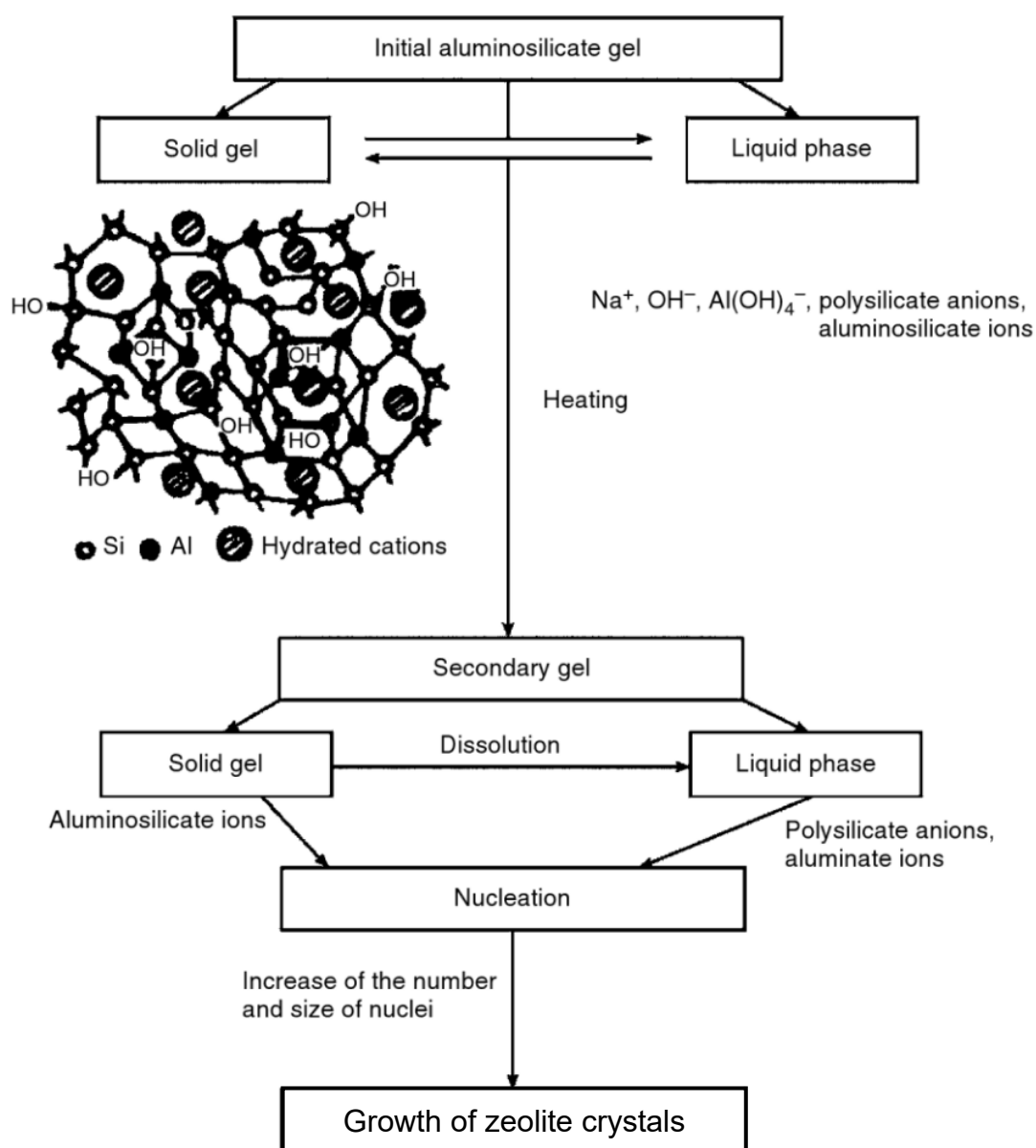


Figure 1.3. Solid-phase transformation mechanism.<sup>41</sup>

The liquid-mediate transport mechanism (Figure 1. 4), on the other hand, claims that the aluminate, silicate, and/or aluminosilicate species indeed participate in the nucleation and crystallization process.<sup>42</sup>

Recently, a synergistic mechanism of two growth processes is also supported to explain the experiment results. For example,<sup>43</sup> Do and his co-workers traced the zeolite crystal evolution from sodium-rich hydrogels and found zeolite nuclei was formed in the equilibrated gel phase derived from primary aggregates, then the nuclei could be diffused into the liquid-solid interface of the equilibrated gel phase and the liquid phase.



**Figure 1.4.** liquid-mediate transport mechanism.<sup>41</sup>

### 1.2.2. Dry-gel conversion (DGC) synthetic route

Since 1990, the crystalline ZSM-5 (MFI) was transferred from a dry amorphous aluminosilicate gel with vapors of water and volatile amines.<sup>44</sup> Several zeolites such as TS-1,<sup>45</sup> Ti-BEA,<sup>45</sup> YNU-2,<sup>46</sup> can be synthesized by using this method as well. This new synthetic method is named by dry-gel conversion (DGC).

## 1.3 YNU-5 zeolite

Since the discovery of large-pore zeolites, such as Y (FAU), BEA and MOR, the catalytic application of zeolites was heavily focused on large-pore zeolites. Zeolite Y, with supercages, are widely used in the fluid catalytic cracking (FCC) of oil.<sup>47</sup> Zeolite BEA and MOR play important roles in the catalytic upgrading of platform molecules from the refinery.<sup>48</sup> Therefore, the syntheses of large-pore zeolites attract intense focus. However, only few types of large-pore zeolite were discovered since 2000, such as (MSE topology, 12-10-10R, 2000),<sup>49, 50</sup> ITQ-27(IWV topology, 12-12R, 2006)<sup>51</sup> and SSZ-65 (SSF topology, 12-12R, 2007).<sup>52</sup>

Typically, MCM-68 (MSE) can be synthesized using N,N,N',N',-tetraethylbicyclo[2.2.2]-oct-7-ene-2,3:5,6-di-pyrrolidinium(TEBOP<sup>2+</sup>) (Figure 1.5a) as OSDA crystallized for 16 days. Attempts were tried to simplify the synthesis of MSE by using FAU as a building units' supplier. This method leads to YNU-3 (Si/Al = 6~7) zeolite with different properties from MCM-68 (Si/Al = 10~12) and shorten the crystallization time to 5 days.<sup>53</sup> It was reported that UZM-35 with a Si/Al ratio of 8 (MSE) can be obtained using a simple OSDA Me<sub>2</sub>Pr<sub>2</sub>N<sup>+</sup> shown in Figure 1.5b.<sup>54</sup> The investigation about the syntheses of new zeolites in a high-concentrated system (FAU as Si & Al sources) was intensively carried out in our group. SSZ-39(AFX)<sup>55</sup> and YNU-5 (YFI)<sup>56</sup> were obtained. YNU-5 is a new discovered zeolite with a novel framework of YFI (shown in Figure 1.6), containing a distinguishable three-dimensional channel system: 2-dimensional 12-ring (0.78 nm × 0.59 nm; large micropore) with channel intersection connected with 8-ring channel (0.44 nm × 0.34 nm; small micropore), thus forming a large space around 7.97 Å that are accessible through 12-ring windows. Besides, there is an isolated 8-ring channel (0.40 nm × 0.29 nm, small micropore) in the framework.

Post-synthetic treatment with HNO<sub>3</sub> acid under a severe condition (130°C, 24 h) change YNU-5 zeolite from the aluminosilicate type to the high silica type, as well as high structural stability and high crystallinity.<sup>57, 58</sup> Ikeda and his co-workers<sup>58</sup> applied Rietveld analysis to detect the T atoms vacancy in dealuminated YNU-5. He found no

T atoms vacancy was detected even though the presence of 4%  $Q^3(0Al)Si$  species confirmed by  $^{29}Si$  MAS NMR. It is possible that  $Q^3(0Al)Si$  species are attributed to homogeneous vacancy at all T sites. This speculation is consistent with the Si-migration during dealumination put forward previously.<sup>57</sup> The high stability and widely controllable Al content render YNU-5 a very promising acid solid catalyst.

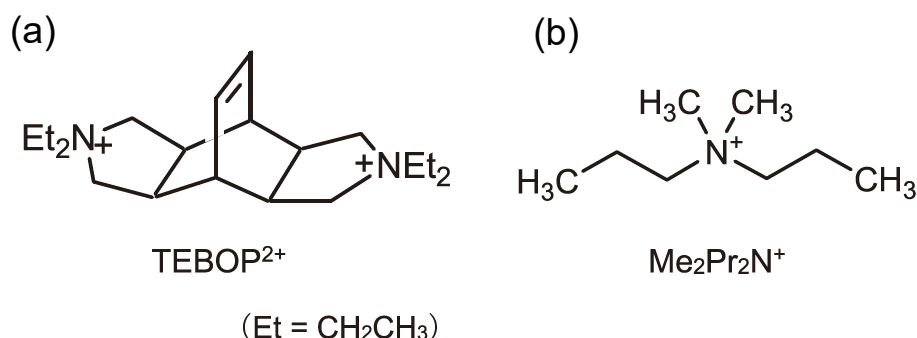


**Figure 1.5.** Structures of cationic moieties of OSDA (a) TEBOP<sup>+</sup>, (b) Me<sub>2</sub>Pr<sub>2</sub>N<sup>+</sup>

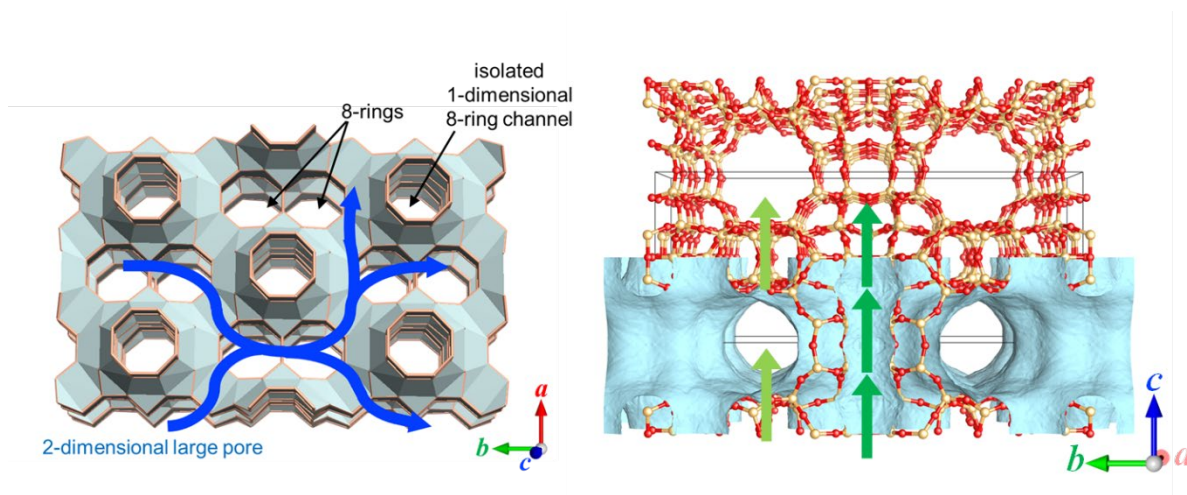


**Figure 1.6.** Crystal structure of YNU-5.

## 1.4 Application as solid acid catalyst

### 1.4.1 Acidity of zeolite

In aluminosilicate-type zeolites, the tetrahedra of  $SiO_{4/2}$  present as electrically neutral, however, the formal charge on the tetrahedra changes from neutral to negative when silicon cation in the framework is substituted by Al atoms. This negative charge is balanced by a metal cation or a hydroxyl proton thus forming a weak Lewis acid site or a strong Brønsted acid sites, respectively. Brønsted acid sites act as protons donors and Lewis acids accept a pair of electrons. Figure 1.7 displays different types of hydroxyl groups and acid sites in zeolite. Figure 1.7a shows the typical bridging hydroxyl groups  $Si-(OH)-Al$  which acts as a strong Brønsted acid site. The silanol

groups Si–OH (or framework defects) at the external surface of zeolite particles are of weak acid strength (in Figure 1.7b). These Si–OH groups are mainly formed from calcination, hydrothermal or acid treatment. If Si migration occurred during dealumination process, these defects may be healed and extra-framework Al species (Figure 1.7c) are formed, acting as Brønsted acid sites. Figure 1.7d is Lewis acid sites at extra-framework Al species and framework defects.

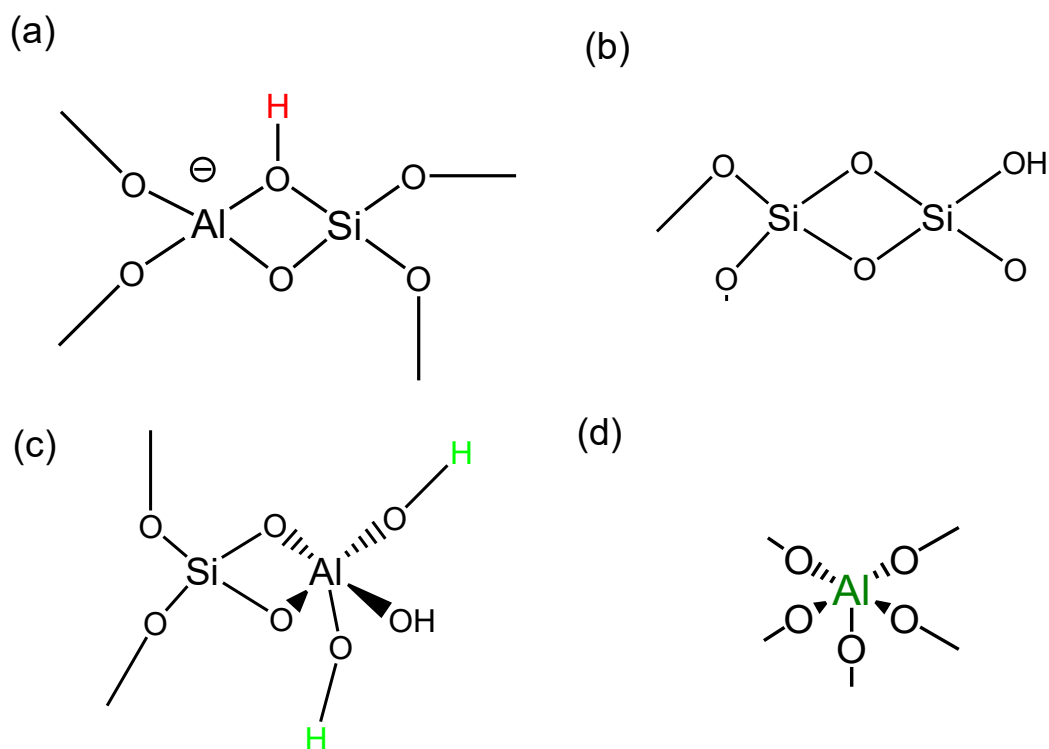


**Figure 1.7.** Schematic representation of the different types of hydroxyl groups and acid sites in zeolites. (a) typical bridging hydroxyl groups Si–OH–Al, (b) terminal Si–OH, (c) octahedrally coordinated extraframework Al species after hydration, (d) coordinated extraframework Al species.

Reactivity in zeolites is based on their active sites, which is directly related to the framework aluminum content. Acid strength is believed to rely on the composition of the zeolite framework (such as Si/Al ratio),<sup>59</sup> the presence of extraframework cations,<sup>60,61</sup> and crystal structure.<sup>62</sup> In 2009, Katada and co-workers<sup>63</sup> found the relationship between local geometry ((i) the distance between tetrahedra at the end of both  $\text{O}_3\text{Si}(\text{OH})\text{AlO}_3$  unit, (ii) the relative orientation of two tetrahedrons) and Brønsted acid sites in zeolites (estimated by ammonia adsorption energy). The longer distance and larger planar angle contribute to higher Brønsted acid strength.



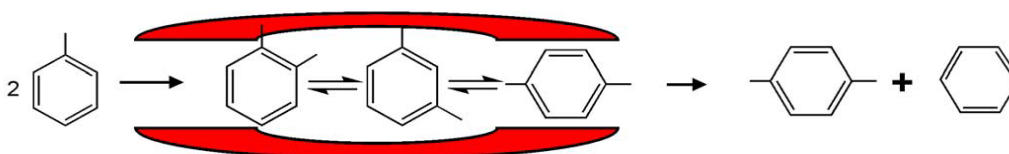
### 1.4.2 Shape selectivity of zeolite

One defining features of zeolites is their shape, or topology of the internal pore structure, which can strongly influence the selectivity of products in chemical transformations.<sup>64</sup> This property of zeolite is named with shape selectivity. There are three basic types of shape-selectivity: reactant shape-selectivity, product shape-selectivity, and transition-state shape selectivity, as shown in Figure 1.8.<sup>64</sup>

- Reactant Selectivity (Dewaxing)



- Product Shape Selectivity (Toluene Disproportionation)



- Transition-State Selectivity (Alkylation of Aromatics)

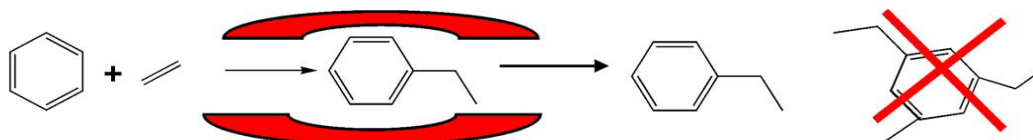


**Figure 1.8.** Examples of classical shape selectivity from the literature.<sup>64</sup>

Reactant shape selectivity excludes bulky molecules which cannot reach the internal acid sites due to the limited size of the pore mouth of channels.<sup>65</sup> This type of selectivity depends on the geometry of the pore entrance and the intrapore diffusional characteristics of the reactant molecules.<sup>64</sup> A classic example is the selective dehydration of alcohols (primary and secondary butanol) on CaA and CaX zeolites.<sup>66</sup> CaA zeolite shows a selective dehydration whereas CaX with larger pore size shows non-selective dehydration.

Product shape selectivity works when the molecules size of products is close to the pore exit of channels. Molecules with a higher diffusion (spatial dimensions fit the pore well) throughout the channel will be in higher percentage in bulk products.<sup>67</sup> A noteworthy instance is the selective disproportionation of toluene to *p*-xylenes over modified ZSM-5.<sup>68</sup>

The reactant and product molecules must diffuse in and out of the pore in a regime. This behavior is called configurational diffusion. Even a slight change of the size of molecules or the pores, there will be a huge difference in the diffusion coefficients.<sup>65</sup>

Transition-state shape selectivity is the steric restriction which the geometry of pores around the active sites imposes on the transition states when reaction taking place at the internal confined pores or channels.<sup>65</sup>

### 1.4.3 Catalytic application

#### 1.4.3.1 Methanol-to-olefins(MTO) reaction

Since first proposed by Mobil Corporation in 1977,<sup>69</sup> methanol to olefins reaction has been receiving great of focus until today because it is one of the most important reaction in C1 chemistry facilitating the production of chemicals and plastics from renewable resources. ZSM-5 and SAPO series zeolites are two excellent catalysts to produce light olefins. There are several excellent reviews about MTO reactions ranging from the fundamental research<sup>70–73</sup> to its commercialization perspective.<sup>74</sup> In general, hydrocarbon pool (HCP) concept proposed by Dahl et al.<sup>75–77</sup> is used to explain the formation of the products including olefins, aromatics, and alkanes. However, there are still debates on the formation of the first C–C bond. In 2007, Bjørgeren et al. put forward a dual-cycle mechanism (shown in Figure 1.9) based on their experiment data over ZSM-5 zeolite.<sup>78</sup> Other studies using different zeolites also have similar evidence of this mechanism.<sup>79–81</sup> The dual-cycle mechanism is the combination of an aromatic cycle and an alkene cycle. As shown in Figure 1.9, the left aromatic cycle, the primary intermediates are methylcyclopentenyl and polymethyl-benzenium, while in the alkene cycle, higher alkenes are the primary intermediates producing light olefins by dealkylation. Higher alkenes also transfer to methylcyclopentenyl through hydrogen transfer and cyclization reactions.

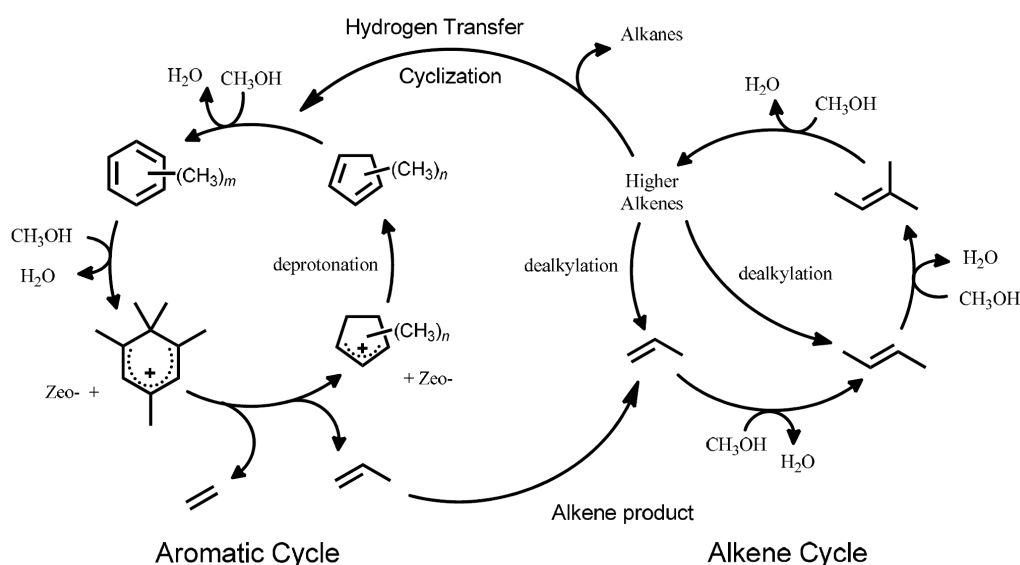


**Figure 1.9.** Scheme of dual-cycle mechanism of MTO reaction.

#### 1.4.3.2 Fluid Catalytic Cracking (FCC)

It is well-known that flow catalytic cracking (FCC) craft is one of the most important processes in petroleum refining to produce high octane gasoline from high boiling point fractions. Catalyst can reduce the activation energy required for the reaction, making the reaction can proceed at a lower temperature, which has obvious advantages in terms of energy saving and environmental preservation. As a new process to replace traditional thermal cracking producing light olefins, hydrocarbon catalytic cracking technology has been extensively investigated. Y type (FAU) zeolite is the most widely used catalyst for FCC. However,  $H^+$ -Y zeolite with low  $SiO_2/Al_2O_3$  shows low hydrothermal stability despite its high initial activity. This problem was solved by the steaming treatment, leading to higher stability of Y zeolite with low  $SiO_2/Al_2O_3$ .<sup>82</sup> On the other hand, ZSM-5 (MFI) is another excellent acid catalyst over FCC reaction, promising high shape selectivity and high activity of cracking paraffins.<sup>83</sup>

#### 1.4.3.3 Limitation of zeolites as solid acid catalyst

Zeolites have many fantastic properties, like uniformed micropores, large specific surface area, strong acidity, and good shape-selectivity, make it widely applied in many fields such as detergents, acid catalysts. However, its limited micropores ( $< 2$  nm) will lead to serious mass transfer and diffusion resistance, resulting in poor catalytic performance, especially in the reaction involving macromolecules.<sup>84,85</sup>

Effectiveness factor  $\eta$  is the parameter to evaluate the degree of catalyst utilization (shown in Figure 1.10).<sup>86</sup> Full utilization of catalysts means  $\eta = 1$ , suggesting the observed reaction rate is equivalent to the intrinsic one without any diffusion constraints. There is intraparticle transport limitation in the case of zeolite using as catalyst. Thiele modules  $\phi$  is another factor to describe the effective utilization of zeolite ( $\phi = 10$ ,  $\eta = 0.1$ , meaning 10% volume of zeolite is used.). For a given reaction system, intrinsic rate coefficient  $k_v$  is fixed, thus there are two routes to increasing the utilization: (i) shortening the diffusion length  $L$ , (ii) improve the effective diffusivity  $D_{eff}$ . The former can be achieved by develop “large cavity” and “wide-pore” zeolites (Figure 1.11a). The latter can be realized by reducing the particle size (shown in Figure 1.11b) or altering the morphology. Another strategy to enhance  $D_{eff}$  is introducing “large pore” system into zeolite particles. The materials containing multi scales of pores was named hierarchical material (Figure 1.11c).

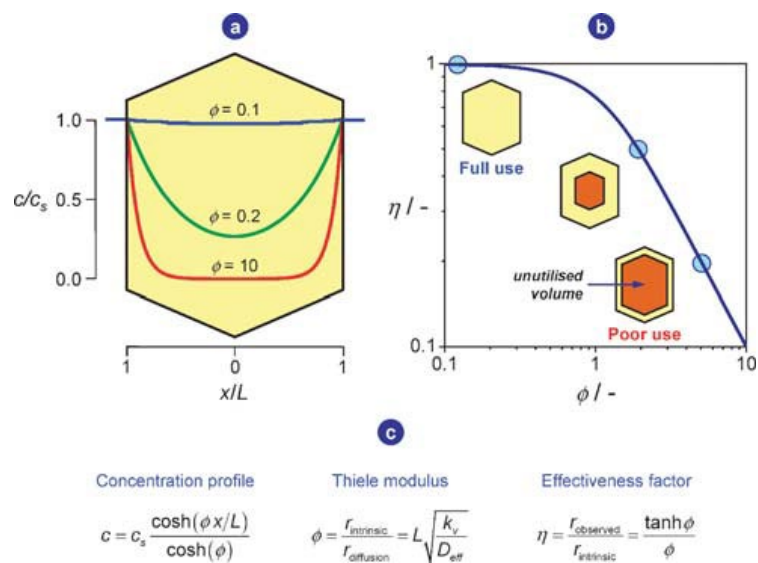


**Figure 1.10.** Change of concentration in a zeolite crystal at different value of Thiele modulus.<sup>86</sup>  
**Assumptions:** Steady-state diffusion and reaction, slab model, first-order irreversible reaction, and isothermal conditions.

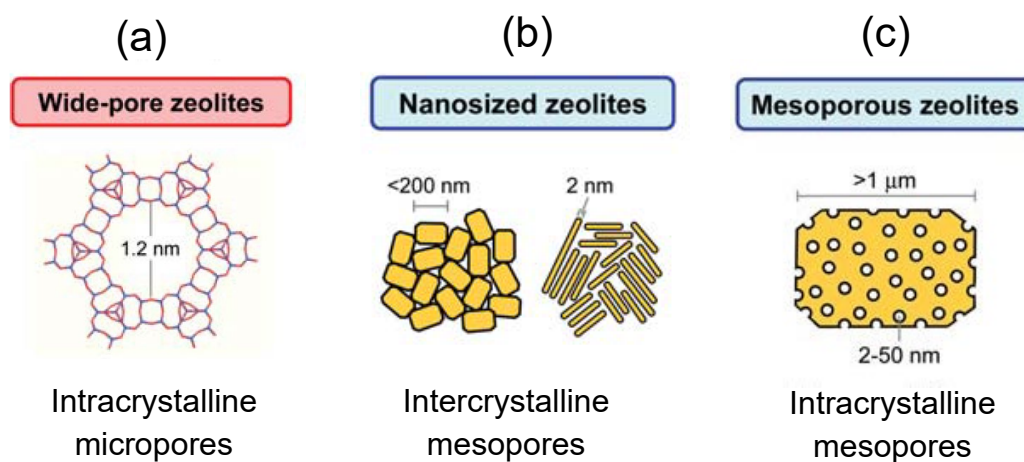


**Figure 1.11.** Three routes of new types of zeolites with enhanced mass transport performance

## 1.5 Hierarchical zeolites

### 1.5.1 Design of Hierarchical Zeolites

Hierarchical zeolites are the zeolites containing a secondary network of mesopores except from the intrinsic micropores. The superior performance of hierarchical materials in many traditional and emerging catalytic applications attracted much attention thus intensive investigations on its syntheses are carried out. The methods can be generally divided into two groups: top-down and bottom-up approaches.

Top-down approaches (Figure 1.12) include (i) post-synthetic demetallation,<sup>87-97</sup> (ii) modification of layered zeolite precursors,<sup>98,99</sup> (iii) Surfactant template,<sup>100-102</sup> (iv) irradiation<sup>103</sup> and (v) ball milling.<sup>104</sup> The post-synthetic demetallation route can be

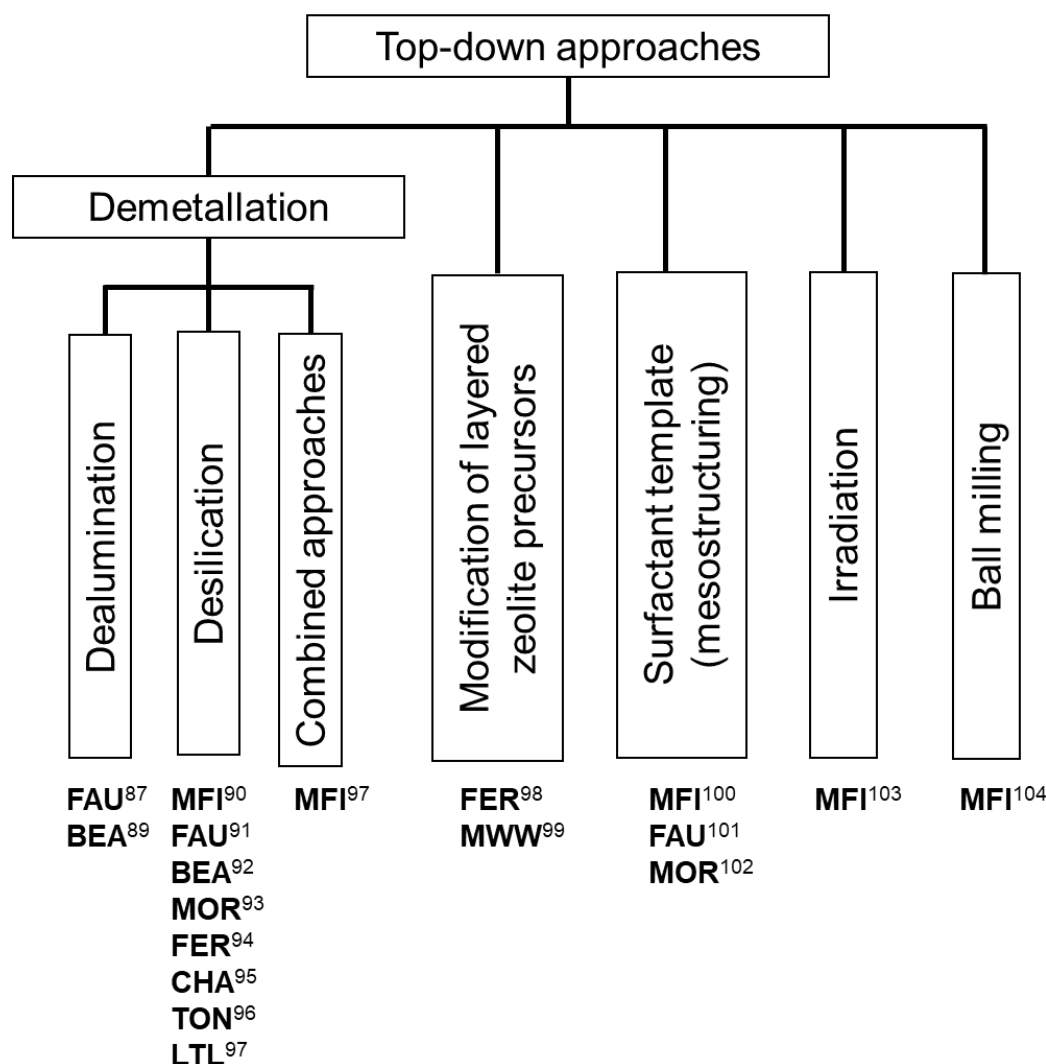


**Figure 1.12.** Top-down synthesis strategies for the hierarchical zeolites of different framework types.

diversified into dealumination,<sup>87,88</sup> desilication<sup>89–96</sup> or combination of dealumination and desilication,<sup>97</sup> depending on the demetallized species such as Al or Si, respectively.

Bottom-up approaches (Figure 1.13) include templating methods and non-templating methods. Templates used in preparing hierarchical zeolites can be generally classified into two categories: hard templates (carbon nanoparticles,<sup>105–107</sup> polymers,<sup>108,109</sup> mesoporous silica,<sup>110</sup> and silanized zeolitic nanounits<sup>111,112</sup>) and soft template (silylated polymers<sup>113</sup> and organosilanes<sup>114–118</sup>).

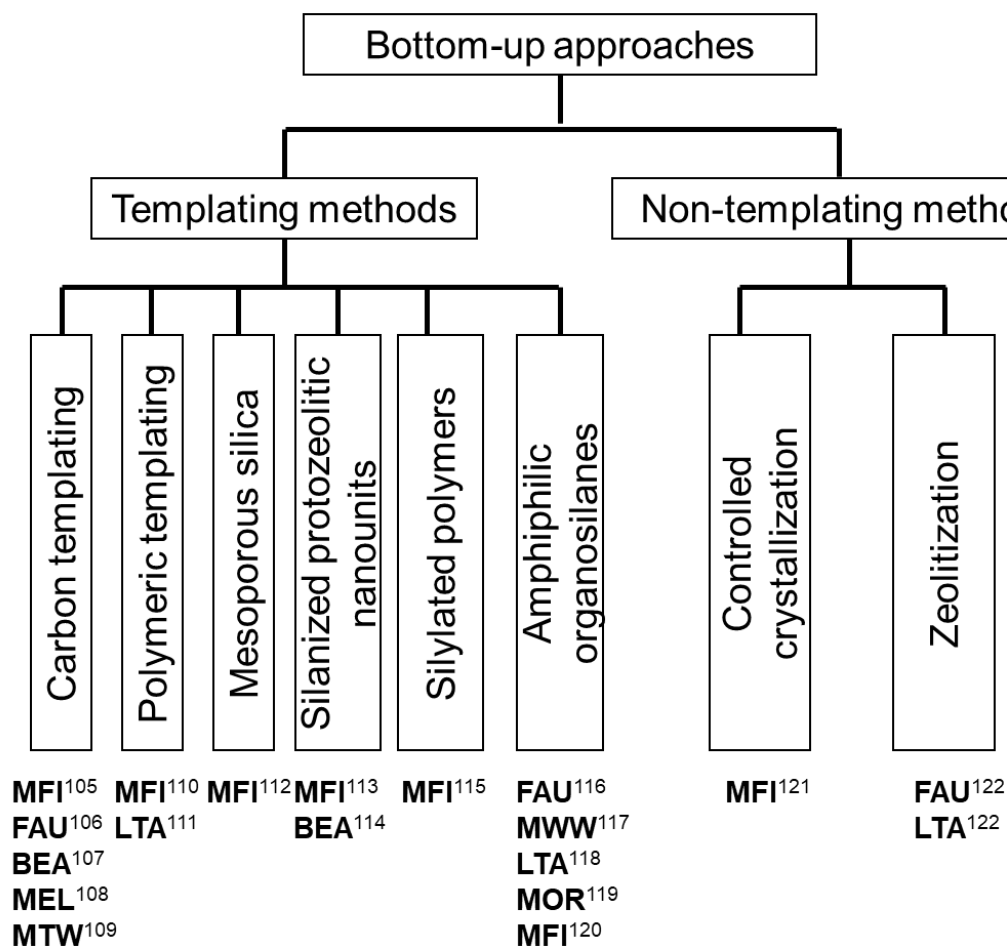


**Figure 1.13.** Bottom-up synthesis strategies for the hierarchical zeolites of different framework types.

For Al-rich FAU type zeolites, the steaming and acid treatment (dealumination) are the most frequently applied method to obtain zeolites with higher Si/Al molar ratio and mesopores for fluid catalytic cracking.<sup>105,106</sup>

Inorganic acid such as HNO<sub>3</sub> aqueous solution is found to be effective to leaching framework Al species, however, the destruction of zeolite structure and crystallinity were simultaneously observed. Therefore, organic acids such as ammonium fluosilicate ((NH<sub>4</sub>)<sub>2</sub>SiF<sub>6</sub>) is another common dealumination agent, which can supplement silicon during dealumination and preserve the crystallinity of zeolite.<sup>107</sup>

### **1.5.2 Catalytic applications of Hierarchical Zeolites**

Compared with traditional zeolite, hierarchical zeolite molecular sieves have both mesoporous structure and microporous structure. They have many significant advantages, especially for reactions involving large molecules. Due to the improvement and optimization of the pore structure of the hierarchical zeolite, its catalytic reaction performance is better than that of the traditional zeolite molecular sieve: (1) The introduction of the mesoporous structure effectively improves its diffusion, so that the reactants can quickly access the active site. The target product can diffuse from the pores to the bulk products, which improves the conversion of reactants and product selectivity; (2) The establishment of a hierarchical pore structure has a significant effect on prolonging catalyst life, and coke deposition can be suppressed. Hierarchical zeolites are mostly used in catalytic cracking, alkylation, isomerization and methanol-to-hydrocarbon reaction systems.

#### **1.5.2.1 Fluid Catalytic Cracking (FCC)**

Zhu<sup>121</sup> et al. introduced mesopores into ZSM-5/mordenite composite zeolites by hydrothermal treatment and investigated the catalytic cracking of *n*-heptane over the fresh and steamed ZSM-5/MOR zeolites by in situ DRIFTS. Treated samples present remarkably faster initial reaction rate. Hierarchical ZSM-5 zeolites were obtained using the combination of base and acid treatments and have superior catalytic performance over the catalytic cracking of biomass.<sup>122</sup> The larger external surface improved the utilization of zeolite acid sites and suppressing the secondary reactions, thus leading to the improvement of the selectivity for gasoline hydrocarbons and light olefins.

#### **1.5.2.2 Methanol-to-hydrocarbon reaction (MTH)**

Ryoo and his coworkers<sup>123</sup> investigated the effect of mesoporosity on catalyst longevity of methanol-to-hydrocarbon (MTH) reactions using MFI zeolites with different degrees of mesoporosity, which were obtained via various strategy: post-synthetic desilication, dry-gel conversion in carbon templates, and hydrothermal synthesis. The experiment results identifies that the lifetime of catalysts can be increased by three times due to the existence of mesopores.

## **1.6 Aims of research**

YNU-5 zeolite, as a new discovered zeolite, is a potential catalyst in chemical reactions due to its three-dimensional large micropore structure and its widely tunable Al content. However, the related investigation is far away from enough. The primary goals of this thesis are to (i) gain fundamental understanding of the relationship between

synthetic conditions and product quality; (ii) to assess the catalytic performance of YNU-5 zeolite over different reaction, (iii) enhance the catalytic performance through introducing mesopores.

## 1.7 References

1. D. W. Breck, J. V. Smith, *Sci. Am.*, **1959**, 200, 85–96.
2. M. E. Davis, R. F. Lobo, *Chem. Mater.*, **1992**, 4, 756–768.
3. W. Loewenstein, *Am. Mineral.*, **1954**, 39, 92–96.
4. Y. Li, J. Yu, *Chem. Rev.*, **2014**, 114, 7268–7316.
5. M. Dusselier, P. Van Wouwe, A. Dewaele, P. A. Jacobs, B. F. Sels, *Science*, **2015**, 349, 78–80.
6. M. E. Davis, *Ind. Eng. Chem. Res.*, **1991**, 30(8), 1675–1683.
7. E. M. Flanigen, R. W. Broach, S. T. Wilson, Wiley-VCH Verlag GmbH & Co. KGaA, **2010**.
8. J. L. Paillaud, B. Harbuzaru, J. Patarin, N. Bats, *Science*, **2014**, 304, 990–992.
9. W. Vermeiren, J. P. Gilson, *Top. Catal.*, **2009**, 52, 1131–1161.
10. C. Baerlocher, L. McCusker, D. Olson, Atlas of Zeolite Framework Types. *Elsevier Science*, **2007**.
11. International Zeolite Association: Structure Commission. Database of Zeolite Structures, <http://www.iza-structure.org/>.
12. F. Schwochow, L. Puppe, *Angew. Chem. Int. Ed. Engl.*, **1975**, 14(9), 620–628.
13. R. F. Lobo, S. I. Zones, M. E. Davis, *J. Incl. Phenom. Mol. Recogen. Chem.*, **1995**, 21, 47–78.
14. R. Szostak, Molecular Sieves, Principles of Synthesis and Identification, 2<sup>nd</sup> Edn, Blackie Academic & Professional, London, **1998**.
15. C. S. Cundy, P. A. Cox, *Chem. Rev.*, **2003**, 103, 663–702.
16. A. Corma, M. E. Davis, *Chem. Phys. Chem.*, **2004**, 5, 304–313.
17. R. Xu, W. Pang, J. Yu, Q. Huo, J. Chen, Chemistry-Zeolites and Porous Materials (in Chinese), 1<sup>st</sup> Edn., Science Press, Beijing, **2004**.
18. D. W. Breck, Zeolite Molecular Sieves, Chemistry, and Use, Wiley, New York, **1974**.
19. M. Maldonado, M. D. Oleksiak, S. Chinta, *J. Am. Chem. Soc.*, **2013**, 135, 2641–2652.
20. X. Meng, F. Xiao, *Chem. Rev.*, **2014**, 114, 1521–1543.
21. P. J. Kooyman, P. Van der Waal, H. van Bekkum, *Zeolites*, **1997**, 2449, 50–53.
22. S. Ivanova, E. Vanhaecke, L. Dreibine, B. Louis, C. Pham, C. Pham-Huu, *Appl. Catal. A Gen.*, **2009**, 359, 151–157.
23. R. Lai, Y. Yan, G. R. Gavalas, *Microporous Mesoporous Mater.*, **2000**, 37, 9–19.
24. J. Grand, H. Awala, H. S. Mintova, *Cryst. Eng. Comm.*, **2016**, 18, 650–664.
25. S. Shimizu, H. Hamada, *Angew. Chem. Int. Ed.*, **1999**, 38, 2725–2721.



26. H. Kessler, *Stud. Surf. Sci. Catal.*, **1989**, 52, 17–37.
27. W. Meise, F. E. Schwocho, *Adv. Chem. Ser.*, **1973**, 121, 169–178.
28. S. G. Fegan, B. M. Lowe, *J. Chem. Soc. Faraday Trans.*, **1986**, 82, 785–799.
29. D. P. Serrano, Van R. Grieken, *Microporous Mesoporous Mater.*, **2001**, 46, 35–46.
30. W. Chaikittisilp, T. Yokoi, T. Okubo, *Microporous Mesoporous Mater.*, **2008**, 116, 188–195.
31. R. F. Lobo, M. E. Davis, *J. Am. Chem. Soc.*, **1995**, 117(13), 3766–3779.
32. D. L. Dorset, S. C. Weston, S. S. Dhingra, *J. Phys. Chem. B*, **2006**, 110(5), 2045–2050.
33. J. Q. Song, B. Marler, H. Gies, *C. R. Chimie*, **2005**, 8(3-4), 341–352.
34. N. Nakazawa, T. Ikeda, N. Hiroshi, Y. Yoshida, Q. Han, S. Inagaki, Y. Kubota, *J. Am. Chem. Soc.*, **2017**, 139, 7989–7997.
35. Y. Kubota, M. M. Helmkamp, S. I. Zones, M. E. Davis, *Micropor. Mater.*, **1996**, 6, 213.
36. S. Lawton, W. Rohrbaugh, *Science*, **1990**, 247, 1319–1321.
37. D. Shantz, A. Burton, R. Lobo, *Microporous Mesoporous Mater.*, **1999**, 31, 61–73.
38. J. Paillaud, P. Caullet, L. Schreyeck, B. Marler, *Microporous Mesoporous Mater.*, **2001**, 42, 177–189.
39. G. Lee, Y. Nakagawa, S. Hwang, M. Davis, P. Wagner, L. Beck, *J. Am. Chem. Soc.*, **2002**, 124, 7024–7034.
40. S. Zones, Y. Nakagawa, L. Yuen, T. Harris, *J. Am. Chem. Soc.*, **1996**, 118, 7558–7567.
41. R. Xu, W. Pang, J. Yu, Q. Huo, J. Chen, *Chemistry-zeolite and porous Materials* (in Chinese), 1<sup>st</sup> Edn., Science Press, Beijing, **2004**.
42. H. C. Hu, T. Y. Lee, *Ind. Eng. Chem. Res.*, **1990**, 29, 749–754.
43. M. H. Do, T. Wang, D. G. Cheng, F. Chen, X. Zhan, J. Gong, *J. Mater. Chem. A*, **2014**, 2, 14360–14370.
44. W. Xu, J. Dong, J. Li, J. Li, F. Wu, *J. Chem. Soc.-Chem. Commun.*, **1990**, 10, 755–756.
45. M. Matsukata, M. Ogura, T. Osaki, P. Rao, M. Nomura, E. Kikuchi, *Top. Catal.*, **1999**, 9, 77–92.
46. T. Ikeda, S. Inagaki, T. Hanaoka, Y. Kubota, *J. Phys. Chem. C*, **2010**, 114, 19641–19648.
47. E. T. C. Vogt, B. M. Weckhuysen, *Chem. Soc. Rev.*, **2015**, 44, 7342–7370.
48. M. Dusselier, M. E. Davis, *Chem. Rev.*, **2018**, 118, 5265–5329.
49. D. C. Calabro, J. C. Cheng, R. A. Crane, Jr. C. T. Kresge, S. S. Dhingra, M. A. Steckel, D. L. Stern, S. C. Weston, U.S. Patent, 6049018, **2000**.
50. D. L. Dorset, S. C. Weston, S. S. Dhingra, *J. Phys. Chem. B*, **2006**, 110, 2045–2050.
51. D. L. Dorset, G. J. Kennedy, K. G. Strohmaier, M. J. DiazCabañas, F. Rey, A. Corma, *J. Am. Chem. Soc.*, **2006**, 128, 8862–8867.
52. S. Elomari, A. W. Burton, K. Ong, A. R. Pradhan, I. Y. Chan, *Chem. Mater.*, **2007**, 19, 5485–5492.
53. Y. Kubota, S. Inagaki, Y. Nishita, K. Itabashi, Y. Tsuboi, T. Syahylah, T. Okubo, *Catal. Today*, **2015**, 243, 85–91.

54. J. G. Moscoso, D. Y. Jan, U.S. Patent 7922997, **2011**.
55. N. Nakazawa, S. Inagaki, Y. Kubota, *Chem. Lett.*, **2016**, 45, 919–921.
56. N. Nakazawa, T. Ikeda, N. Hiyoshi, Y. Yoshida, Q. Han, S. Inagaki, Y. Kubota, *J. Am. Chem. Soc.*, **2017**, 139(23), 7989–7997.
57. N. Nakazawa, Y. Yoshida, S. Inagaki, Y. Kubota, *Microporous Mesoporous Mater.*, **2019**, 280, 66–74.
58. T. Ikeda, Y. Yoshida, N. Nakazawa, S. Inagaki, Y. Kubota, *Microporous Mesoporous Mater.*, **2020**, 302, 110197.
59. P. A. Jacobs, *Catal. Rev. Sci. Eng.*, **1982**, 24, 415–440.
60. M. Niwa, K. Suzuki, K. Isamoto, N. Katada, *J. Phys. Chem. B*, **2006**, 110, 264–269.
61. T. Noda, K. Suzuki, N. Katada, M. Niwa, *J. Catal.*, **2008**, 259, 203–210.
62. N. Katada, M. Niwa, *Catal. Surv. Asia*, **2004**, 8, 161–170.
63. N. Katada, K. Suzuki, T. Noda, G. Sastre, M. Niwa, *J. Phys. Chem. C*, **2009**, 113, 19208–19217.
64. T. F. Degnan, Jr. *J. Catal.*, **2003**, 216, 32–46.
65. P. B. Weisz, *Pure Appl. Chem.*, **1980**, 52, 2091–2103.
66. P. B. Weisz, V. J. Frillette, *J. Phys. Chem.*, **1960**, 64, 382–382.
67. C. Song, J. M. Garcés, Y. Sugi, Introduction to Shape-Selective Catalysis, **1999**, chapter 1.
68. A. Corma, F. Llopi, J. B. Monton, *J. Catal.*, **1993**, 140, 384–394.
69. C. D. Chang, A. J. Silvestri, *J. Catal.*, **1977**, 47, 249–259.
70. M. Stocker, *Microporous Mesoporous Mater.*, **1999**, 29, 3–48.
71. W. Wang, M. Acc. Hunger, *Chem. Res.*, **2008**, 41, 895–904.
72. D. Chen, K. Moljord, A. Holmen, *Microporous Mesoporous Mater.*, **2012**, 164, 239–250.
73. U. Olsbye, S. Svelle, M. Bjorgen, P. Beato, T. V. W. Janssens, F. Joensen, S. Bordiga, K. P. Lillerud, *Angew. Chem., Int. Ed.*, **2012**, 51, 5810–5831.
74. P. Tian, Y. Wei, M. Ye, Z. Liu, *ACS Catal.*, **2015**, 5, 1922–1938.
75. M. Dahl, S. Kolboe, *Catal. Lett.*, **1993**, 20, 329–336.
76. M. Dahl, S. Kolboe, *J. Catal.*, **1994**, 149, 458–464.
77. M. Dahl, S. Kolboe, *J. Catal.*, **1996**, 161, 304–309.
78. M. Bjørgen, S. Svelle, F. Joensen, J. Nerlov, S. Kolboe, F. Bonino, L. Palumbo, S. Bordiga and U. Olsbye, *J. Catal.*, **2007**, 249, 195–207.
79. J. B. Wang, Y. X. Wei, J. Z. Li, S. T. Xu, W. N. Zhang, Y. L. He, J. R. Chen, M. Z. Zhang, A. M. Zheng, F. Deng, X. W. Guo, Z. M. Liu, *Catal. Sci. Technol.*, **2016**, 6, 89–97.
80. J. R. Chen, J. Z. Li, C. Y. Yuan, S. T. Xu, Y. X. Wei, Q. Y. Wang, Y. Zhou, J. B. Wang, M. Z. Zhang, Y. L. He, S. L. Xu, Z. M. Liu, *Catal. Sci. Technol.*, **2014**, 4, 3268–3277.
81. M. Z. Zhang, S. T. Xu, J. Z. Li, Y. X. Wei, Y. J. Gong, Y. Y. Chu, A. M. Zheng, J. B. Wang, W. N. Zhang, X. Q. Wu, F. Deng, Z. M. Liu, *J. Catal.*, **2016**, 335, 47–57.
82. J. Klinowski, J. M. Thomas, C. A. Fyfe, G. C. Gobbi, *Nature*, **1982**, 296, 533–536.

83. A. Aitani, T. Yoshikawa, T. Ino, *Catal. Today*, **2000**, *60*, 111–117.
84. A. R. Teixeira, Qi X, C. C. Chang, W. Fan, W. C. Conner, P. J. Dauenhauer, *J. Phy. Chem. C*, **2015**, *118*, 22166–22180.
85. S. Brandani, *Chem. Eng. Tech.*, **2016**, *39*, 1194–1198.
86. R. Baur, R. Krishna, *Catal. Today*, **2005**, *105*, 173–179.
87. A. Feng, Y. Yu, L. Mi, Y. Cao, Y. Yu, L. Song, *Microporous Mesoporous Mater.*, **2019**, *280*, 211–218.
88. H. J. Cho, N. S. Gould, V. Vattipalli, S. Sabnis, W. Chaikittisilp, T. Okubo, W. Fan, *Microporous Mesoporous Mater.*, **2019**, *278*, 387–396.
89. J. C. Groen, J. A. Moulijn, J. Pérez-Ramírez, *J. Mater. Chem.*, 2006, *16*, 2121–2131.
90. M. Gackowski, K. Tarach, J. Podobiński, S. Jarczewski, P. Kuśtrowski, J. Datka, *Microporous Mesoporous Mater.*, **2018**, *263*, 282–288.
91. M. H. Ahmed, O. Muraza, A. K. Jamil, E. N. Shafei, Z. H. Yamani, K. H. Choi, *Energy Fuels*, **2017**, *31*, 5482–5490.
92. V. Paixão, A. P. Carvalho, J. Rocha, A. Fernandes, A. Martins, 2010 *Microporous Mesoporous Mater.*, **2010**, *131*, 350–357.
93. J. C. Groen, L. A. Peffer, J. A. Moulijn, J. Pérez-Ramírez, *Microporous Mesoporous Mater.*, **2004**, *69*, 29–34.
94. L. Sommer, D. Mores, S. Svelle, M. Stöcker, B. M. Weckhuysen, U. Olsbye, *Microporous Mesoporous Mater.*, **2010**, *132*, 384–394.
95. P. Matias, C. S. Couto, I. Graça, J. M. Lopes, A. P. Carvalho, F. R. Ribeiro, M. Guisnet, *App. Catal. A: Gen.*, **2011**, *399*(1-2), 100–109.
96. N. P. Tangale, S. K. Sonar, P. S. Niphadkar, P. N. Joshi, *J. Ind. Eng. Chem.*, **2016**, *40*, 128–136.
97. S. Yang, C. Yu, S. Huang, *Angew. Chem. Int. Ed.*, **2017**, *56*, 12553–12556.
98. Z. Zhao, W. Zhang, P. Ren, X. Han, U. Müller, B. Yilmaz, X. Bao, *Chem. Mater.*, **2013**, *25*(6), 840–847.
99. J. Grzybek, W. J. Roth, B. Gil, A. Korzeniowska, M. Mazur, J. Čejka, R. E. Morris, *J. Mater. Chem. A*, **2019**, *7*(13), 7701–7709.
100. V. N. Shetti, J. Kim, R. Srivastava, M. Choi, R. Ryoo, *J. Cat.*, **2008**, *254*(2), 296–303.
101. G. Rioland, S. Albrecht, L. Josien, L. Vidal, T. J. Daou, *New J. Chem.*, **2015**, *39*, 2675–2681.
102. T. Tago, D. Aoki, K. wakai, T. Masuda, *Top. Catal.*, **2009**, *52*, 865–871.
103. Y. Liu, M. Li, Z. Chen, Y. Cui, J. Lu, Y. Liu, *Angew. Chem. Int. Ed.*, **2021**, *60*, 7659–7663.
104. N. L. Michels, S. Mitchell, J. Pérez-Ramírez, *ACS Catal.*, **2014**, *4*, 2409–2417.
105. H. Tao, H. Yang, Y. Zhang, J. Ren, X. Liu, Y. Wang, G. Lu, *J. Mater. Chem. A*, **2013**, *1*, 13821–13827.
106. J. O. Abildstrøm, Z. N. Ali, U. V. Mentzel, J. Mielby, S. Kegsnæs, M. Kegsnæs, *New J. Chem.*, **2016**, *40*(5), 4223–4227.

107. X. Wei, P. G. Smirniotis, *Microporous Mesoporous Mater.*, **2005**, *89*, 170–178.
108. R. Wang, W. Liu, S. Ding, Z. Zhang, J. Li, S. Qiu, *Chem. Commun.*, **2010**, *46*(39), 7418–7420.
109. X. Meng, F. Nawaz, F. S. Xiao, *Nano Today*, **2009**, *4*(4), 292–301.
110. F. Z. Zhang, M. Fuji, M. Takahashi, *Chem. Mater.*, **2005**, *17*(5), 1167–1173.
111. D. P. Serrano, J. Aguado, J. M. Rodriguez, A. Peral, *J. Mater. Chem.*, **2008**, *18*(35), 4210–4218.
112. V. P. Caldeira, A. Peral, M. Linares, A. S. Araujo, R. A. Garcia-Muñoz, D. P. Serrano, *App. Catal. A: Gen.*, **2017**, *531*, 187–196.
113. H. Wang, T. J. Pinnavaia, *Angew. Chem. Int. Ed.*, **2006**, *45*, 7765–7768.
114. A. Inayat, I. Knoke, E. Spiecker, W. Schwieger, *Angew. Chem., Int. Ed.*, **2012**, *51*, 1962–1965.
115. C. H. L. Tempelman, M. T. Portilla, M. E. Martínez-Armero, B. Mezari, N. G. R. De Caluwé, C. Martínez, E. J. M. Hensen, *Microporous Mesoporous Mater.*, **2016**, *220*, 28–38.
116. K. Cho, H. S. Cho, L. C. De Ménorval, R. Ryoo, *Chem. Mater.*, **2009**, *21*, 5664–5673.
117. X. F. Li, R. Prins, J. A. van Bokhoven, *J. Catal.*, **2009**, *262*, 257–265.
118. M. Choi, H. Cho, R. Srivastava, *Nature Mater.*, **2006**, *5*, 718–723.
119. J. Lin, T. Yang, C. Lin, J. Sun, *Catal. Commun.*, **2018**, *115*, 82–86.
120. T. Yutthalekha, C. Wattanakit, C. Warakulwit, W. Wannapakdee, K. Rodponthukwaji, T. Witoon, J. Limtrakul, *J. Clean. Prod.* **2017**, *142*, 1244–1251.
121. N. Zhu, Y. Wang, D. Cheng, F. Chen, X. Zhan, *App. Catal. A: Gen.*, **2009**, *362*, 26–33.
122. H. X. Vu, M. Schneider, U. Bentrup, *Ind. Eng. Chem. Res.*, **2015**, *54*, 1773–1782.
123. J. Kim, M. Choi, R. Ryoo, *J. Catal.*, **2010**, *269*, 219–228.

## ***Chapter Two***

# **The Synthesis of YNU-5 Zeolite and Its Application to the Catalysis in the Dimethyl Ether-to-Olefin Reaction**

*During prior investigations of the synthesis of the novel zeolite YNU-5 (YFI), it was found that a very slight amount of an impurity phase contaminated the desired zeolitic phase. This impurity was very often ZSM-5 (MFI). The phase composition was determined to be sensitive to the water in the synthesis mixture, and it was possible to obtain a pure phase and also to intentionally generate a specific impurity phase. In the present work, trials based on the dimethyl ether-to-olefin (DTO) reaction using a fixed-bed downflow reactor were performed to assess the effect of the purity of YNU-5 on its catalytic performance. Dealuminated pure YNU-5 exhibited rapid deactivation due to coking at time on stream (TOS) values exceeding 5 min. Surprisingly, this deactivation was greatly suppressed when the material contained a trace amount of ZSM-5 consisting of nano-sized particles. The formation of ZSM-5 nanoparticles evidently improved the performance of the catalytic system during the DTO reaction. The product distributions obtained from this reaction using highly dealuminated and very pure YNU-5 resembled those generated by 12-ring rather than 8-ring zeolite catalysts. The high selectivity for desirable C3 and C4 olefins during the DTO reaction over YNU-5 is beneficial.*

**Keywords:** zeolite; YNU-5; solid acid catalyst; DTO reaction

## **2.1 Introduction**

Zeolites are crystalline aluminosilicates that possess an exceptional combination of properties, including high thermal stability, Brønsted acidity, and microporosity, due to their well-defined channel systems.<sup>1,2</sup> These materials have been used in a diverse range of applications, including as ion exchangers, adsorbents, and catalysts for many refining and petrochemical processes.<sup>3-6</sup> Even though there are a variety of chemical compositions in zeolite-like materials, aluminosilicates are the most typical. Zeolites possessing a high Si/Al ratio and a three-dimensional (3D) channel system including

large pore (that is, 12-ring) channels are of particular interest, since they combine high thermal and hydrothermal stability with superior resistance to pore blockage.<sup>7,8</sup> Some examples of high-silica, large-pore microporous aluminosilicates that are especially promising on the basis of the above criteria are beta (**\*BEA**),<sup>8–13</sup> MCM-68 (**MSE**), and related **MSE**-type materials. Another interesting example is CIT-1 (**CON**), which has a 12-12-10-ring pore system. This material was first synthesized as a borosilicate,<sup>14</sup> after which the Al-containing borosilicate **CON** ([Al,B]-**CON**) was successfully crystallized.<sup>15</sup> Al-containing **CON**-type zeolites have exhibited excellent catalytic performance in the methanol-to-olefin (MTO) reaction because of their unique structures and their ability to promote the ready accessibility and diffusion of reactants.<sup>15–17</sup>

Some small-pore (that is, 8-ring) zeolite frameworks such as **CHA** (having an 8-8-8-ring system) can also be applied to the MTO reaction, and **CHA** can also be used as a catalyst for the NH<sub>3</sub>-selective catalytic reduction (SCR) reaction. Very recently, our own group has found that the **AFX** framework (having an 8-8-8-ring structure) is an even more interesting catalyst for the NH<sub>3</sub>-SCR process.<sup>18</sup> In addition, it should be noted that mordenite (**MOR**) has 12-ring straight channels with intersecting 8-ring pores, and is one of the most industrially useful zeolite catalysts. It is thus expected that combinations of 12-ring and 8-ring pores will provide useful materials.

Our group has successfully synthesized the new aluminosilicate zeolite YNU-5 having a 12-12-8-ring pore system together with an independent 8-ring system, using dimethyl- dipropylammonium (Me<sub>2</sub>Pr<sub>2</sub>N<sup>+</sup>) as the organic structure-directing agent (OSDA).<sup>19</sup> This material was given the framework type code **YFI** by the International Zeolite Association (IZA).<sup>20</sup> After the synthesis and structural determination of this substance, it was characterized with regard to potential catalytic applications in three respects: (1) by obtaining information regarding critical factors that affect the successful crystallization of YNU-5, (2) by establishing framework stabilization when preparing a high-silica YNU-5 catalyst, and (3) by assessing the relationship between phase purity (that is, the presence of very small amounts of an impurity phase) and catalytic performance.

Regarding issue (2), our work demonstrated that YNU-5 only crystallizes at a Si/Al ratio of approximately 9 in the product. Although dealumination was possible using a liquid phase post-synthetic treatment with nitric acid, the framework stability of this material was determined to be sensitive to the dealumination conditions. Specifically, a reflux temperature (oil-bath temperature 130 °C rather than 80 °C) promoted framework stability by allowing the migration of Si to fill site defects generated by the removal of framework Al.<sup>21</sup> This simple technique for stabilizing the framework is very valuable because it guarantees the thermal and hydrothermal stability of the catalyst

during use and/or regeneration. A remaining challenge that corresponds to issue (1) is that the synthesis window is very narrow, and in most cases, a very slight amount of an impurity phase contaminates the desired YNU-5 product. In our previous work,<sup>21</sup> several competing phases, such as MCM-68 (**MSE**), ZSM-5 (**MFI**), and beta (**\*BEA**), were observed following slight changes in the gel composition (especially the amount of water) during synthesis. Even after optimization of the synthesis conditions, trace amounts of **MFI** or **MOR** were frequently still observed as an impurity.

To address issue (3), I focused on the catalytic performance of YNU-5 with regard to the dimethyl ether (DME)-to-olefin (DTO) reaction. This reaction, together with the MTO reaction, is important as an alternative to the thermal cracking of ethane (supplied from nonpetroleum fossil-based resources such as natural gas or shale gas) because thermal cracking alone cannot satisfy the demand for propylene. In addition, butenes and higher molecular weight olefins are currently more in demand than ethylene. During these acid-catalyzed reactions, I found that even trace amounts of impurities in the YNU-5 catalyst greatly affected the catalytic performance, which was unexpected because this effect is not often observed. Therefore, in order to employ this material in catalytic applications, it is essential to establish how these impurities affect the performance of YNU-5.

We report here additional systematic investigations of the optimal synthetic conditions (specifically, gel composition, crystallization state, and time span) and of the effect of small concentrations of **MFI** impurities on the catalytic performance of YNU-5 during the DTO reaction.

## 2.2 Experimental

### 2.2.1. Measurements

Powder X-ray diffraction (XRD; Ultima-IV, Rigaku, Akishima, Tokyo, Japan) data were collected using Cu K $\alpha$  radiation and operating at 40 kV and 20 mA to examine the crystallinity and phase purity of the zeolite catalysts. The Si/Al molar ratios in the bulk materials were determined by inductively coupled plasma—atomic emission spectrometry (ICP-AES; ICPE-9000, Shimadzu Ltd., Kyoto, Japan). In preparation for these analyses, a catalyst sample (20 mg) was suspended in Milli-Q (Merck KGaA, Darmstadt, Germany) water (5 g) within a Teflon beaker followed by the addition of 47% HF (120 mg) at room temperature, ultrasonication for 2 min to provide dissolution, and dilution with Milli-Q water (90 g). The crystal sizes and morphologies of the zeolite catalysts were observed by means of field emission scanning electron microscopy (FE-SEM; JSM-7001F, JEOL Ltd., Akishima, Tokyo, Japan). Solid-state magic angle

spinning nuclear magnetic resonance (MAS NMR) data were collected using a spectrometer (AVANCEIII 600, Bruker Co., Billerica, Massachusetts, USA) operated at 600 MHz for  $^1\text{H}$  analyses and 119.2 MHz for  $^{29}\text{Si}$  analyses. All MAS NMR spectra were recorded at room temperature with a 4 mm diameter  $\text{ZrO}_2$  tube. The  $^{29}\text{Si}$  chemical shifts were determined based on that of hexamethylcyclotrisiloxane at  $-9.66$  ppm. Dipolar-decoupling (DD) MAS NMR data were acquired using 1024 pulses with a recycle time of 30 s at a spinning rate of 10 kHz. The coke contents of the spent catalysts were determined by thermogravimetric/differential thermal analysis (TG-DTA) on a Thermo plus EVO II TG8120 (Rigaku). The temperature was raised from room temperature to  $800^\circ\text{C}$  with the rate of  $10^\circ\text{C}\cdot\text{min}^{-1}$  under air flow ( $30\text{ cm}^3\cdot\text{min}^{-1}$ ). The weight loss observed from 300 to  $700^\circ\text{C}$  was ascribed to coke.

### 2.2.2. Typical YNU-5 Synthesis Procedure

The YNU-5 zeolite was typically synthesized as follows.<sup>19,21</sup> Initially, an aqueous  $\text{Me}_2\text{Pr}_2\text{N}^+\text{OH}^-$  solution ( $2.847\text{ mmol}\cdot\text{g}^{-1}$ , 11.94 g, 34.0 mmol), aqueous NaOH solution ( $9.048\text{ mmol}\cdot\text{g}^{-1}$ , 3.32 g, 30.0 mmol), aqueous KOH solution ( $6.075\text{ mmol}\cdot\text{g}^{-1}$ , 4.94 g, 30.0 mmol), colloidal silica (21.59 g; Ludox AS-40, DuPont de Nemours Inc., Wilmington, Delaware, USA, 40.2 wt%  $\text{SiO}_2$ , 8.68 g  $\text{SiO}_2$ , 144.4 mmol  $\text{SiO}_2$ ), and Milli-Q water (1.50 g) were combined in a 150 mL Teflon vessel. The vessel was tightly capped and the mixture stirred for 3 h on a hot plate while maintaining a temperature of approximately  $60^\circ\text{C}$ . This procedure was essential to obtaining a clear solution. After cooling to room temperature, a FAU-type zeolite (Tosoh Co., Tokyo, Japan, HSZ-350HUA, 5.03 g;  $\text{Si}/\text{Al} = 5.5$ ) was added and the resulting suspension was stirred for 10 min at room temperature. It should be noted that the synthesis results were found to be sensitive to the FAU-type zeolite manufacturer's lot that was employed, and so the starting gel composition had to be slightly tuned depending on the lot number. For a typical example in this work, the molar composition of the starting gel was  $0.265\text{SiO}_2$  (from FAU) –  $0.735\text{SiO}_2$  (from colloidal silica) –  $0.025\text{Al}_2\text{O}_3$  (from FAU) –  $0.17\text{Me}_2\text{Pr}_2\text{N}^+\text{OH}^-$  –  $0.15\text{NaOH}$  –  $0.15\text{KOH}$  –  $7.5\text{H}_2\text{O}$ . This mixture was transferred to a 125 mL Teflon-lined stainless-steel autoclave that was subsequently sealed and allowed to stand statically for 4 days in a convection oven at  $160^\circ\text{C}$ . After cooling the autoclave to room temperature, the resulting solid was separated by filtration, washed several times with de-ionized water, and dried overnight. The as-synthesized YNU-5 zeolite was obtained as a white powder (6.72 g) and was calcined at  $550^\circ\text{C}$  for 6 h to remove occluded organics to give the final product (6.31 g) as a white powder ( $\text{Si}/\text{Al} = 9.1$ ). In order to examine the effect of  $\text{H}_2\text{O}/\text{SiO}_2$  ratio (w) in the starting mixture on the YNU-5 synthesis, the amount of input water was varied as follows. Input amounts were 10.50, 8.70, 6.91, 5.11, 3.31, 1.50,  $-0.30$ , and  $-3.91$  g, where w values were 10.0, 9.5, 9.0, 8.5,



8.0, 7.5, 7.0, and 6.0, respectively. The negative values mean that the evaporation of excess water by stirring the mixture at approximately 60 °C on a hot plate.<sup>19,21</sup>

The four representative samples used in the present study were prepared by varying the rotation rate (x, in rpm) of autoclaves in the oven and crystallization period (y, in days). The “rotation” means rotating the autoclave to mix the contents well; this technique is often used for screening experiments because it is more convenient than the typical stirring system. The rotation rate is one of the important variables for zeolite synthesis.<sup>22,23</sup> The YNU-5 samples were synthesized under conditions for which the (x, y) values were (0, 4), (0, 7), (20, 4), and (20, 7), and are designated herein as YFI-A, YFI-B, YFI-C, and YFI-D, respectively. The typical procedure described above corresponds to the synthesis of YFI-A.

### ***2.2.3. Preparation of MFI-Type Zeolite Nanocrystals***

The typical procedure used to prepare nanocrystals of MFI was as follows. An aqueous solution of  $\text{Me}_2\text{Pr}_2\text{N}^+\text{OH}^-$  (Sachem Inc., Austin, Texas, USA, 2.691 mmol·g<sup>-1</sup>, 1.26 g, 3.4 mmol), NaOH (11.980 mmol·g<sup>-1</sup>, 0.26 g, 3.0 mmol) and KOH (7.914 mmol·g<sup>-1</sup>, 0.38 g, 3.0 mmol), and colloidal silica (2.65 g; Ludox AS-40, DuPont de Nemours Inc., 40.2 wt% SiO<sub>2</sub>, 1.07 g SiO<sub>2</sub>, 17.8 mmol SiO<sub>2</sub>) was transferred into a 23 mL Teflon cup, after which the mixture was stirred at 60 °C. During this process, 0.295 g of water evaporated from the mixture, after which dealuminated FAU-type zeolite (0.60 g; SiO<sub>2</sub>: 69.7 wt%, Al<sub>2</sub>O<sub>3</sub>: 6.8 wt%, H<sub>2</sub>O: 23.5 wt%, Si/Al = 8.7) was added to the clear solution and the resulting suspension stirred for 10 min. The final gel composition was 1.0SiO<sub>2</sub> – 0.016Al<sub>2</sub>O<sub>3</sub> – 0.136Me<sub>2</sub>Pr<sub>2</sub>N<sup>+</sup>OH<sup>-</sup> – 0.12NaOH – 0.12KOH – 5.6H<sub>2</sub>O. This mixture was added to a 23 mL Teflon-lined stainless steel autoclave that was maintained at 160 °C in a convection oven without rotation for 7 days. The precipitated solid was separated by centrifugation, washed several times with de-ionized water, and dried overnight at 80 °C. The as-synthesized MFI nanocrystals (0.46 g) were calcined at 550 °C for 6 h to remove occluded organics, giving a product (0.42 g, Si/Al = 20) designated herein as MFInano(20). For comparison purposes, micron-sized ZSM-5 crystals (Si/Al = 19.7), denoted as MFImicron(20), were obtained using a synthesis procedure previously reported in the literature.<sup>24</sup>

### ***2.2.4. Post-Synthesis Modification***

The calcined YNU-5 samples were converted to protonated dealuminated analogues using various acid treatments. Direct dealumination of the calcined YNU-5 (typically 1.0 g) was accomplished by refluxing with 0.1–13.4 mol·L<sup>-1</sup> HNO<sub>3</sub> solutions (60 mL (g-sample)<sup>-1</sup>) in a 200 mL round bottom flask at 130 °C in an oil bath for 24 h. These conditions also stabilized the framework of the material due to Si migration.<sup>19,21</sup>

The dealuminated versions of YFI-A, B, C, and D are referred to herein as deAl-YFI-A, B, C, and D(n), respectively, where n indicates the Si/Al ratio. In this work, as an example, deAl-YFI-A(51), deAl-YFI-B(57), deAl-YFI-C(55), and deAl-YFI-D(63) were prepared by treatment with a 2.0 mol·L<sup>-1</sup> HNO<sub>3</sub> solution, while deAl-YFI-C(287) was prepared with a 13.4 mol·L<sup>-1</sup> HNO<sub>3</sub> solution under reflux conditions.

In the case of physical mixtures of calcined YNU-5 and small amounts of MFInano(20) or MFImicron(20), the calcined materials were first mixed after which the mixture was treated with a HNO<sub>3</sub> solution as described above. These mixtures are designated as deAl-[YFI-C + 3 wt% MFInano(20)] and deAl-[YFI-C + 3 wt% MFImicron(20)], respectively.

### ***2.2.5. Procedure for the DTO Reaction***

Each catalyst was pelletized without a binder, roughly crushed, and then sieved to obtain 500–600 µm particles. These catalyst particles (typically 100 mg) were placed in a fixed-bed reactor (a down-flow quartz tube microreactor with a 9 mm internal diameter) situated in an electric furnace. Each sample was first pretreated at 550 °C for 1 h under an air flow at 40 cm<sup>3</sup> (N.T.P.) min<sup>-1</sup> and then maintained at 400 °C under a He flow at 40 cm<sup>3</sup> (N.T.P.) min<sup>-1</sup>, acting as a carrier gas. While maintaining the specimen at 400 °C, DME (at a partial pressure of 5.0 kPa) was introduced through the top of the reactor. The contact time, W/F (where W value is catalysts weight and F value is flow rate of DME), was 20 g-cat h mol<sup>-1</sup> in these trials but could be varied by changing the flow rate or catalyst amount if necessary. The reactants and products were analyzed by gas chromatography (GC 2014, Shimadzu) using a DB-5 capillary column (Agilent Technologies Inc., Santa Clara, California, USA; id 0.53 mm, length 30 m, 5.00 µm thick stationary phase) and an HP-PLOT/Q capillary column (Agilent Technologies; id 0.53 mm, length 30 m, 40.0 µm thick stationary phase) together with a flame ionization detector.

## **2.3. Results and Discussion**

### ***2.3.1. Synthetic Investigations of YNU-5***

In our previous paper, I reported a drastic effect of the H<sub>2</sub>O/SiO<sub>2</sub> molar ratio (w) in the starting gel on the resulting zeolitic phases. Specifically, relatively water-rich conditions promoted crystallization of a zeolitic phase with a higher framework density (FD<sub>Si</sub><sup>19</sup>), and it was speculated that a more concentrated gel solution enhanced the degree of interaction between the OSDA molecules and the silicate. Further and more detailed investigations of the effects of the H<sub>2</sub>O/SiO<sub>2</sub> molar ratio were performed in the present study.

Initially,  $w$  was varied from 10 to 6 in 0.5 intervals, and the results are shown in Figure 2.1. Over this entire range, the major phase was always YFI. However, below a value of 10, an MFI phase was clearly present as a contaminant. The level of this impurity decreased with decreases in the water content, such that pure YNU-5 was obtained at  $w = 7.5$ . As shown in Figure 2.1, there were no impurity phases other than MFI in the range of 10–7.5. When  $w$  was 7.0 or smaller, a MOR phase began to appear although the YFI phase was still almost pure at  $w = 7.0$ . This result is consistent with the hypothesis<sup>21</sup> that more water-rich conditions favor the formation of materials with higher  $FD_{Si}$  values. In fact, the  $FD_{Si}$  values of MOR and MFI are 17.0 and 18.4, respectively.<sup>19</sup>

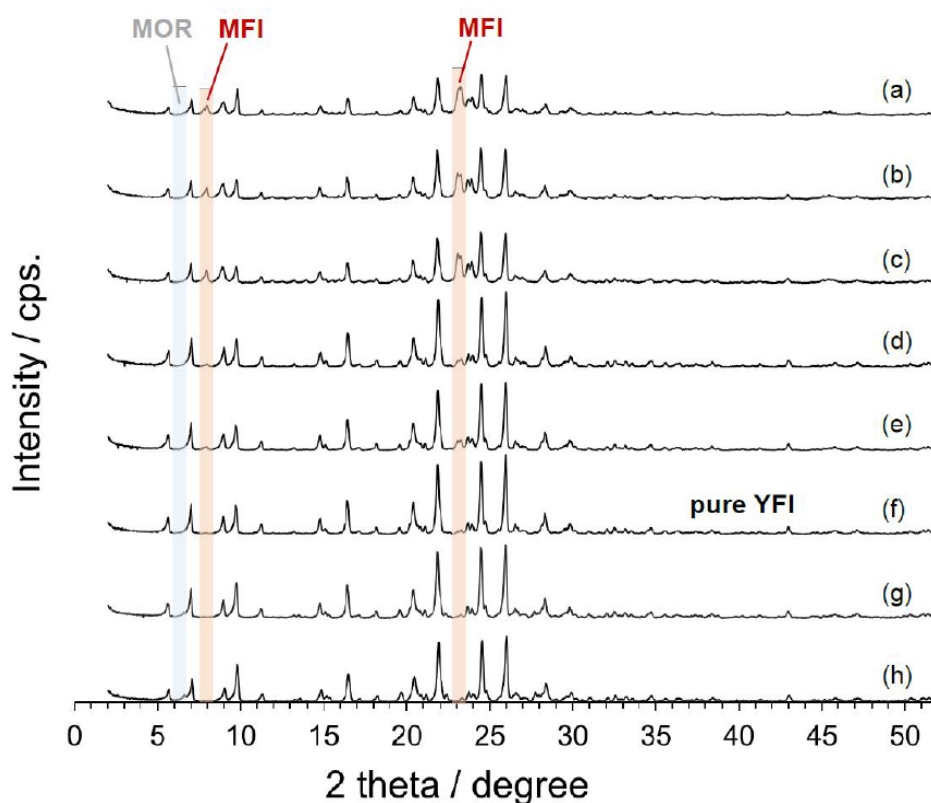


**Figure 2.1.** Powder X-ray diffraction patterns showing the effect of water content ( $w = \text{H}_2\text{O}/\text{SiO}_2$  molar ratio) in the starting gel on the phase-purity of the product of YNU-5 synthesis. The  $w$  values in this series were (a) 10, (b) 9.5, (c) 9, (d) 8.5, (e) 8, (f) 7.5, (g) 7, and (h) 6. The starting gel with molar composition  $0.265\text{SiO}_2$  (from FAU) –  $0.735\text{SiO}_2$  (from colloidal silica) –  $0.025\text{Al}_2\text{O}_3$  (from FAU) –  $0.17\text{Me}_2\text{Pr}_2\text{N}^+\text{OH}^-$  –  $0.15\text{NaOH}$  –  $0.15\text{KOH}$  –  $w\text{H}_2\text{O}$  was heated under static conditions at  $160^\circ\text{C}$  for 4 days. The FAU was HSZ-350HUA (Lot #35UA8301B).

The crystals of the contaminant phases were readily distinguished from the major YFI phase in the FE-SEM images (Figure 2.2). The MFI phase consisted of sub-micron or nano-sized pillar-like crystals (Figure 2.2b), whereas the MOR impurity comprised

micron-sized crystals (Figure 2.2c). The fact that a slight change in the water content in the starting gel promoted the formation of impurities suggests that the structure-directing ability of the OSDA,  $\text{Me}_2\text{Pr}_2\text{N}^+\text{OH}^-$ , was not very high.

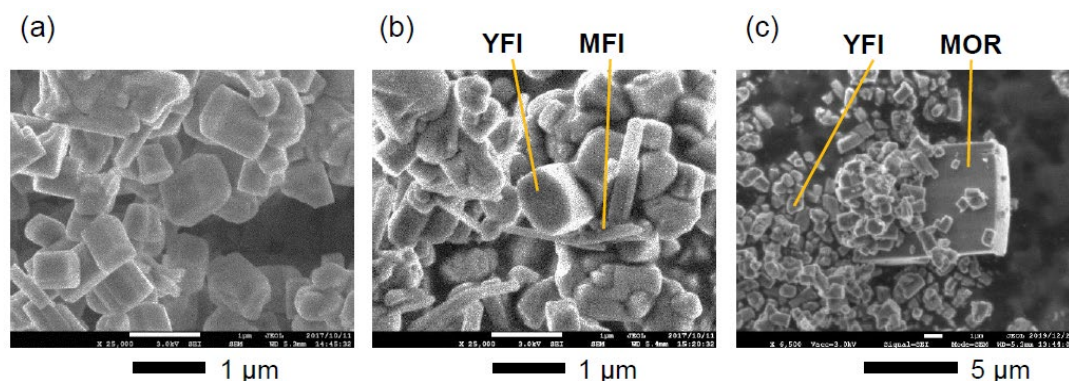


**Figure 2.2.** Field emission scanning electron microscopy (FESEM) images of the (a) pure YFI, (b) YFI with trace MFI, and (c) YFI with trace MOR.

The effect of the crystallization period on the YNU-5 product was also investigated, and the time-course of crystallization is presented in Figure 2.3. The composition of starting mixture and the synthesis conditions are shown in the caption. Figure 2.3a shows the powder XRD pattern of the FAU-type zeolite used as the starting material, while Figure 2.3b demonstrates that the YFI phase began to appear while the major phase was still FAU after 1 day. The FAU phase completely disappeared and a pure YFI phase was observed after 2 days. After 4 days, peaks assignable to an MFI phase appeared and the intensity of these peaks gradually increased upon prolonged heating. In the early stage of the synthesis, it appears that the FAU transformed to YFI; however, it is more likely that the FAU initially dissolved and that some fragments were responsible for the crystallization of YFI, based on other examples of hydrothermal conversion such as from FAU to MSE,<sup>25</sup> \*BEA to AFI,<sup>26,27</sup> and \*BEA to \*STO.<sup>28</sup> During the investigation on the time-course of crystallization in this work (see Figure 2.3), the same high level of solids recovery was consistently obtained after 2 days. Even after 1 day, a significant decrease in solid recovery was not observed, indicating that the crystallization rate of the YFI was much greater than the dissolution rate of FAU. The co-crystallized MFI that appeared after 4 days may not have been transformed from YFI but rather was generated as a result of independent nucleation from the mother gel. The FE-SEM image in Figure 2.2b is consistent with this hypothesis because it shows that crystals of YFI and MFI existed independently. Crystallization for a span of 2–3 days appears to have given the highest degree of phase purity. However, in the present work, I tuned the synthesis conditions so as to require crystallization times in the range of 4–7 days, and found interesting results with regard to the catalytic performance of the materials.

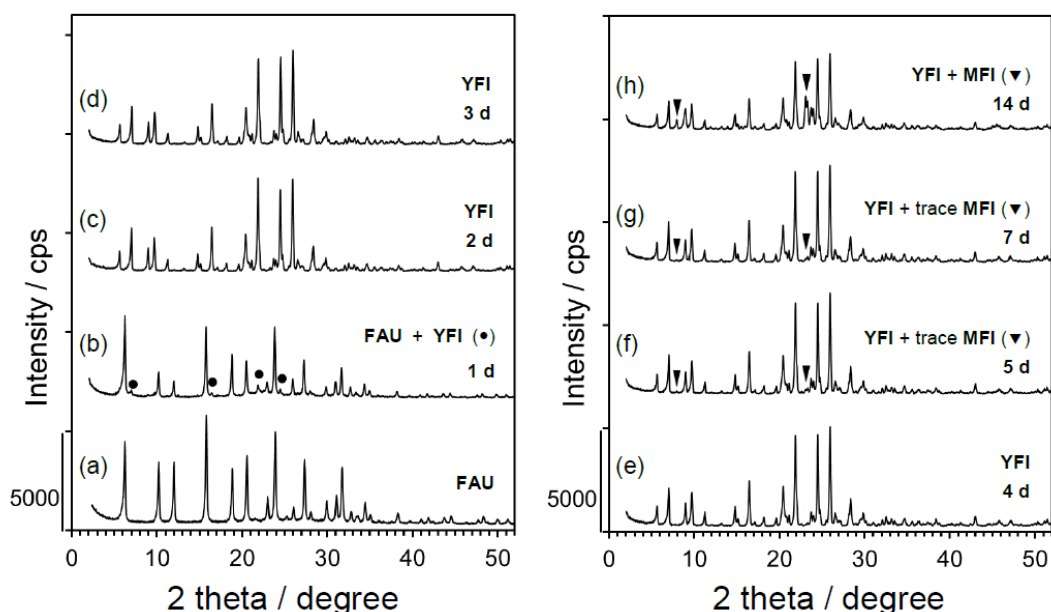


**Figure 2.3.** Phase changes over time as reflected in the powder X-ray diffraction patterns of (a) the starting material (FAU) and (b–h) as-synthesized samples crystallized under static conditions at 160 °C. The starting molar composition was  $0.265\text{SiO}_2$  (from FAU) –  $0.735\text{SiO}_2$  (from colloidal silica) –  $0.025\text{Al}_2\text{O}_3$  (from FAU) –  $0.17\text{Me}_2\text{Pr}_2\text{N}^+\text{OH}^-$  –  $0.15\text{NaOH}$  –  $0.15\text{KOH}$  –  $7.0\text{H}_2\text{O}$ . The FAU was HSZ-350HUA (Lot #35UA3Y02).

Rotation of the synthesis vessel during the synthesis (see Section 2.2) is sometimes a key factor affecting the final products. As an example, topological changes from MFI to TON-type zeolites when using *n*-butylamine and 1,6-diaminohexane as the OSDAs were observed upon going from static to rotating conditions in a prior work.<sup>22</sup> Thus, to further examine the relationship between synthesis conditions and the formation of second phases, the effects of rotation and the crystallization period were also investigated in the present research. In these trials, the rotation rate (*x*, in rpm) and crystallization period (*y*, in days) were varied such that the (*x*, *y*) pairs were (0, 4), (0, 7), (20, 4), and (20, 7), while keeping the other parameters constant. The resulting samples are denoted herein as YFI-A, YFI-B, YFI-C, and YFI-D, respectively, and the results are summarized in Figure 2.4.

These data demonstrate that the appearance of trace amounts of MFI as an impurity was more effectively suppressed when *x* was larger and *y* was smaller. The best results were obtained at (*x*, *y*) = (20, 4), such that the corresponding YFI-C sample comprised a pure YFI phase (Figure 2.4c). In addition, regardless of the rotation rate, longer crystallization times increased the probability of forming the MFI impurity, although the amounts of this phase remained almost negligible.

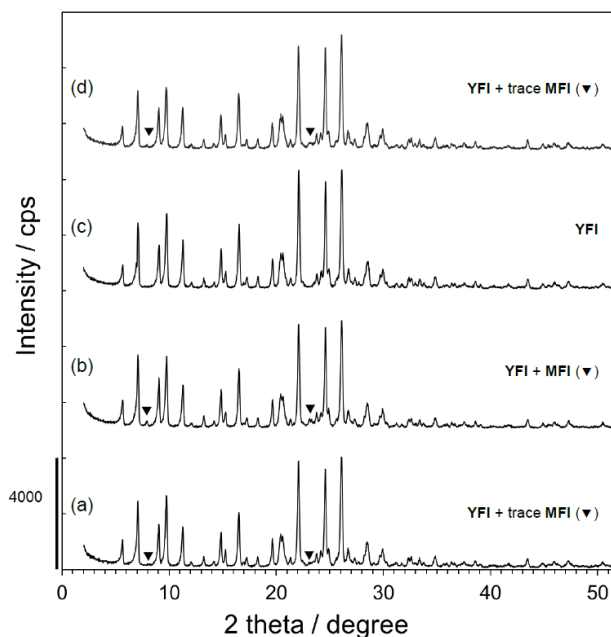


**Figure 2.4.** Powder X-ray diffraction patterns for calcined forms of (a) YFI-A, (b) YFI-B, (c) YFI-C, and (d) YFI-D crystallized while varying the rotation rate ( $x$ , rpm) and crystallization period ( $y$ , days), with ( $x$ ,  $y$ ) values of (a) (0, 4), (b) (0, 7), (c) (20, 4), and (d) (20, 7). The nomenclature for these samples is explained in Section 2.2. The starting molar composition was  $0.265\text{SiO}_2$  (from FAU) –  $0.735\text{SiO}_2$  (from colloidal silica) –  $0.025\text{Al}_2\text{O}_3$  (from FAU) –  $0.17\text{Me}_2\text{Pr}_2\text{N}^+\text{OH}^-$  –  $0.15\text{NaOH}$  –  $0.15\text{KOH}$  –  $7.0\text{H}_2\text{O}$ . The FAU was HSZ-350HUA (Lot #35UA3Y02).

### 2.3.2. Effects of a Trace of MFI on the Physicochemical Properties of YFI Samples

The effects of trace amounts of MFI, the most frequent contaminant, on some physicochemical properties of bulk YNU-5 samples were investigated, employing the YFI-A–D that are discussed in the previous section and shown in Figure 2.4. Since the original material was composed of a very pure YFI phase, it was possible to establish the effects of contaminants by comparing this specimen with three other samples: YFI-A, B, and D. The trace amount of MFI did not affect the bulk chemical composition of the material as revealed by ICP analysis (Table 2.1).

**Table 2.1.** Elemental analysis and related data of YFI samples.

sample <sup>a</sup>	Si <sup>b</sup> /mmol g <sup>-1</sup>	Al <sup>b</sup> /mmol g <sup>-1</sup>	Na <sup>b</sup> /mmol g <sup>-1</sup>	K <sup>b</sup> /mmol g <sup>-1</sup>	Si/Al <sup>c</sup>	Si/Al <sup>d</sup>
YFI-A	14.87	1.537	0.211	0.864	9.7	13.5
YFI-B	14.01	1.468	0.160	0.761	9.5	14.1
YFI-C	14.44	1.564	0.116	0.784	9.2	15.0
YFI-D	14.43	1.442	0.176	0.799	10.0	14.1

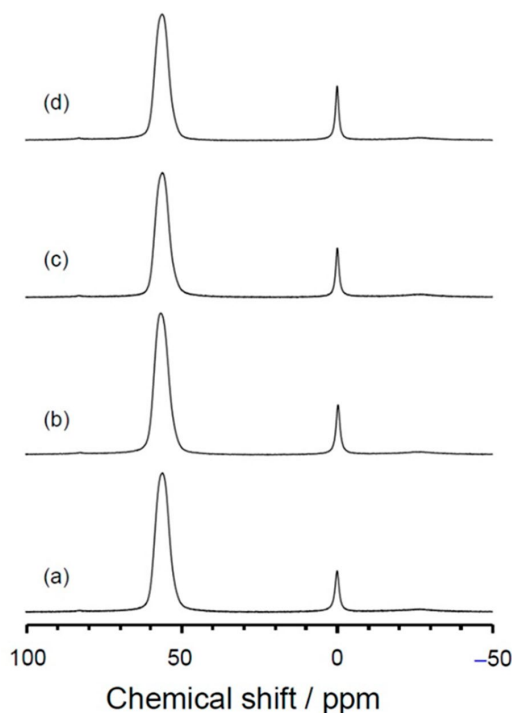
a. The nomenclature for the samples is explained in the Section 2.2.2.

b. Amounts in the bulk materials were determined by means of inductively coupled plasma-atomic emission spectrometry (ICP-AES).

c. The Si/Al molar ratios in the bulk materials based on ICP analyses.

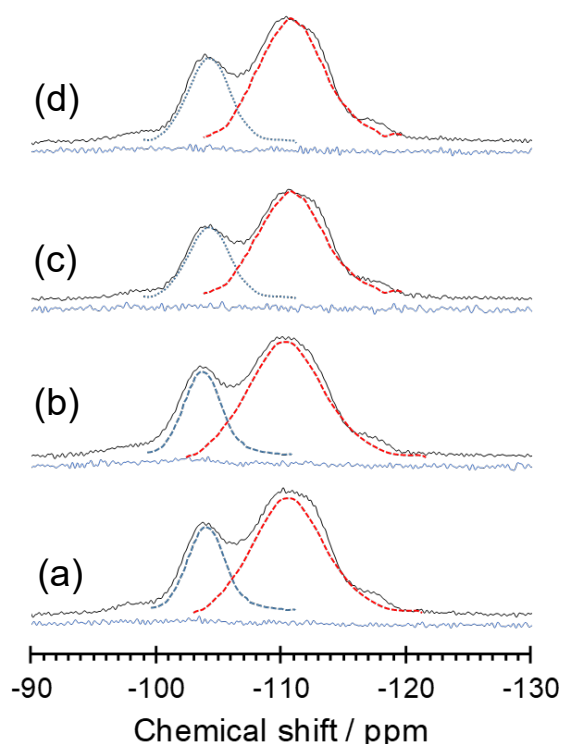
d. The Si/Al molar ratios in the framework based on <sup>29</sup>Si magic angle spinning nuclear magnetic resonance (<sup>29</sup>Si MAS NMR) spectra as shown in Figure 2.6.

Figure 2.5 presents the <sup>27</sup>Al MAS NMR spectra of the YNU-5 samples (YFI-A–YFI-D) acquired immediately after removing the OSDA by calcination at 550 °C for 6 h. All these spectra are similar and the major peaks in the range of 50–60 ppm are assignable to tetrahedral aluminum, indicating that the majority of the aluminum atoms were incorporated into the framework.

**Figure 2.5.** <sup>27</sup>Al magic angle spinning nuclear magnetic resonance (<sup>27</sup>Al MAS NMR) spectra obtained from the calcined (a) YFI-A, (b) YFI-B, (c) YFI-C, and (d) YFI-D.

The nomenclature for these samples is explained in the Section 2.2.2.

The minor peak at approximately 0 ppm is ascribed to octahedral Al, which tends to appear in calcined samples and was not observed in the as-synthesized YNU-5 samples. Figure 2.6 provides the  $^{29}\text{Si}$  MAS NMR spectra of the calcined YNU-5 samples. The spectra for samples A, B, and D (Figure 2.6a,b,d, respectively) are seen to be similar to that produced by the pure calcined YNU-5 sample YFI-C (Figure 2.6c). It is interesting to note that the framework Si/Al ratios estimated from the  $^{29}\text{Si}$  MAS NMR spectra are slightly higher than the bulk Si/Al ratios determined by ICP analysis (Table 2.1), which is consistent with the  $^{27}\text{Al}$  MAS NMR results. At this stage, no obvious differences were observed among samples A–D.



**Figure 2.6.**  $^{29}\text{Si}$  MAS NMR spectra obtained from the calcined (a) YFI-A, (b) YFI-B, (c) YFI-C, and (d) YFI-D.

The blue lines are  $^{29}\text{Si}$  CPMAS NMR spectra.

The nomenclature for these samples is explained in the Section 2.2.2.

To assess the application of these materials as solid acid catalysts, samples A–D (in calcined form) were dealuminated with  $2\text{ mol}\cdot\text{L}^{-1}\text{ HNO}_3$  in a  $130\text{ }^\circ\text{C}$  oil bath for 24 h.<sup>20</sup> It was confirmed by XRD that the samples maintained a high degree of crystallinity after dealumination (see Figure 2.7). Figure 2.8 shows the ammonia temperature-programmed desorption ( $\text{NH}_3$ -TPD) profiles for these same samples along with the acid amounts (that is, the number of acid sites) estimated from the so-called h-peak for each material.<sup>29,30</sup>



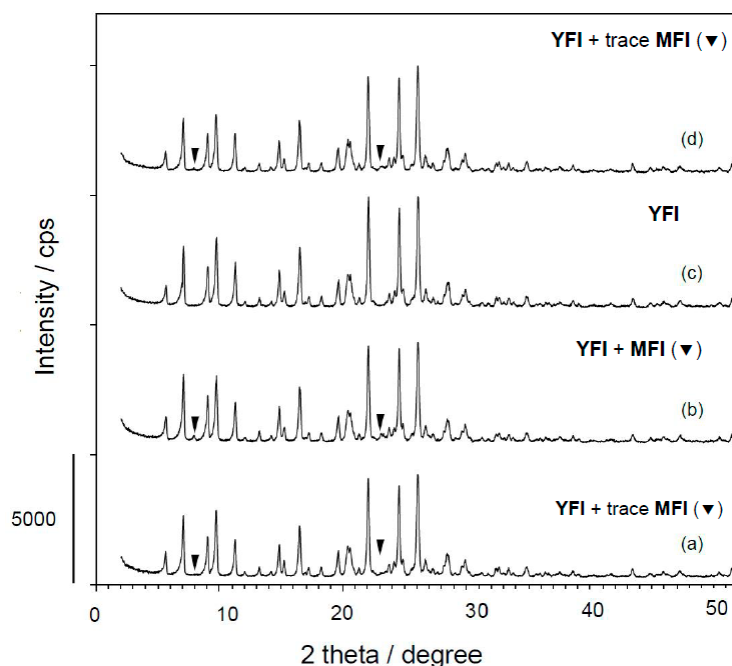


**Figure 2.7.** Powder X-ray diffraction patterns obtained from the (a) deAl-YFI-A(51), (b) deAl-YFI-B(57), (c) deAl-YFI-C(55), and (d) deAl-YFI-D(63).

The nomenclature for these samples is explained in the Section 2.2.4.

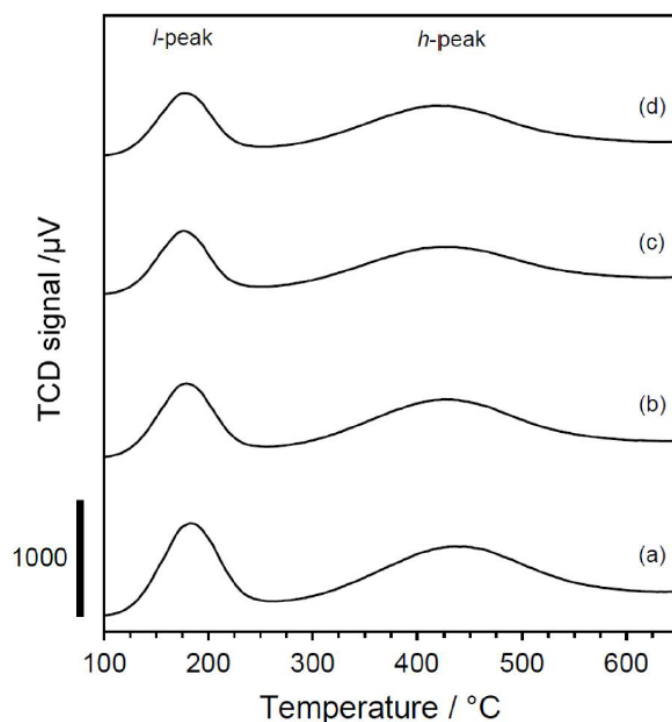


**Figure 2.8.** The  $\text{NH}_3$ -temperature programmed desorption profiles for the (a) deAl-YFI-A(51), (b) deAl-YFI-B(57), (c) deAl-YFI-C(55), and (d) deAl-YFI-D(63). The acid concentrations determined from the  $h$  peaks are (a) 0.258, (b) 0.290, (c) 0.224, and 0.249  $\text{mmol}\cdot\text{g}^{-1}$ , respectively. The Al levels determined by ICP analysis are (a) 0.325, (b) 0.319, (c) 0.267, and 0.301  $\text{mmol}\cdot\text{g}^{-1}$ , respectively. As explained in Section 2.4, the dealuminated versions of YFI-A, B, C, and D are referred to herein as deAl-YFI-A, B, C, and D( $n$ ), respectively, where  $n$  indicates the Si/Al ratio.

The discrepancy between the Al content ( $0.224 \text{ mmol-Al g}^{-1}$ ) determined by ICP analysis (see Figure 2.8 caption) and the number of acid sites ( $0.249 \text{ mmol}\cdot\text{g}^{-1}$ ) estimated by  $\text{NH}_3$ -TPD for the pure YFI (YFI-C) was not unexpected and was in good agreement with the results of our previous studies concerning other zeolites.<sup>31</sup> Underestimation of acid amounts by  $\text{NH}_3$ -TPD compared to the Al content determined by ICP analysis is very common and there are some possible reasons for this. These include the existence of non-acidic extra-framework Al atoms,<sup>32</sup> inaccessible tetrahedral Al sites in the framework, and residual  $\text{K}^+$  at  $[\text{Si-O-Al}]^-$  sites in the framework. These effects are typical in the case of the parent samples before dealumination; however, the number of acid sites in each dealuminated YFI sample was closer to the bulk Al content, together with a K/Al molar ratio of less than 0.01. At the dealuminated stage, the  $\text{NH}_3$ -TPD profiles are very similar between the YFI-A–D specimens, regardless of the effects discussed immediately above.

Overall, the similarities in the Si/Al ratios, framework characteristics, and even acid properties indicate that the presence of trace amounts of impurities had no obvious effects on the physicochemical properties of the YNU-5 in the case that the extent of contamination was as low as in these specimens.

### **2.3.3. DTO Reaction over the YFI Catalyst**

#### *2.3.3.1. Effect of MFI as a Trace Contaminant*

The conversion of DME is an attractive alternative approach to the sustainable production of olefins and could replace the classical routes based on the thermal cracking of ethane.<sup>33</sup> DME is commonly obtained from the dehydration of methanol acquired from non-fossil resources such as natural gas, coal, biomass, or waste gasification/reforming.<sup>34</sup> Due to its low cost and high hydrocarbon selectivity, the DTO reaction has become increasingly attractive in recent years.<sup>35,36</sup> The present work focused on performing this reaction catalyzed by zeolite-based solid acid materials with the expectation of obtaining high selectivity for propylene and butenes.<sup>31</sup> In the previous section, I reported almost no effect of trace contamination on the physicochemical properties of these catalysts. In contrast, small amounts of impurities had profound effects on the DTO reaction when using deAl-YFI-C(55) (that is, a pure YFI phase) and deAl-YFI-B(57) (YFI containing approximately 3 wt% of an MFI phase).

Figure 2.9a,b shows the conversions as well as product distributions over deAl-YFI-C(55) and deAl-YFI-B(57), respectively. The conversions were high after a short TOS (5 min) over both catalysts. However, in the case of the deAl-YFI-C(55), a rapid decrease in conversion was observed as the TOS increased. In fact, conversion

decreased to <40% at a TOS of 65 min. This result demonstrates that the pure YNU-5 catalyst deactivated rapidly during the DTO reaction. After the removal of acid sites on the external surfaces and pore mouths (preferentially the 12-ring pores) by the acid treatment, the remaining acid sites on the pore mouths of isolated 8-rings may have directly promoted coke formation.<sup>21</sup> The detailed location of the remaining acid site after deep dealumination will be investigated in future work. The most surprising finding was that this phenomenon changed when deAl-YFI-B(57) was used as the catalyst, such that the deactivation of the YNU-5 was greatly suppressed, and the conversion remained high even at a TOS of 305 min. The thermogravimetric analysis of the spent catalysts indicated there was no significant difference in the amount of coke deposition between deAl-YFI-C(55) and deAl-YFI-B(57) in Figure 2.9. This suggests that the long-lived active sites in deAl-YFI-B(57) are not influenced by currently observed coke formation even though some different active sites are deactivated.

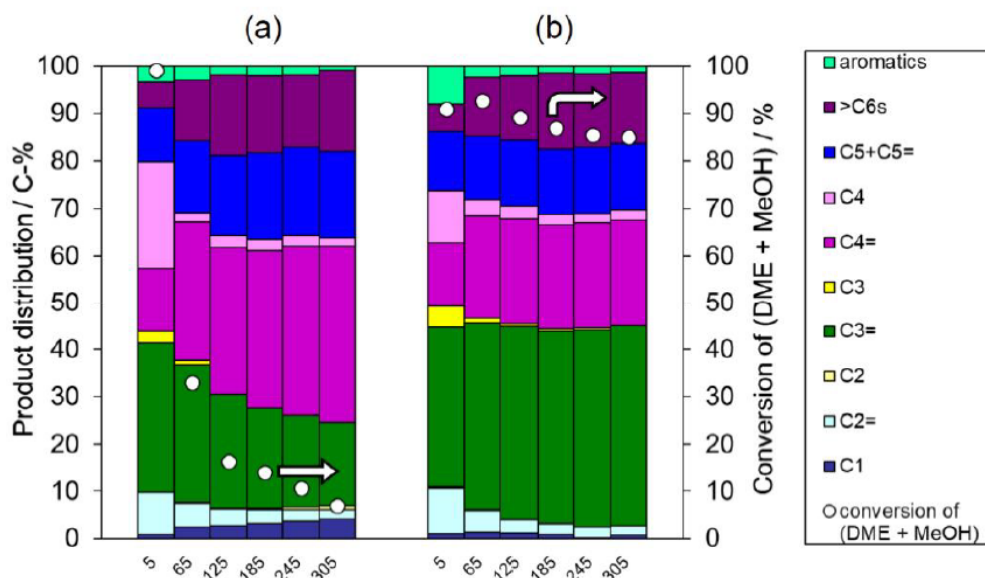


**Figure 2.9.** Results from the dimethyl ether (DME)-to-olefin (DTO) reaction over the (a) deAl-YFI-C(55) and (b) deAl-YFI-B(57). Pretreatment conditions: 550 °C, 1 h under an air flow of 40 cm<sup>3</sup>(N.T.P.) min<sup>-1</sup>. Reaction conditions: catalyst weight, 100 mg;  $W/F = 20$  g-cat h mol<sup>-1</sup>; pellet size, 500–600 μm; He flow rate, 40 cm<sup>3</sup>·(N.T.P.)·min<sup>-1</sup>; temperature, 400 °C. As explained in Section 2.4, the dealuminated versions of YFI-A, B, C, and D are referred to herein as deAl-YFI-A, B, C, and D(*n*), respectively, where *n* indicates the Si/Al ratio. Coke amounts in the spent catalysts estimated by thermogravimetric analyses were (a) 91 and (b) 105 mg (g-cat)<sup>-1</sup>.

To determine if the small amounts of impurities were responsible for the significant changes in performance, I intentionally mixed YFI-C (that is, pure YNU-5) with trace amounts of MFI<sub>nano</sub>(20) or MFI<sub>micron</sub>(20), dealuminated using a standard technique to compare with deAl-YFI-B(57), and used the resulting deAl-[YFI-C + 3 wt% MFI<sub>nano</sub>(20)] and deAl-[YFI-C + 3 wt% MFI<sub>micron</sub>(20)] (as defined in Section 2.4) as catalysts for the DTO reaction. Note that the abbreviations MFI<sub>nano</sub>(20) and MFI<sub>micron</sub>(20) used here are as defined in Section 2.3. The particle sizes and morphologies of these samples were confirmed by FE-SEM, as shown in Figure 2.10. The MFI<sub>nano</sub>(20) or MFI<sub>micron</sub>(20) was added at 3 wt% based on physically mixing pure calcined YNU-5 (YFI-C) with MFI<sub>micron</sub>(20) so that the YFI-C:MFI<sub>micron</sub>(20) weight ratio was 97:3, 95:5, or 90:10. Comparing the YFI-B to these mixtures, the amount of the MFI phase in the YFI-B was estimated to be 3 wt%.

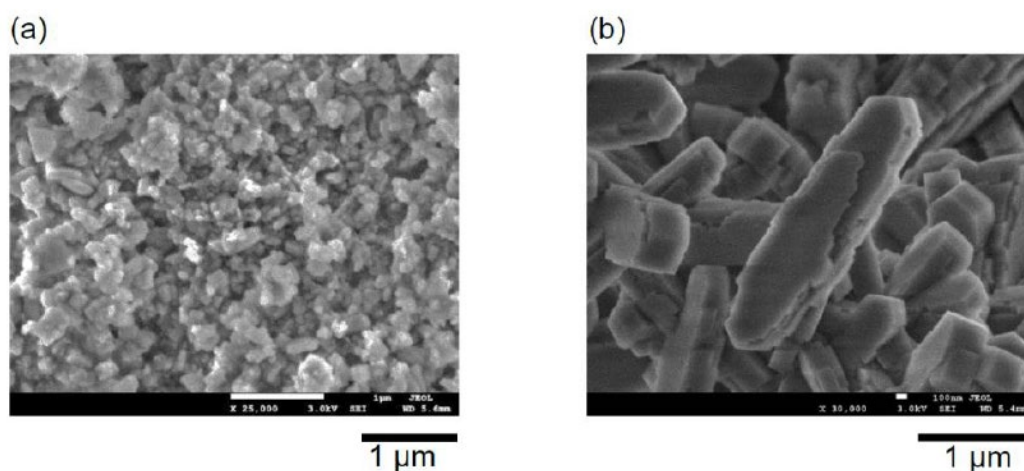


**Figure 2.10.** Field emission scanning electron microscopy images of the (a) MFI<sub>nano</sub>(20) and (b) MFI<sub>micron</sub>(20). The nomenclature for these samples is explained in Section 2.3.

To allow a comparison with the deAl-YFI-B(57) (Figure 2.9b), the catalytic performances of the physical mixtures are summarized in Figure 2.11a,b. During the initial stage of the reaction (TOS < 5 min), the YFI phase evidently acted as the main catalyst. However, the deAl-YFI-C(55) was rapidly deactivated due to coke formation (Figure 2.9a). After this initial stage (TOS > 5 min), it appears that the MFI phase primarily catalyzed the reaction. Compared to the data for deAl-YFI-C(55) in Figure 2.8a, it is evident that deactivation was effectively suppressed when using the deAl-[YFI-C + 3 wt% MFI<sub>nano</sub>(20)] (Si/Al = 57, Figure 2.11a) or deAl-[YFI-C + 3 wt% MFI<sub>micron</sub>(20)] (Si/Al = 62, Figure 2.11b). Only minimal deactivation was observed in both cases at TOS values between 5 and 185 min. Unexpectedly, with further increases in TOS, a significant decrease in conversion occurred when using the deAl-[YFI-C + 3 wt% MFI<sub>micron</sub>(20)]. In contrast, the conversion was maintained at 80% at a TOS of 305 in the case of the nanosized MFI deAl-[YFI-C + 3 wt% MFI<sub>nano</sub>(20)].

In this case, the selectivity for propene (a C3=) greatly increased as well. It should be noted that the samples made via the intentional physical mixing of MFInano showed very similar catalytic performance (Figure 2.11a) to that in Figure 2.9b, which suggests that trace levels of MFInano were responsible for the long life of the deAl-YFI-B(57). The fact that typical micron-sized MFI particles exhibited a lesser effect (Figure 2.11b) indicates the advantage of the nano-sized MFI contaminant. A control experiment was carried out as follows. MFInano(20) was physically mixed with inert material Si<sub>3</sub>N<sub>4</sub> at the weight ratio of 3:97 after which the mixture was treated with a HNO<sub>3</sub> solution as described in Section 2.4. The solid mixture was designated as deAl-[Si<sub>3</sub>N<sub>4</sub> + 3 wt% MFInano(20)] and was used as catalyst for DTO reaction (Figure 2.11c). As a result, the deAl-[Si<sub>3</sub>N<sub>4</sub> + 3 wt% MFInano(20)] showed stable activity as well as the similar product distribution pattern to that in Figure 2.11a, which further confirms this extraordinary advantage of MFInano(20). The most interesting aspect of these data is that the formation of a trace amount of co-crystallized MFI along with the crystallization of YNU-5 produced similar results to the material with added MFInano.

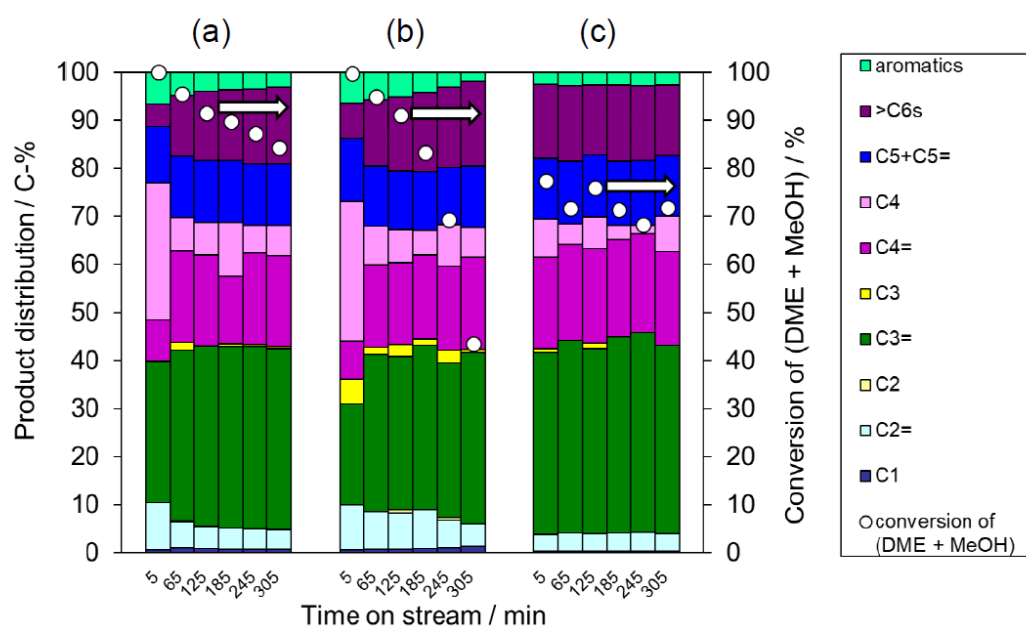


**Figure 2.11.** Results from the DTO reaction over the (a) deAl-[YFI-C + 3 wt% MFInano(20)] (Si/Al = 62), (b) deAl-[YFI-C + 3 wt% MFImicron(20)] (Si/Al = 62), and (c) deAl-[Si<sub>3</sub>N<sub>4</sub> + 3 wt% MFInano(20)]. The nomenclature for these samples is explained in Section 2.4 for (a) and (b), and Section 3.3.1 for (c). Pretreatment conditions: 550 °C, 1 h under air at a flow rate of 40 cm<sup>3</sup>(N.T.P.) min<sup>-1</sup>. Reaction conditions: catalyst weight, 100 mg; *W/F* = 20 g-cat h mol<sup>-1</sup>; pellet size, 500–600 μm; He flow rate, 40 cm<sup>3</sup>·(N.T.P.)·min<sup>-1</sup>; temperature, 400 °C. Coke amounts in the spent catalysts estimated by thermogravimetric analyses were (a) 114 and (b) 94 mg (g-cat)<sup>-1</sup>.

### 2.3.3.2. Catalytic Characteristics of Pure YNU-5

Because I succeeded in obtaining very pure YNU-5, I investigated the intrinsic catalytic features of this 12-12-8-ring zeolite by comparing its catalytic performance with those of 8-ring and 12-ring zeolites. SSZ-13 (having a CHA topology with an 8-8-8-ring pore system) and beta (having a \*BEA topology with a 12-12-12-ring pore system) were used as model catalysts for the DTO reaction. Figure 2.12 summarizes the product distributions obtained from this reaction when catalyzed by the SSZ-13 (Si/Al = 136, Figure 2.12a), deAl-YFI-C(287) (Figure 2.12b,c), and beta (Figure 2.12d) materials.

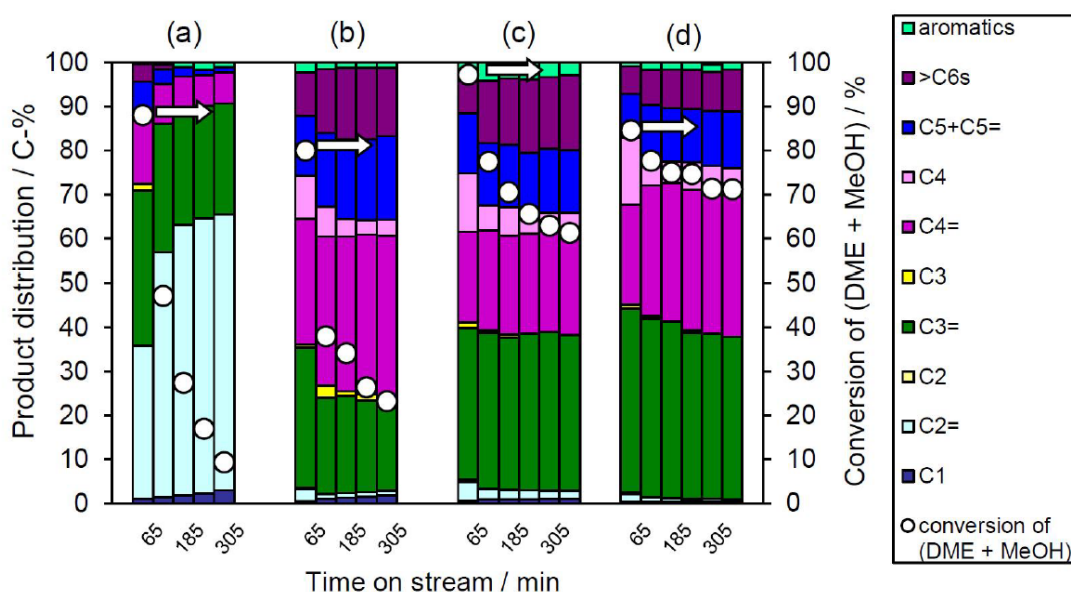


**Figure 2.12.** Results from the DTO reaction over the (a) SSZ-13 (Si/Al = 136), (b,c) deAl-YFI-C(287), and (d) beta (Si/Al = 250). Pretreatment conditions: 550 °C; 1 h under an air flow of 40 cm<sup>3</sup>·(N.T.P.)·min<sup>-1</sup>. Reaction conditions: catalyst weight, 100 mg;  $W/F = 20$  g-cat h mol<sup>-1</sup> with the exception of (c) where  $W/F = 79$  g-cat h mol<sup>-1</sup>; pellet size, 500–600 μm; He flow rate, 40 cm<sup>3</sup>(N.T.P.) min<sup>-1</sup>; reaction temperature, 400 °C. The nomenclature for deAl-YFI-C(287) is explained in Section 2.4. Coke amounts in the spent catalysts estimated by thermogravimetric analyses were (a) 91, (b) 29, (c) 25, and (d) 19 mg (g-cat)<sup>-1</sup>.

It is obvious that the SSZ-13 gave very high C2= selectivity as high as 35% at a conversion of 88% (Figure 2.12a). In contrast, the C3= and C4= selectivities obtained from the beta were remarkably high, with a combined [C3= + C4=] selectivity of approximately 65% in conjunction with a conversion of 85% (Figure 2.12d). Thus, the product distributions tended to reflect the pore system in the catalyst. To obtain comparable conversion levels, the  $W/F$  value was increased by a factor of 4 when using the YNU-5, with the results presented in Figure 2.12c. The DTO reaction catalyzed by the highly dealuminated YNU-5 (deAl-YFI-C(287)) gave a product distribution pattern

that was very similar to that obtained from the reaction over the beta specimen (Si/Al = 250) (Figure 2.12c,d). At a conversion of 80%, the selectivity for [C3= + C4=], which are the products in growing demand at present,<sup>37-39</sup> was close to 60% (Figure 2.12c), suggesting that this material could have practical applications. Thus, the behavior of the highly dealuminated YNU-5 was closer to that of a 12-ring system rather than an 8-ring zeolite catalyst. This result could assist in determining the locations of acid sites in the YNU-5 catalyst, and more detailed investigations of these effects are currently underway in our laboratory.

## 2.4. Conclusions

Following the successful synthesis and structural determination of YNU-5 having a YFI framework,<sup>19</sup> it became important to assess several aspects of this material with regard to potential catalytic applications. This included defining the factors that affect crystallization,<sup>21</sup> preparing a high-silica YNU-5 catalyst with a stable framework,<sup>21</sup> and establishing the relationship between very small amounts of impurity phases and catalytic performance. The present study examined the first and third issues. During the synthesis investigation, it was found that a very slight amount of an impurity phase tended to be formed along with the desired product YNU-5. This minor phase was very often MFI. The phase selection was sensitive to the levels of water in the synthesis mixture, such that a pure phase could be produced but it was also possible to intentionally form specific trace impurities. Dealuminated pure YNU-5 showed rapid deactivation at TOS values greater than 5 min, while the presence of low levels of ZSM-5 as an impurity reduced the extent of deactivation. At a TOS of 305 min, conversions up to 80% were observed. During the initial reaction stage, the YNU-5 acted as the primary catalyst and showed selectivity for propene as high as 30%. When TOS was between 5 and 305 min, ZSM-5 was the main catalyst and provided selectivity for propene up to 40%. This enhanced selectivity was observed only in the case that the ZSM-5 comprised nanoparticles. It is worth noting that the ZSM-5 impurity in the synthesis system of YNU-5 was unlike typical ZSM-5 specimens in that it appeared in the form of nano-sized particles. The presence of this nanoparticle contaminant phase evidently improved the performance of the catalytic system during the DTO reaction. Based on the product distribution obtained using highly dealuminated, very pure YNU-5 as a solid acid catalyst, this material behaves more like a 12-ring zeolite. The highly dealuminated YNU-5 also shows increased selectivity for high value C3 and C4 olefins, which suggests potential practical applications.

## 2.5 References

1. M.E. Davis, *Chem. Mater.*, **2014**, 26, 239–245.
2. J. C. Groen, T. Bach, U. Ziese, A. M. Paulaime-van Donk, K. P. de Jong, J. A. Moulijn, J. Pérez-Ramírez, *J. Am. Chem. Soc.*, **2005**, 127, 10792–10793.
3. V. Van Speybroeck, K. Hemelsoet, L. Joos, M. Waroquier, R. G. Bell, C. R. Catlow, *Chem. Soc. Rev.*, **2015**, 44, 7044–7111.
4. Jr. T. F. Degnan, *J. Catal.*, **2003**, 216, 32–46.
5. D. M. Ruthven, S. C. Reyes, *Microporous Mesoporous Mater.*, **2007**, 104, 59–66.
6. T. F. Jr. Degnan, *Top. Catal.*, **2000**, 13, 349–356.
7. M. A. Camblor, P. A. Barrett, M. Díaz-Cabañas, L. A. Villaescusa, M. Puche, T. Boix, E. Pérez, H. Koller, *Microporous Mesoporous Mater.*, **2001**, 48, 11–22.
8. K. S. N. Reddy, B. S. Rao, V. P. Shiralkar, *Appl. Catal. A Gen.*, **1993**, 95, 53–63.
9. E. S. Shamsoum, T. R. Schuler, A. K. Ghosh, U.S. Patent 5,227,558, 13 July **1993**.
10. G. J. Gajda, R. T. Gajek, U.S. Patent 5723710A, 3 March **1998**.
11. R. L. Wadlinger, G. T. Kerr, E. J. Rosinski, U.S. Patent 3,308,069, 7 March **1967**.
12. A. Corma, M. Camblor, P. Esteve, A. Martinez, J. Perezpariente, *J. Catal.*, **1994**, 145, 151–158.
13. A. Corma, L. T. Nemeth, M. Renz, S. Valencia, *Nature*, **2001**, 412, 423–425.
14. R. F. Lobo, M. E. Davis, *J. Am. Chem. Soc.*, **1995**, 117, 3766–3779.
15. M. Yoshioka, T. Yokoi, T. Tatsumi, *ACS Catal.*, **2015**, 5, 4268–4275.
16. S. P. Elangovan, M. Ogura, M. E. Davis, T. Okubo, *J. Phys. Chem. B*, **2004**, 108, 13059–13061.
17. T. Mathew, S. P. Elangovan, T. Yokoi, T. Tatsumi, M. Ogura, Y. Kubota, A. Shimojima, T. Okubo, *Microporous Mesoporous Mater.*, **2010**, 129, 126–135.
18. H. Kubota, C. Liu, T. Toyao, Z. Maeno, M. Ogura, N. Nakazawa, S. Inagaki, Y. Kubota, K. Shimizu, *ACS Catal.*, **2020**, 2334–2344.
19. N. Nakazawa, T. Ikeda, N. Hiyoshi, Y. Yoshida, Q. Han, S. Inagaki, Y. Kubota, *J. Am. Chem. Soc.*, **2017**, 139, 7989–7997.
20. Database of Zeolite Structures. Available online: <http://www.iza-structure.org/databases/> (accessed on 16 March 2020).
21. N. Nakazawa, Y. Yoshida, S. Inagaki, Y. Kubota, *Microporous Mesoporous Mater.*, **2019**, 280, 66–74.
22. R. Kawase, A. Iida, Y. Kubota, K. Komura, Y. Sugi, K. Oyama, H. Itoh, *Ind. Eng. Chem. Res.*, **2007**, 46, 1091–1098.
23. Y. Kubota, S. Tawada, K. Nakagawa, C. Naitoh, N. Sugimoto, Y. Fukushima, T. Hanaoka, Y. Imada, Y. Sugi, *Microporous Mesoporous Mater.*, **2000**, 37, 291–301.



24. S. Inagaki, S. Shinoda, Y. Kaneko, K. Takechi, R. Komatsu, Y. Tsuboi, H. Yamazaki, J. Kondo, Y. Kubota, *ACS Catal.*, **2013**, *3*, 74–78.
25. S. Inagaki, Y. Tsuboi, Y. Nishita, T. Syahylah, T. Wakihara, Y. Kubota, *Chem. Eur. J.* **2013**, *19*, 7780–7786.
26. H. Maekawa, Y. Kubota, Y. Sugi, *Chem. Lett.*, **2004**, *33*, 1126–1127.
27. Y. Kubota, H. Maekawa, S. Miyata, T. Tatsumi, Y. Sugi, *Microporous Mesoporous Mater.*, **2007**, *101*, 115–126.
28. R. K. Ahedi, Y. Kubota, Y. Sugi, *Bull. Chem. Soc. Jpn.*, **2003**, *76*, 883–890.
29. M. Niwa, N. Katada, *Catal. Surv. Jpn.*, **1997**, *1*, 215–226.
30. M. Niwa, N. Katada, *Chem. Rec.*, **2013**, *13*, 432–455.
31. S. Park, Y. Watanabe, Y. Nishita, T. Fukuoka, S. Inagaki, Y. Kubota, *J. Catal.*, **2014**, *319*, 265–273.
32. M. Sawa, M. Niwa, Y. Murakami, *Zeolite*, **1990**, *10*, 532–538.
33. T. Cordero-Lanzac, A. Ateka, P. Pérez-Uriarte, P. Castaño, A. T. Aguayo, J. Bilbao, *Ind. Eng. Chem. Res.*, **2018**, *57*, 13689–13702.
34. C. Seidel, A. Jörke, B. Vollbrecht, A. Seidel-Morgenstern, A. Kienle, *Chem. Eng. Sci.*, **2018**, *175*, 130–138.
35. A. S. Al-Dughaiter, H. de Lasa, *Fuel*, **2014**, *138*, 52–64.
36. M. A. Deimund, L. Harrison, J. D. Lunn, Y. Liu, A. Malek, R. Shayib, M. E. Davis, *ACS Catal.*, **2016**, *6*, 542–550.
37. X. Zhu, S. Liu, Y. Song, L. Xu, *Appl. Catal. A Gen.*, **2005**, *288*, 134–142.
38. V. Blay, E. Epelde, R. Miravalles, L. A. Perea, *Catal. Rev.*, **2018**, *60*, 278–335.
39. P. Boulens, E. Pellier, E. Jeanneau, J. N. Reek, H. Olivier-Bourbigou, P. A. R. Breuil, *Organometallics*, **2015**, *34*, 1139–1142.

## Chapter Three

# Hexane cracking reaction over YNU-5 zeolite

*This chapter shows the results of hexane-cracking using YNU-5 zeolites as catalyst. In this part, the effect of dealumination and temperature on the reaction results were investigated. Dealuminated YNU-5 zeolites with various Si/Al ratios were prepared by acid treatment using different concentration  $\text{HNO}_3$  acid solutions. The proton form of YNU-5 without dealumination having Si/Al ratio around 9 deactivated rapidly during the reaction due to heavy coke formation, whereas properly dealuminated YNU-5 with lower Al content exhibited high catalytic selectivity of propylene and durability to coke formation for hexane cracking at the reaction temperature of 550 to 650°C. By decreasing Al content, the selectivity of propylene increased, and the selectivity of ethylene decreased due to less content of Lewis and strong Bronsted acid sites based on the result of  $\text{NH}_3$  TPD profiles, which suppress secondary reaction producing coke precursor.*

**Keywords:** zeolite; YNU-5; solid acid catalyst; hexane cracking reaction

### 3.1 Introduction

As extremely essential raw materials in petrochemicals, the demand for light olefins is desperate and the current supply cannot match the demand. It is of much significance to improve and optimize the industrial craft of producing light olefins. There are two major strategies of production of light olefins: (i) steam cracker, and (2) Fluid catalytic cracking (FCC). Compared to conventional steam cracking craft, FCC craft has many advantages.<sup>1,2</sup> For example: (1) the relatively low reaction temperature, which greatly reduces the energy consumption and increases the life of the reactor; (2) the higher selectivity of low-carbon olefins; (3) possibility of obtaining different product distributions by designing catalysts with specific pore structure and acidic centers regulation. Therefore, to enable the reaction to proceed at low temperature, long-term efficiency, and high yield, it is particularly important to discover synthesize a catalyst with excellent performance. ZSM-5 zeolite has received extensive attention as a catalytic cracking catalyst.<sup>1-5</sup> However, due to its small microporous channels,

some reactions involving macromolecules are restricted. In decades, zeolites with large pore framework (the definition of large pore was explained in Chapter 1.) were investigated in FCC process since the first commercial introduction of zeolite Y about 60 years ago.<sup>2, 6-8</sup> Zeolite Y has been the primarily used catalyst in FCC process due to its specific properties: (1) large pore-size about 0.74 nm in diameter, (2) strong Brønsted acidity; (3) extraordinary thermal and hydrothermal stability.<sup>9</sup>

MCM-68, with a three-dimensional (12-10-10R, MSE) is another excellent catalyst for FCC process. The investigation of the catalytic performance of MCM-68 for hexane cracking reaction has been carried out, identifying the excellent performance.<sup>10-14</sup> Properly dealuminated MCM-68 zeolite exhibits the high selectivity to propylene (45–50%) and durability to coke formation during hexane cracking, regardless of the reaction temperature, which is attributed to the control of the position and density of acid sites originating from the framework Al atoms.<sup>10</sup>

These studies imply that zeolites with large pore channel system and strong Brønsted acidity are promising candidate for FCC. YNU-5 is a new discovered zeolite with a novel framework of YFI (shown in Figure 1.7), containing a distinguishable three-dimensional channel system: 2-dimensional 12-ring (0.78 nm × 0.59 nm; large micropore) with channel intersection connected with 8-ring channel (0.44 nm × 0.34 nm; small micropore), thus forming a large space around 7.97 Å that are accessible through 12-ring windows. The specific structure renders YNU-5 another promising candidate for hexane cracking reaction. Therefore, this chapter focused on the catalytic performance of YNU-5 zeolites in hexane cracking reaction.

## 3.2 Experimental

### 3.2.1. Measurements

Powder X-ray diffraction (XRD; Ultima-IV, Rigaku, Akishima, Tokyo, Japan) data were collected using Cu K $\alpha$  radiation and operating at 40 kV and 20 mA to examine the crystallinity and phase purity of the zeolite catalysts. The Si/Al molar ratios in the bulk materials were determined by inductively coupled plasma—atomic emission spectrometry (ICP-AES; ICPE-9000, Shimadzu Ltd., Kyoto, Japan). In preparation for these analyses, a catalyst sample (20 mg) was suspended in Milli-Q (Merck KGaA, Darmstadt, Germany) water (5 g) within a Teflon beaker followed by the addition of 47% HF (120 mg) at room temperature, ultrasonication for 2 min to provide dissolution, and dilution with Milli-Q water (90 g). The crystal sizes and morphologies of the zeolite catalysts were observed by means of field emission scanning electron microscopy (FE-SEM; JSM-7001F, JEOL Ltd., Akishima, Tokyo, Japan). Solid-state magic angle

spinning nuclear magnetic resonance (MAS NMR) data were collected using a spectrometer (AVANCEIII 600, Bruker Co., Billerica, Massachusetts, USA) operated at 600 MHz for  $^1\text{H}$  analyses and 119.2 MHz for  $^{29}\text{Si}$  analyses. All MAS NMR spectra were recorded at room temperature with a 4 mm diameter  $\text{ZrO}_2$  tube. The  $^{29}\text{Si}$  chemical shifts were determined based on that of hexamethylcyclotrisiloxane at  $-9.66$  ppm. Dipolar-decoupling (DD) MAS NMR data were acquired using 1024 pulses with a recycle time of 30 s at a spinning rate of 10 kHz. The coke contents of the spent catalysts were determined by thermogravimetric/differential thermal analysis (TG-DTA) on a Thermo plus EVO II TG8120 (Rigaku). The temperature was raised from room temperature to  $800^\circ\text{C}$  with the rate of  $10^\circ\text{C}\cdot\text{min}^{-1}$  under air flow ( $30\text{ cm}^3\cdot\text{min}^{-1}$ ). The weight loss observed from 300 to  $700^\circ\text{C}$  was ascribed to coke.

### **3.2.2. *Typical synthesis of YNU-5 zeolite***

Please see Section 2.2.2.

### **3.2.3. *Post-synthesis treatments of YNU-5 zeolites***

#### **3.2.3.1 *Ion-exchange of calcined YNU-5 to $\text{NH}_4^+$ form***

Ion exchange of the calcined samples to the  $\text{NH}_4^+$ -form was performed using an  $\text{NH}_4\text{NO}_3$  solution as follows.  $\text{NH}_4\text{NO}_3$  (2.0 g) and the calcined sample (1.0 g) were suspended in  $\text{H}_2\text{O}$  (50 mL) in a 250 mL polypropylene bottle. The bottle was capped tightly and allowed to stand at  $80^\circ\text{C}$  for 24 h with occasional release of pressure and careful shaking. After cooling, the sample was separated by filtration and washed with de-ionized water. This process was repeated twice, after which the sample was dried overnight at room temperature. The resulting zeolite was again calcined in a muffle furnace, during which the temperature was raised from ambient to  $550^\circ\text{C}$  over a period of 6 h, and kept at the same temperature for 6 h to give the sample in  $\text{H}^+$  form. The  $\text{NH}_4^+$ -forms of the YFI-type zeolites are denoted as  $\text{NH}_4^+$ -YNU-5. Non-dealuminated H-YNU-5 was generated in situ from  $\text{NH}_4^+$ -YNU-5 in the reactor or in some case for characterization.

#### **3.2.3.2 *Typical procedure of dealumination***

The calcined YNU-5 samples were converted to protonated dealuminated analogues using various acid treatments. Direct dealumination of the calcined YNU-5 (typically 1.0 g) was accomplished by refluxing with  $\text{HNO}_3$  solutions ( $60\text{ mL (g-sample)}^{-1}$ ) in a 200 mL round bottom flask at  $130^\circ\text{C}$  in an oil bath for 24 h. These conditions also stabilized the framework of the material due to Si migration. The dealuminated versions of YFI are referred to herein as deAl-YFI ( $n$ ), respectively,

where  $n$  indicates the Si/Al ratio. In this work, as an example, deAl-YFI(22), deAl-YFI(35), and deAl-YFI(75) were prepared by treatment with a 0.35, 0.5, and 2.0 mol L<sup>-1</sup> HNO<sub>3</sub> aqueous solution under reflux conditions, respectively.

### 3.2.3 Catalytic reaction

An appropriate amount of each zeolite catalyst was pelletized without any binder, roughly crushed and then sieved to obtain catalyst pellets with 500–600  $\mu\text{m}$  in size. The cracking of  $n$ -hexane (hexane hereafter) was performed under atmospheric pressure in a down-flow quartz-tube microreactor (shown in Figure 3.1) with 8 mm of inner diameter. Prior to running the reaction, 100 mg of catalyst pellets were packed in a fixed-bed of the reactor, and preheated at 550 °C for 1 h in a stream of air. After pretreatment, the feed was switched over to a helium stream containing an appropriate amount of hexane (W/F = 19.6 g-cat. h (mol-hexane)<sup>-1</sup>). The reaction was performed at 550°C for 305 min. After reaction, the system was cooled down to room temperature in a helium stream and then the used catalyst was recovered. The reactants and products were separated by a CP-Al<sub>2</sub>O<sub>3</sub>/KCl PLOT capillary column (i.d., 0.53 mm; length 50 m; Agilent Technology) and analyzed by using GC-2014 (Shimadzu) with a flame-ionization detector. The conversion of hexane and the selectivity to each product are calculated on the carbon-basis of the initial amount of hexane.

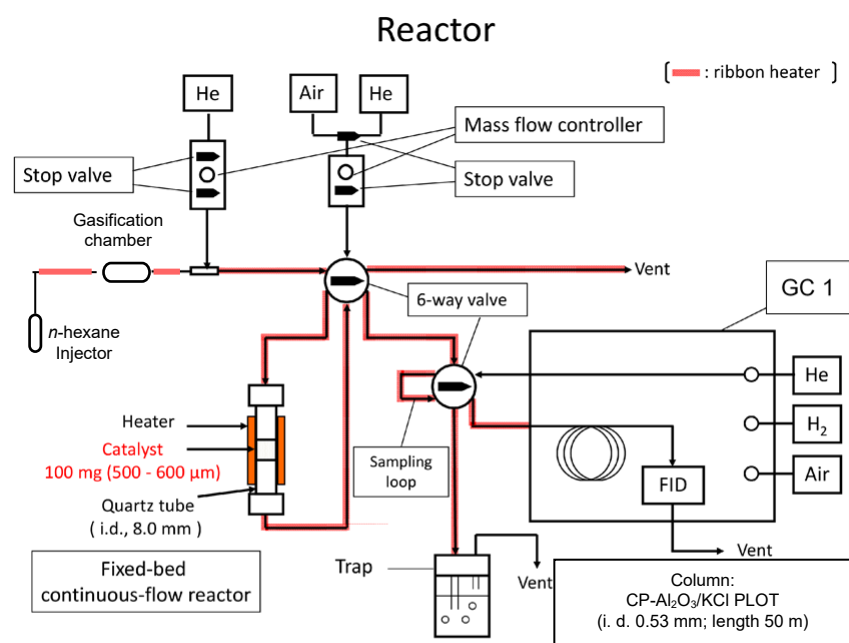


**Figure 3.1.** Set-up of  $n$ -hexane reaction

### 3.3 Results and Discussion

#### 3.3.1 Dealumination of YNU-5 zeolites

##### 3.3.1.1 $\text{NH}_3$ TPD profiles

A major objective of this study was to assess the catalytic performance of YNU-5 zeolite over *n*-hexane cracking reaction as a solid acid catalyst and the impact of post-synthesis treatment by acid treatment on the related acidic properties of YNU-5 zeolites. Whereas  $^{27}\text{Al}$  MAS NMR was applied to assess changes in the Al coordination upon dealumination, the temperature-programmed desorption (TPD) of ammonia method was applied to estimate the number of acid sites.

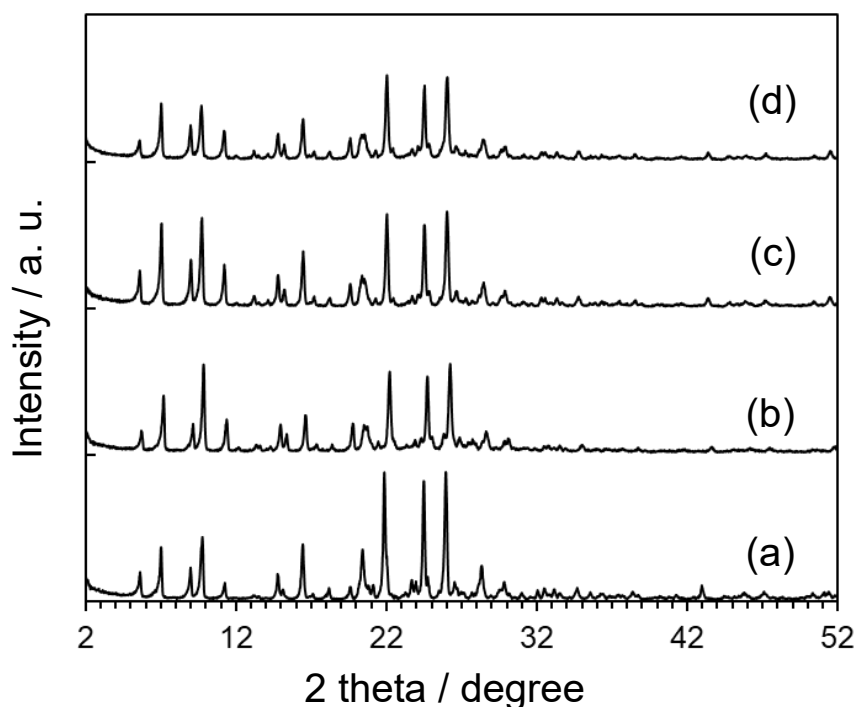


**Figure 3.2.** XRD patterns of (a) YFI\_cal(9), (b) deAl-YFI(22), (c) deAl-YFI(35), and (d) deAl-YFI(75).

Dealuminated YNU-5 zeolites with various Al contents were prepared by acid treatment. Figure 3.2 displays the XRD patterns of the resultant products. All samples exhibited a typical and intense diffraction of YFI zeolite, identifying that crystalline YFI structure was retained after acid treatment. As previous reported, the hydrothermal stability of YNU-5 zeolites can be enhanced after strict condition due to Si migration during dealumination process. The possible schematic of Si-migration<sup>15</sup> is shown in

Figure 3.3. Neighboring Si atoms are firstly hydrolyzed by the acid producing monosilicic acid species. These monosilicic groups move towards adjacent side defects through condensation. After many repetitions, the defects move to the outer surface. Table 3.1 shows the Acid amounts and Al content of these samples. Acid amount was estimated from  $\text{NH}_3$  TPD profiles (shown in Figure 3.4) and Al content was determined by ICP AES analysis. A close to linear decrease in the bulk Si/Al ratio of dealuminated zeolites is evidenced with increasing  $\text{HNO}_3$  concentration (from 0.35 to 2.0 M), confirming the preferential removal of Al atoms in the tire range of treatment conditions.

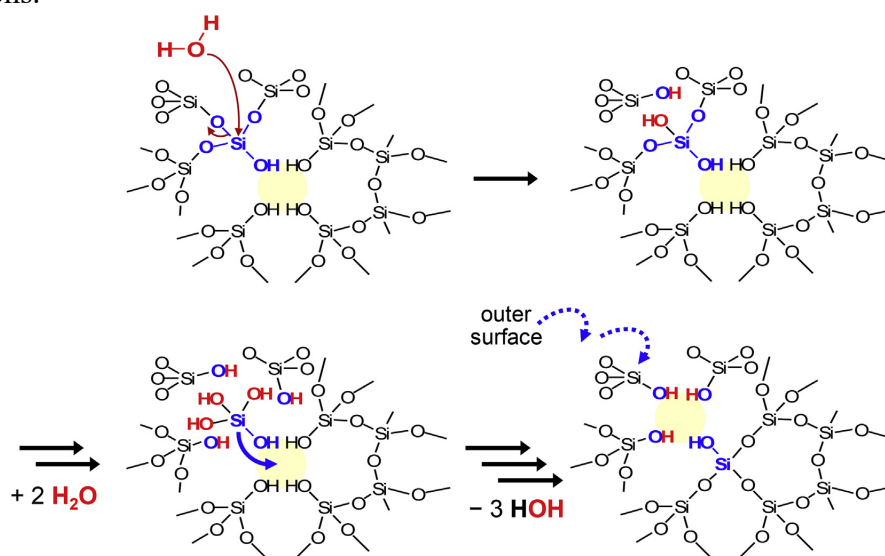


**Figure 3.3.** Mechanistic speculation of Si-migration in molecular level.

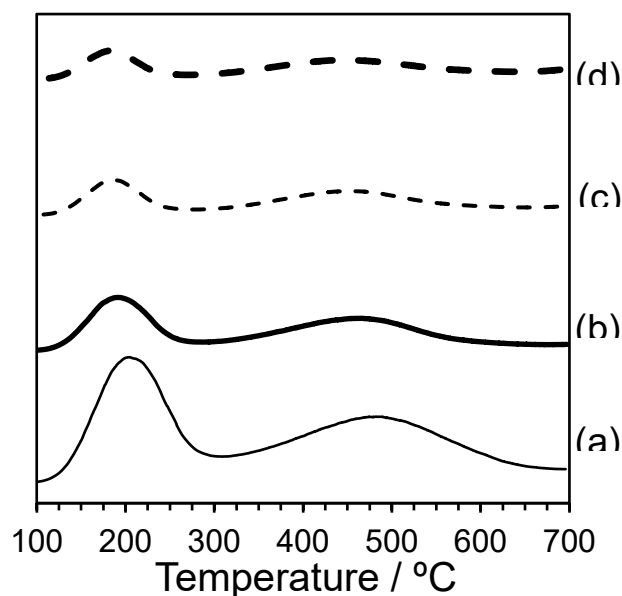


**Figure 3.4.**  $\text{NH}_3$ -TPD profiles of (a)  $\text{H}^+$ -YFI(10), (b) deAl-YFI(22), (c) deAl-YFI(35), and (d) deAl-YFI(75). Pretreatment: 600°C, 1 h under He, TCD detector.  $\text{H}^+$ -YFI(10) was generated in situ from  $\text{NH}_4^+$ -YNU-5 after pretreatment.

**Table 3.1.** Acid amount and Al content of YNU-5 zeolite samples

	Catalyst	Al content <sup>a</sup>	Number of acid sites <sup>b</sup>
	(Si/Al ratio) <sup>a</sup>	/ mmol g <sup>-1</sup>	/ mmol g <sup>-1</sup>
(a)	NH <sub>4</sub> -YFI(10)	1.121	1.380
(b)	deAl-YFI (22)	0.649	0.678
(c)	deAl-YFI(35)	0.371	0.426
(d)	deAl-YFI(75)	0.224	0.258

a ICP-AES.

b NH<sub>3</sub>-TPD, pretreatment: 600°C, 1 h under He, TCD detector.

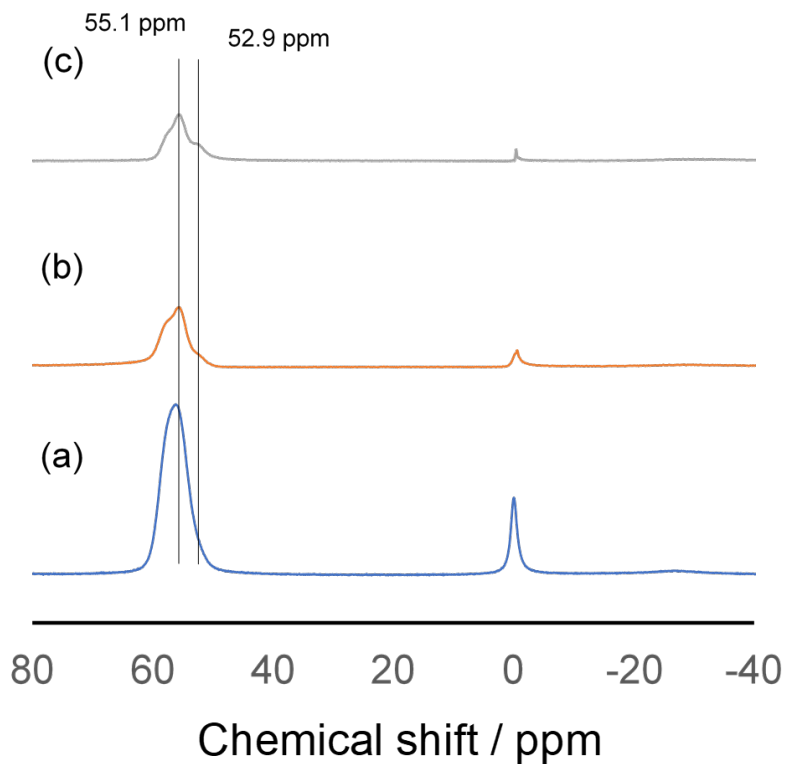
### 3.3.1.2 <sup>27</sup>Al MAS NMR

Figure 3.5 displays the <sup>27</sup>Al MAS NMR spectra of parent YNU-5 only calcined and the dealuminated YNU-5 zeolite with various Si/Al ratios. For concision, the resultant samples were designated as YFI\_cal, deAl-YFI(35), and deAl-YFI(75) as described in section 3.3.2. <sup>27</sup>Al MAS NMR is an efficient probe to determine the coordination and the local structure of aluminum species in zeolites. Extraframework Al (octahedral Al) atoms is located around 0 ppm, and tetrahedral Al is in the range of 50–60 ppm.<sup>1</sup> It is easy to find a primary peak at ca. 56 ppm in the spectrum of YFI\_cal (Figure 3.5a) which is consistent with those previous reports. With increase of the HNO<sub>3</sub> concertation, namely the degree of dealumination, the peaks (ca. 51 ppm) corresponding to tetrahedral Al obviously decreased. The spectrum of sample deAl-YFI(75) exhibits a shoulder peak around 53 ppm, which is speculated to be the framework aluminum atoms inside isolated 8-ring channels. It's difficult to remove this kind of Al atoms because the diffusion of H<sub>2</sub>O molecular is weak.

### 3.3.1.3 N<sub>2</sub> adsorption

The nitrogen adsorption–desorption isotherms of YFI\_cal(9) and deAl-YFI(75) are shown in Figure 3.6. No significant change of micropore volume estimated by the *t*-plot method were observed and no mesopores was formed after dealumination.





**Figure 3.5.**  $^{27}\text{Al}$  MAS NMR spectra of (a) YFI\_cal, (b) deAl-YFI(35), and (c) deAl-YFI(75).

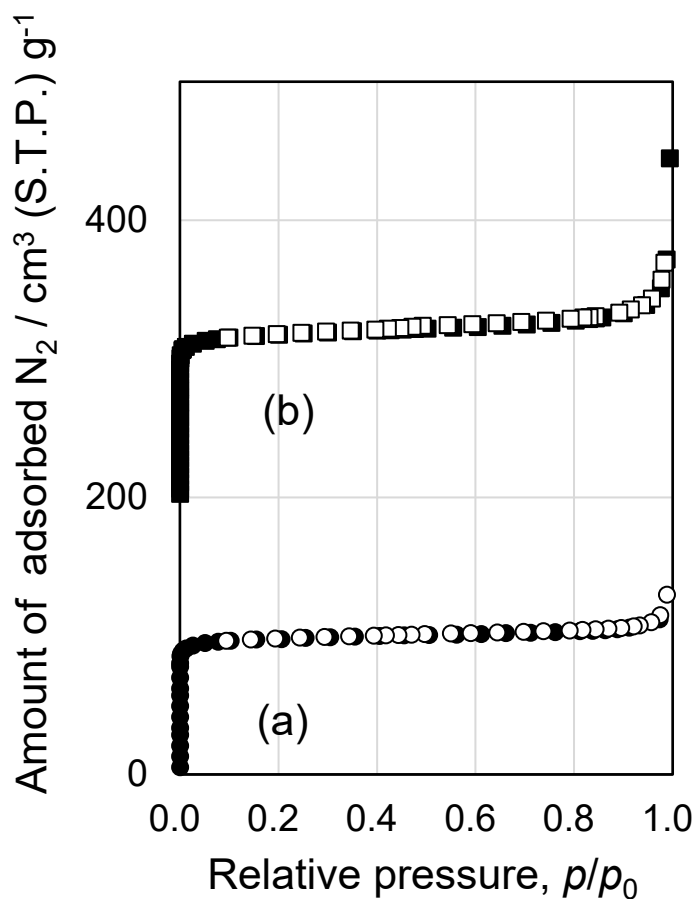


**Figure 3.6.**  $\text{N}_2$  isotherms of (a) YFI\_cal (9), (b) deAl-[YFI-BT](75). The number in the parentheses is Si/Al ratio. The isotherms (b) is offset vertically by  $200 \text{ cm}^3 (\text{S.T.P.}) \text{ g}^{-1}$ , respectively. Filled and unfilled symbols indicate adsorption and desorption, respectively.

### 3.3.2 Hexane cracking reaction

#### 3.3.2.1 Hexane cracking over MFI and BEA catalysts

Figure 3.7 shows the variation in both hexane conversion and the product distribution during the cracking of *n*-hexane at 550°C over ZSM-5, YNU-5, and beta type zeolite catalyst. I intended to investigate the intrinsic catalytic features of this 12-12-8ring zeolite by comparing its catalytic performance with those of 8-ring and 12-ring zeolites. ZSM-5 (having a MFI topology with 10-10-10-ring pore system) and beta (having a \*BEA topology with 12-12-12-ring pore system) were used as model catalyst for the hexane cracking reaction. At the TOS = 5 min, it is obvious that ZSM-5 gave high C2= selectivity as high as 26% and C3= 22% at the conversion of 98%. In the case of beta zeolite, the C3= selectivity (32%) is remarkably high and lower C2= (14%) selectivity at the conversion of 70%. Similarly, the C2= and C3= selectivity obtained from deAl-YFI(22) were 15% and 37% at the conversion of 84%, respectively. However, deAl-YFI(22) experienced a very rapid deactivation due to the large amount of coke (121 mg (g-catalyst)<sup>-1</sup>). Thus, the behavior of deAl-YFI(22) was closer to that of a 12-ring system. This result tells that the product distribution of hexane cracking has direct relationship with the topology of catalyst.

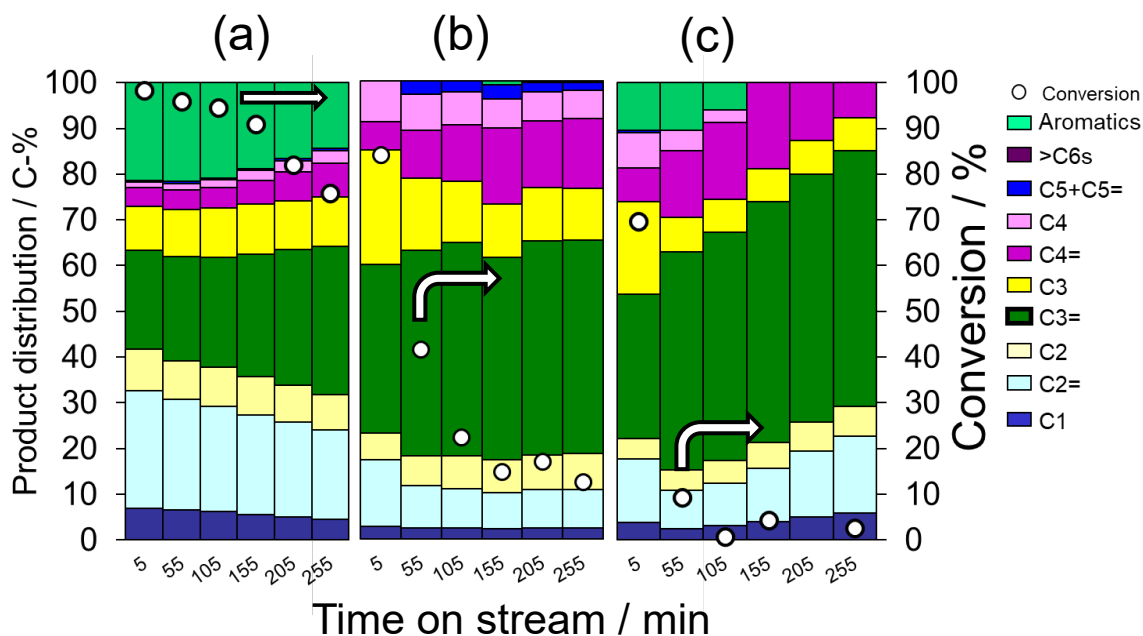


**Figure 3.7.** Product distribution and conversion of hexane over (a) ZSM-5 (12), (b) deAl-[YFI-BT](22), and (c) H<sup>+</sup>-BEA<sub>OSDAF</sub>\_IE. The number in the parentheses is Si/Al ratio. Reaction conditions: catalyst, 100 mg, temperature, 550°C; W/F, 19.6-cat h (mol-hexane)<sup>-1</sup>; He gas flow rate, 40 cm<sup>3</sup> (N.T.P.) min<sup>-1</sup>. Coke amounts on the spent catalysts are estimated to be 107, 121, and 33 mg (g-catalyst)<sup>-1</sup> for (a), (b), and (c), respectively.

### 3.3.2.2 Hexane cracking over dealuminated YNU-5 zeolites

In this section, the effects of dealumination on the catalytic performances in cracking reaction were discussed. As shown in Figure 3.8b, H-YFI(10) generated in situ from NH<sub>4</sub>-YFI(10) exhibited a poor catalytic stability and a low propylene selectivity. This rapid deactivation may be caused by the large amount of acid sites (Table 3.1), which would accelerate the secondary reactions among products, leading to a large amount of coke (145 mg (g-catalyst)<sup>-1</sup> at TOS of 305 min). Therefore, the catalytic performances of dealuminated YNU-5 zeolites with a lower amount of acid were considered. It is obvious that the catalytic stability increased with the degree of dealumination increasing, simultaneously, coke amount significantly decreased from 145 to 12 mg (g-catalyst)<sup>-1</sup> because of less acid amounts. deAl-YFI(75) gave a good catalytic stable, namely, an enhanced resistance to coking.

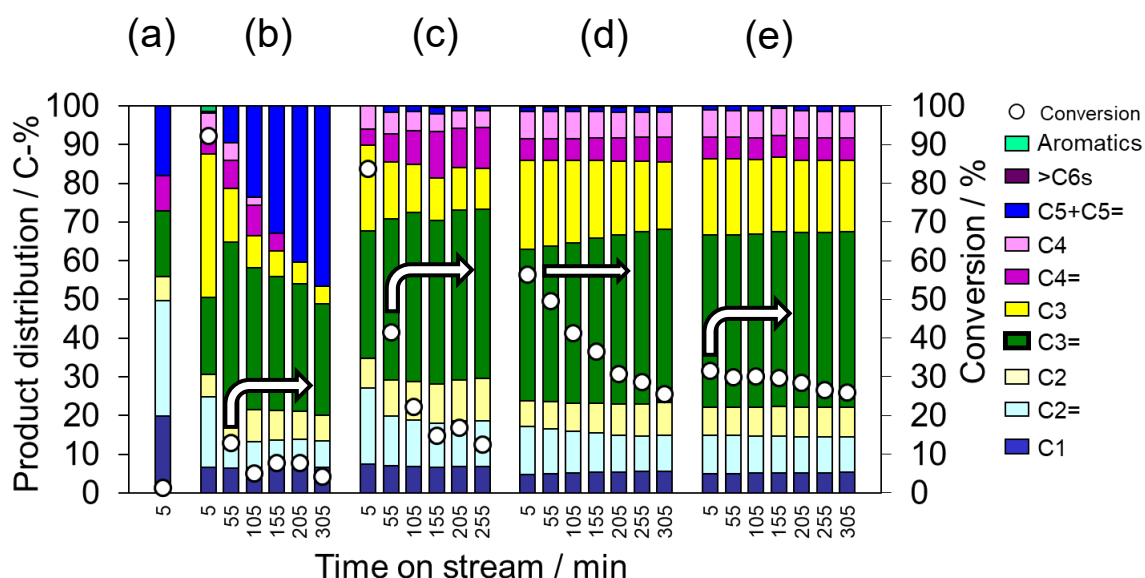


**Figure 3.8.** Product distribution and conversion of hexane over (a) blank, (b) H<sup>+</sup>-YNU-5(10), (c) deAl-YFI(22), (d) deAl-YFI(35) and (e) deAl-YFI (75). The number in the parentheses is Si/Al ratio. Reaction conditions: catalyst, 100 mg, temperature, 550°C; W/F, 19.6-cat h (mol-hexane)<sup>-1</sup>; He gas flow rate, 40 cm<sup>3</sup> (N.T.P.) min<sup>-1</sup>. Coke amounts on the spent catalysts are estimated to be 145, 121, 34 and 12 mg (g-catalyst)<sup>-1</sup> for (a), (b), (c) and (d), respectively.

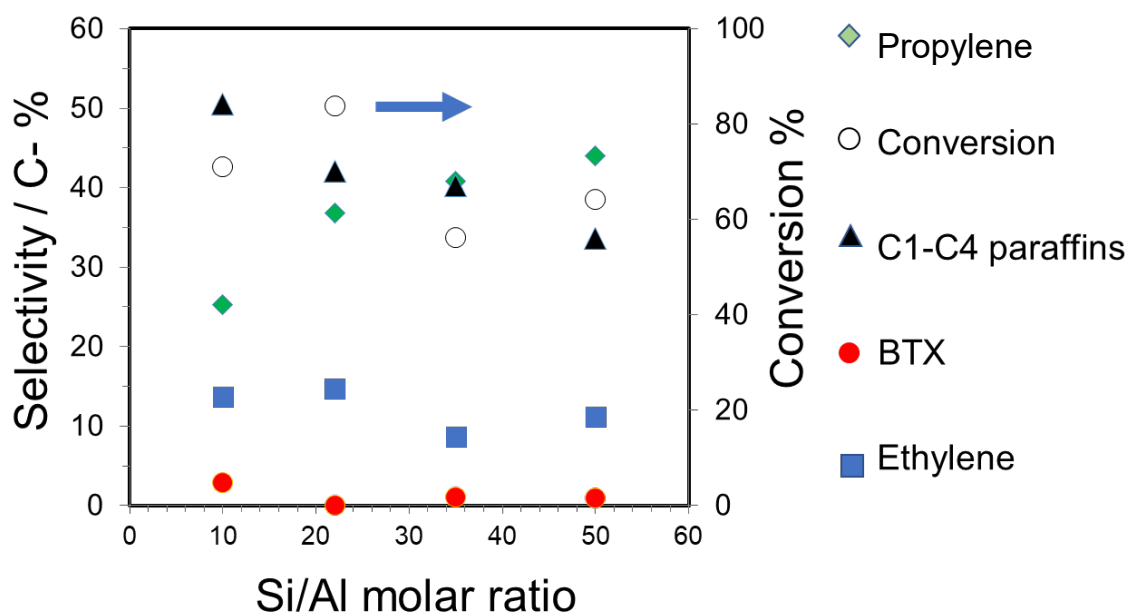


**Figure 3.9.** Products selectivity and conversion of hexane on YNU-5 zeolite with various Si/Al ratio. Catalysts: H-YFI(10), deAl-YFI(22), deAl-YFI(38), deAl-YFI(51)

Reaction conditions: 100 mg, temperature, 550°C; W/F, 7.7 or 19.6-cat h (mol-hexane)<sup>-1</sup>; He gas flow rate, 40 cm<sup>3</sup> (N.T.P.) min<sup>-1</sup>. TOS = 5 min.

Except for the stability, the selectivity and conversion are both important as well. To obtain comparable conversion levels, the W/F value was tuned to 7.7 g-cat h mol<sup>-1</sup> when using the H-YFI(10), with the results presented in Figure 3.9. The conversions of different sample were controlled with the range of 56% to 83% at the TOS of 5 min. The selectivity of C2=, C3=, C1-C4 paraffins, and BTX (benzene, toluene, xylene) are summarized in Figure 3.9 as well. The selectivity of C3= obviously became higher with the higher Si/Al ratio, increasing from 22% at the conversion of 71% to 43% at the conversion of 64% in the case of H-YFI(10) and deAl-YFI(50), respectively. Simultaneously, the selectivity of C2= slightly decreased from 14% to 11%. More interesting, selectivity of C1-C4 paraffine has an obvious decrease from 53% to 34%. This result could be explained by the removal of strong acid sites in YNU-5 zeolite,  $\beta$ -scission to form lighter olefins were suppressed. The desorption peak of chemically adsorbed NH<sub>3</sub> shift to relative lower temperature area show in Figure 3.4.

Figure 3.10 gives the product distribution and conversion of hexane over deAl-YFI(75) at different temperature. The direct hydrothermal cracking conversion of hexane was ca. 10%, with the primary product 39% C2= and 21% C3=. Dealuminated YNU-5 zeolite kept high catalytic stability even at 600°C, which was getting lower at 650°C. The initial conversion of hexane at the TOS of 5 significantly increased from 31% to 56% when reaction temperature changed from 550 to 600°C. Additionally, the propene selectivity is about 41% and is much larger than that of propane (16%) and expected as a primary cracking product even at a higher conversion.

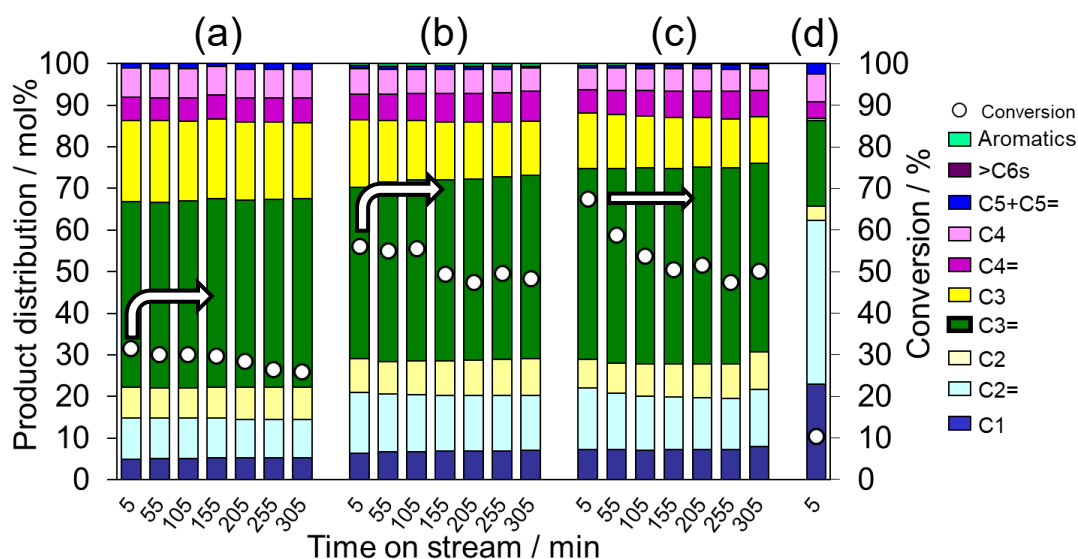


**Figure 3.10.** Product distribution and conversion of hexane over deAl-YFI(75) at (a) 550°C, (b) 600°C, and (c) 650°C. (d): Blank at 650°C. The number in the parentheses is Si/Al ratio. Reaction conditions: catalyst, 100 mg, temperature, 550°C; W/F, 19.6-cat h (mol-hexane)<sup>-1</sup>; He gas flow rate, 40 cm<sup>3</sup> (N.T.P.) min<sup>-1</sup>. Coke amounts on the spent catalysts are estimated to be 12, 24 and 27 mg (g-catalyst)<sup>-1</sup> for (a), (b), and (c), respectively.

### 3.4 Conclusions and outlook

This chapter focused on the catalytic performance of YNU-5 in hexane cracking reaction. Properly dealuminated YNU-5 catalyst exhibits high resistance to coking and good catalytic stability even at high temperature of 650°C. More importantly, it also has high selectivity of light olefins C3= and C2=. Based on these results, YNU-5 is a useful cracking catalyst.

Outlook: A further improvement of catalytic activity is necessary. There are two methods: (1) developing the synthesis of nanoparticle-sized YNU-5 zeolites, (2) introducing multiple porous structure into the framework.

### 3.5 References

1. A. Aitani, T. Yoshikawa, T. Ino, *Catal. Today*, **2000**, 60, 111–117.
2. T. F. Degnan, G. K. Chitnis, P. H. Schipper, *Microporous Mesoporous Mater.*, **2000**, 35, 245–252.
3. J. S. Buchanan, *Catal. Today*, **2000**, 55(3), 207–212.
4. P. Zhang, X. Guo, H. Guo, X. Wang, *J. Mol. Catal. A: Chem.*, **2007**, 261(2), 139–146.

5. O. D. Mante, F. A. Agblevor, S. T. Oyama, R. McClung, *App. Catal. A: Gen.*, **2012**, *445*, 312–320.
6. C. Marcilly, *J. Catal.*, **2003**, *216*, 47–62.
7. A. F. Masters, T. Maschmeyer, *Microporous Mesoporous Mater.*, **2011**, *142*, 423–438.
8. C. Martínez, A. Corma, *Coord. Chem. Rev.*, **2011**, *255*, 1558–1580.
9. J. García-Martínez, K. Li, G. Krishnaiah, *Chem. Commun.*, **2012**, *48*(97), 11841–11843.
10. S. Inagaki, K. Takechi, K., Y. Kubota, *Chem. Commun.*, **2010**, *46*(15), 2662–2664.
11. Y. Kubota, S. Inagaki, K. Takechi, *Catal. Today*, **2014**, *226*, 109–116.
12. Y. Kubota, S. Inagaki, *Top. Catal.*, **2015**, *58*(7), 480–493.
13. Q. Han, K. Enoda, S. Inagaki, Y. Kubota, *Chem. Lett.*, **2017**, *46*(9), 1434–1437.
14. S. Inagaki, S. Park, H. Yamazaki, J. N. Kondo, Y. Kubota, *Microporous Mesoporous Mater.*, **2018**, *272*, 16–23.
15. N. Nakazawa, Y. Yoshida, S. Inagaki, Y. Kubota, *Microporous Mesoporous Mater.*, **2019**, *280*, 66–74.

## Chapter Four

# Introduction of hierarchical structure into YNU-5 zeolite and its enhanced catalytic performance for cracking of hexane

*Hierarchical structure was successfully created in YNU-5 zeolite by a direct base-treatment. Although the unmodified YNU-5 catalyst was significantly deactivated by heavy coking in hexane cracking, the dealuminated catalyst was much less deactivated. Furthermore, the mesopore/micropore hierarchical structure in the YNU-5 zeolite catalyst suppressed deactivation more than the non-hierarchical, dealuminated YNU-5 with the similar Si/Al ratio. An increase in hexane conversion was also observed for the YNU-5 with hierarchical structure.*

**Keywords:** YNU-5, desilication, hierarchical structure, hexane cracking

### 4.1 Introduction

High-silica zeolites have strong potential as solid acid catalysts,<sup>1</sup> and any new framework should be considered for catalytic application. YNU-5 (YFI topology)<sup>2</sup> is a new large-pore aluminosilicate zeolite that I first synthesized recently using  $\text{Me}_2\text{Pr}_2\text{N}^+$  as a simple organic structure-directing agent (OSDA).<sup>3</sup> This has a 12–12–8-ring pore system<sup>3,4</sup> and is highly attractive as a solid catalyst in the petrochemical field. I have already found that the thermal stability of the framework is enhanced by post-synthesis treatment,<sup>4</sup> which makes this material promising catalysts. The YNU-5 has been first applied to dimethyl ether-to-olefin (DTO) reaction as the solid acid catalyst.<sup>3</sup> Afterwards, very pure YNU-5 was found to have a tendency to be rapidly deactivated by coking even when the material is dealuminated.<sup>5</sup> This tendency also exists in other reactions such as paraffin cracking. To get rid of this deactivation, at least two strategies for making the mass transfer easier would be effective. One strategy is decreasing the particle size into the nanometer range in order to increase the number of pore-mouth.<sup>6,7</sup> However, I have not been successful in changing the particle size of YNU-5 by tuning the synthesis conditions due to the narrow synthesis window. Another strategy is the creation of intra-particle mesopores to improve the mass transfer within the catalyst,

leading to the enhanced catalytic performance.<sup>8</sup> When the YNU-5 zeolite has the porosities of multiple levels such as micropores/mesopores can be called "hierarchical YNU-5". In general, the preparation method of hierarchical zeolites<sup>9–12</sup> can be classified into (1) top-down strategies involving the post-synthetic treatment of previously grown zeolite or zeolite precursor and (2) bottom-up approaches depending on the modification of the zeolite synthesis protocol.

In this work, I planned to take the route (1) via base-treatment procedure<sup>13–15</sup> to prepare the hierarchical YNU-5.

The catalytic properties were evaluated by the cracking of *n*-hexane (hereafter referred to as hexane) as a probe reaction. The catalytic cracking of paraffin including hexane is useful for producing light olefins including propylene and ethylene. Propylene is a highly demanded compound and the current supply does not satisfy the demand. Ethylene is also very useful synthetic intermediate. The propylene/ethylene selectivity is sensitive to the acid properties of the catalyst. Therefore, besides the suppression of deactivation, the selectivity to both propylene and ethylene in the hexane cracking over new zeolite such as YNU-5 catalyst is also an interesting and important issue. In this work, I investigated the preparation of hierarchical YNU-5 zeolite by post-synthetic treatment with aqueous NaOH solution. Catalytic properties for hexane cracking were also examined while performing physicochemical characterization of the catalyst.

## 4.2 Experimental

### 4.2.1 Materials

The commercially available reagents were used as received without further purification. The suppliers and cautions are described in each section when necessary. "Pure water" is Milli-Q grade water unless otherwise noted. The FAU-type zeolite is the HSZ-350HUA, Si/Al = 5.5, purchased from Tosoh Corporation.

### 4.2.2 Measurements

Powder X-ray diffraction (XRD) data were collected on an Ultima-IV diffractometer (Rigaku, Tokyo, Japan) using Cu K $\alpha$  radiation and operating at 40 kV and 20 mA to examine the crystallinity and phase purity of the zeolite catalysts. The crystal sizes and morphologies of the zeolite catalysts were observed by means of field emission scanning electron microscopy (FE-SEM; JSM-7001F, JEOL, SU8000 and SU9000, Hitachi High-Tech Corporation, Japan). Cross-sectional specimens were



prepared by ion milling using an IB-09010CP cross section polisher (JEOL Corp., Tokyo, Japan). Nitrogen adsorption-desorption measurements were carried out using a BELSORP max II (MicrotracBEL Corp., Osaka, Japan). The Si/Al molar ratios in the bulk materials were determined by inductively coupled plasma-atomic emission spectrometry (ICP-AES; ICPE-9000, Shimadzu Kyoto, Japan). In preparation for these analyses, a catalyst sample (20 mg) was suspended in pure water (5 g) within a Teflon beaker followed by the addition of 47% HF (120 mg) at room temperature, ultrasonication for 2 min to provide dissolution, and dilution with pure water (95 g). The coke contents of the spent catalysts were estimated by thermogravimetric/differential thermal analysis (TG-DTA) on a Thermo plus EVO II TG8120 (Rigaku, Tokyo, Japan). The temperature was raised from room temperature to 800 °C with the rate of 10°C min<sup>-1</sup> under air flow (30 cm<sup>3</sup> min<sup>-1</sup>). The weight loss observed from 300 to 700°C was ascribed to coke. The number of acid sites was estimated by using the temperature-programmed desorption (TPD) of ammonia on a BELCAT-B (MicrotracBEL Corp., Osaka, Japan).

#### ***4.2.3. Typical synthesis of YNU-5 zeolite***

Please see Chapter two section 2.2.1.

#### ***4.2.4. Preparation of Hierarchical YNU-5 zeolite***

Alkaline treatment of YFI zeolite was carried out in a round-bottom flask using an oil bath pre-heated at the desired temperature (65–105°C). To 60 mL NaOH aqueous solution (0.05M–0.2M) was added 1.0 g calcined YFI zeolite and the whole mixture was stirred for 0.5–3 h. After the treatment, the zeolite suspension was immediately cooled down using ice bath an ice-water, and the mixture was subjected to centrifugation (4000 rpm, 30 min). The residue was thoroughly washed with de-ionized water, and the centrifugation-washing process was repeated for another 2 times until pH of the supernatant became 7, and the resulting solid was dried at 80 °C overnight. The residue was thoroughly washed with pure water until pH became neutral, and the resulting solid was dried at 80°C overnight. This dried sample is designated as “YFI-BT”.

#### ***4.2.5. Post-synthesis treatments of YNU-5 zeolites***

##### ***4.2.5.1 Ion-exchange of calcined YNU-5 to NH<sub>4</sub><sup>+</sup> form***

Ion exchange of the calcined samples to the NH<sub>4</sub><sup>+</sup>-form was performed using an NH<sub>4</sub>NO<sub>3</sub> solution as follows. NH<sub>4</sub>NO<sub>3</sub> (2.0 g) and the calcined sample (1.0 g) were

suspended in H<sub>2</sub>O (50 mL pure water) in a 250 mL polypropylene bottle. The bottle was capped tightly and allowed to stand at 80°C for 24 h with occasional release of pressure and careful shaking. After cooling, the sample was separated by filtration and washed with de-ionized water. This process was repeated twice, after which the sample was dried overnight at room temperature. The resulting zeolite was again calcined in a muffle furnace, during which the temperature was raised from ambient to 550°C over a period of 6 h, and kept at the same temperature for 6 h to give the sample in H<sup>+</sup> form. The NH<sub>4</sub><sup>+</sup>-forms of the YFI-type zeolites are denoted as NH<sub>4</sub><sup>+</sup>-YNU-5. In a typical experiment, 860.4 mg of NH<sub>4</sub><sup>+</sup>-YNU-5 was obtained from 999.8 mg of calcined YNU-5. Non-dealuminated H-YNU-5 was generated in situ from NH<sub>4</sub><sup>+</sup>-YNU-5 in the reactor or in some case for characterization.

#### ***4.2.5.2 Typical procedure of dealumination***

The calcined YNU-5 samples were converted to protonated dealuminated analogues using various acid treatments. Direct dealumination of the calcined YNU-5 (typically 1.0 g) was accomplished by refluxing with HNO<sub>3</sub> solutions (60 mL (g-sample)<sup>-1</sup>) in a 200 mL round-bottom flask at 130°C in an oil bath for 24 h. These conditions also stabilized the framework of the material due to Si migration. The dealuminated versions of YFI are referred to herein as deAl-YFI (*n*), respectively, where *n* indicates the Si/Al ratio. In this work, as an example, deAl-YFI(22), deAl-YFI(35), and deAl-YFI(75) were prepared by treatment with a 0.35, 0.5, and 2.0 mol L<sup>-1</sup> HNO<sub>3</sub> aqueous solution under reflux conditions, respectively. In this section, all the resultant solids were recovered by suction filtration followed by thorough washing with de-ionized water.

#### ***4.2.5.3 Typical procedure of dealumination***

Alkaline treatment of YFI zeolite was carried out in a round-bottom flask using an oil bath pre-heated at 105°C. To 60 mL NaOH aqueous solution was added 1.0226 g calcined YFI zeolite and the whole mixture was stirred for 1 h. After the treatment, the zeolite suspension was immediately cooled down using ice bath and ice-water, and the mixture was subjected to centrifugation (4000 rpm, 30 min). The residue was thoroughly washed with de-ionized water, and the centrifugation-washing process was repeated for another 2 times until pH of the supernatant became 7, and the resulting solid was dried at 80 °C overnight. This dried sample (712.6 mg) is designated as “YFI-BT”. The YFI-BT sample was subsequently converted to protonated, dealuminated analogues, denoted as “deAl-[YFI-BT]”, using acid treatments with HNO<sub>3</sub> solutions. The procedure for acid-treatment is similar to that described in section 2.3. Accordingly, the each sample of deAl-[YFI-BT](35) and deAl-[YFI-BT](61) was obtained by

treatment with a solution of  $0.35 \text{ mol L}^{-1}$  and  $2.0 \text{ mol L}^{-1}$   $\text{HNO}_3$  under reflux conditions, respectively. The values in parentheses are molar ratios determined by ICP-AES. The samples deAl-[YFI-BT](35) (381.7 mg) and deAl-[YFI-BT](61) (253.0 mg) were obtained from 540.7 mg and 489.9 mg of YFI-BT samples, respectively.

### 4.3. Catalytic reaction

An appropriate amount of each zeolite catalyst was pelletized without any binder, roughly crushed and then sieved to obtain catalyst pellets with 500–600  $\mu\text{m}$  in size. The cracking of *n*-hexane (hexane hereafter) was performed under atmospheric pressure in a down-flow quartz-tube microreactor with 8 mm of inner diameter. Prior to running the reaction, 100 mg of catalyst pellets were packed in a fixed-bed of the reactor, and preheated at  $550^\circ\text{C}$  for 1 h in a stream of air. After pretreatment, the feed was switched over to a helium stream containing an appropriate amount of hexane ( $\text{W/F} = 19.6 \text{ g-cat. h (mol-hexane)}^{-1}$ ). The reaction was performed at  $550^\circ\text{C}$  for 305 min. After reaction, the system was cooled down to room temperature in a helium stream and then the used catalyst was recovered. The reactants and products were separated by a CP- $\text{Al}_2\text{O}_3/\text{KCl}$  PLOT capillary column (i.d., 0.53 mm; length 50 m; Agilent Technology) and analyzed by using GC-2014 (Shimadzu) with a flame-ionization detector. The conversion of hexane and the selectivity to each product are calculated on the carbon-basis of the initial amount of hexane.

## 4.4. Results and Discussion

### 4.4.1. Preparation of hierarchical YNU-5 zeolite

Hierarchical structure was successfully created in YNU-5 zeolite by a direct base-treatment. The introduction of mesopores through base treatment is clearly revealed by the presence of hysteresis loop shown in the  $\text{N}_2$  sorption isotherms. Three parameters including alkalinity, duration, and temperature, having effect on forming mesopores in zeolite were investigated in this chapter. The resultant products are designated as YFI\_BT ( $x \text{ M}$ ,  $y^\circ\text{C}$ ,  $z \text{ h}$ ), where value  $x$ ,  $y$ ,  $z$  mean NaOH concentration, treatment temperature, and duration. The characteristic type I isotherms of the microporous zeolites transformed into a type I+IV isotherms, with an enhanced adsorbed amount of  $\text{N}_2$  at intermediate and high relative pressure (shown in Figure 4.1–4.3). Figure 4.1, 4.2,

and 4.3 exhibit the effect of alkalinity, duration, and temperature, respectively. The corresponding XRD patterns are shown in Figure 4.4, 4.5, and 4.6, respectively.

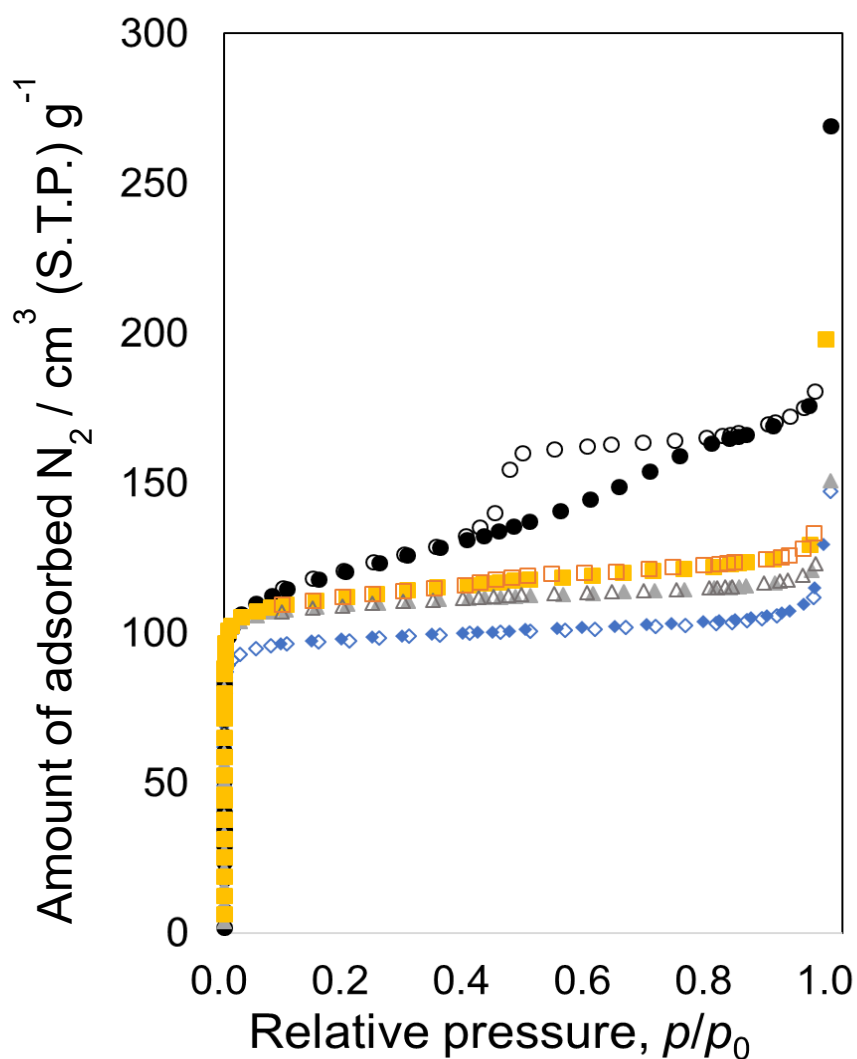


**Figure 4. 1.** N<sub>2</sub> isotherms of the non-hierarchical and hierarchical zeolite samples. Filled and unfilled symbols indicate adsorption and desorption, respectively.  $\diamond$ : YFI\_cal,  $\triangle$ : YFI\_BT(0.02 M, 65°C, 0.5 h),  $\square$  YFI\_BT(0.1 M, 65°C, 0.5 h),  $\circ$  YFI\_BT(0.2 M, 65°C, 0.5 h).

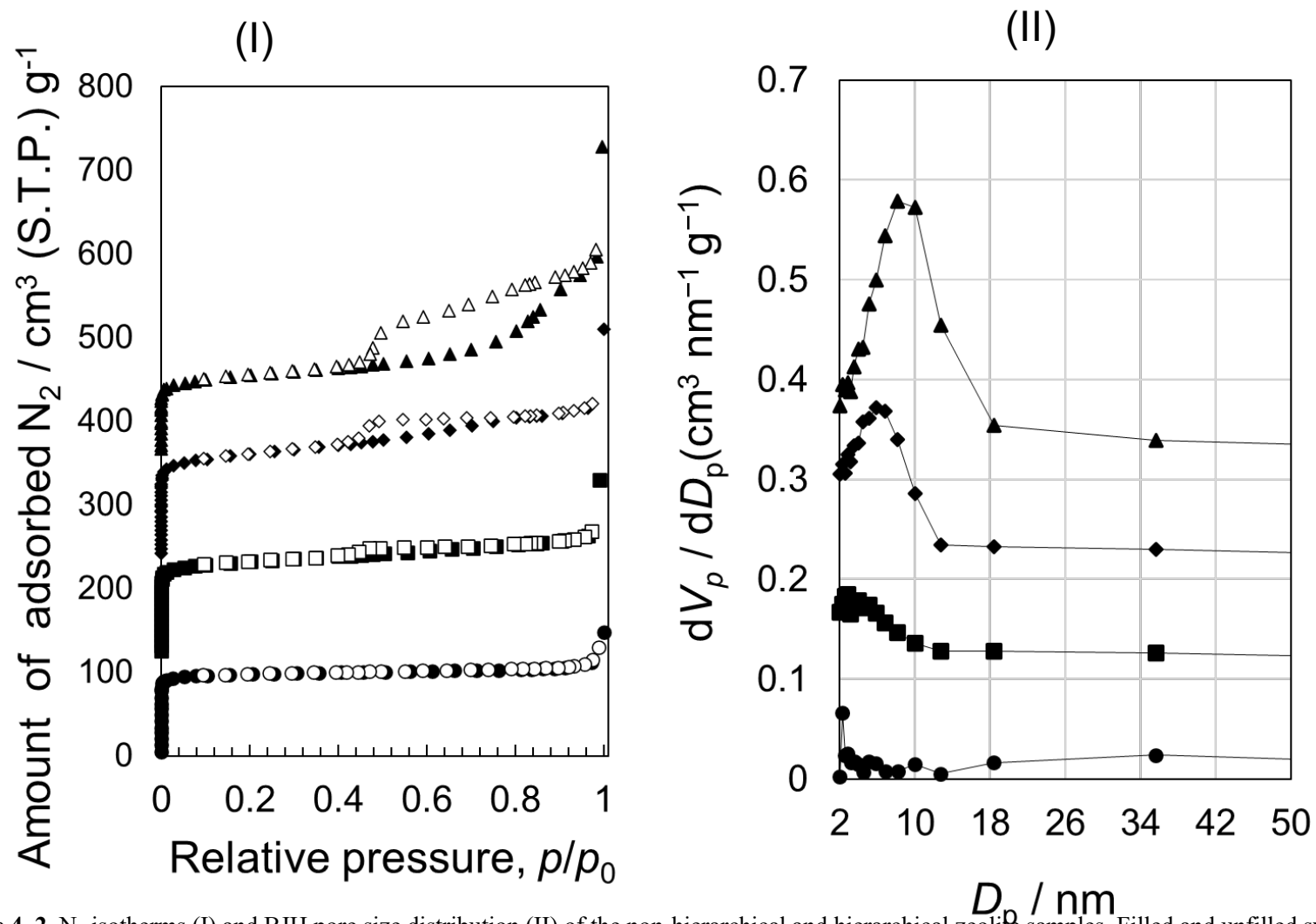


**Figure 4. 2.**  $N_2$  isotherms (I) and BJH pore size distribution (II) of the non-hierarchical and hierarchical zeolite samples. Filled and unfilled symbols indicate adsorption and desorption, respectively.  $\circ$ : YFI\_cal,  $\square$ : YFI\_BT(0.2 M, 65°C, 1 h),  $\diamond$ : YFI\_BT(0.2 M, 65°C, 2 h),  $\triangle$ : YFI\_BT(0.2 M, 65°C, 3 h).

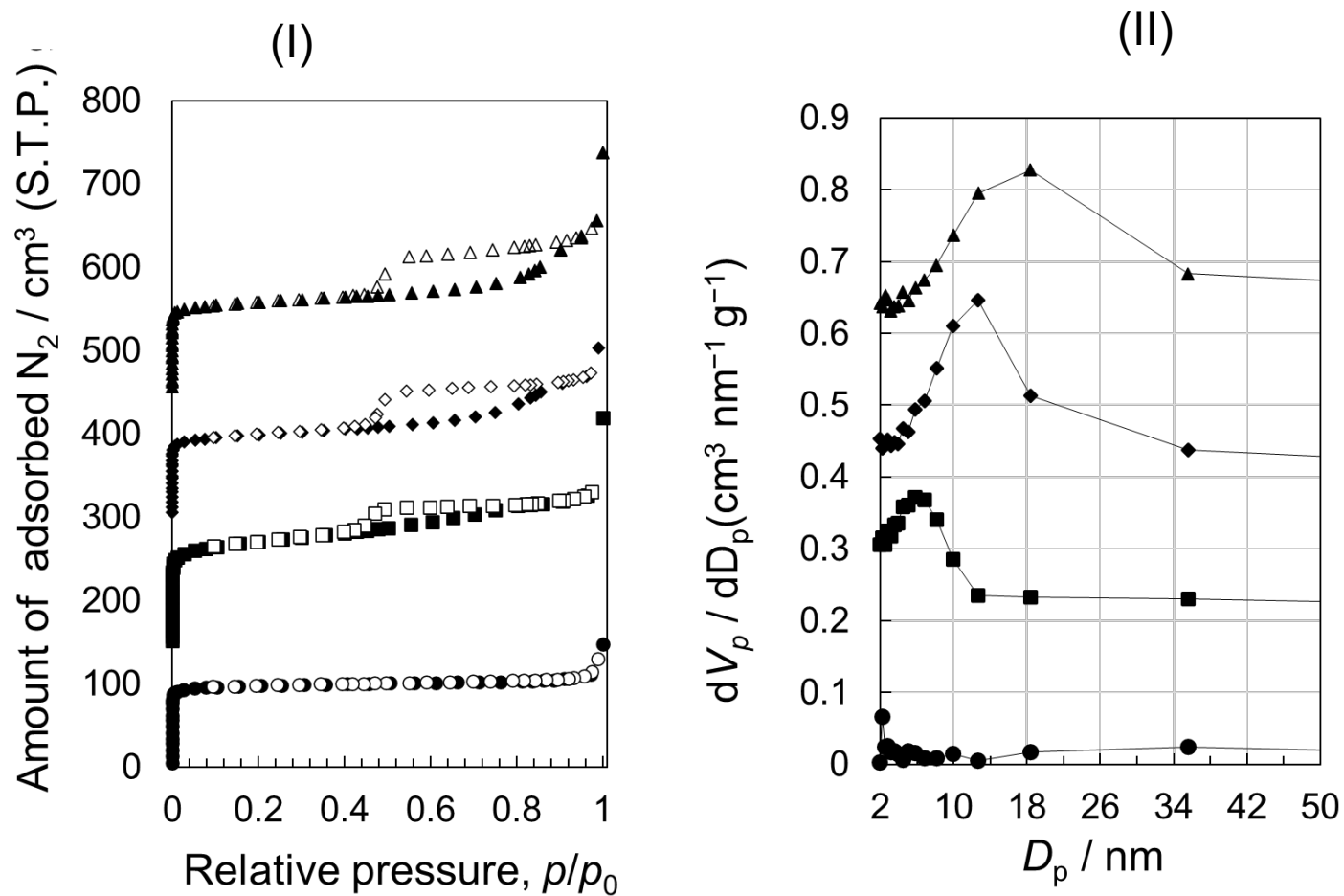


**Figure 4. 3.**  $N_2$  isotherms (I) and BJH pore size distribution (II) of the non-hierarchical and hierarchical zeolite samples. Filled and unfilled symbols indicate adsorption and desorption, respectively.  $\circ$ : YFI\_cal,  $\square$ : YFI\_BT(0.2 M, 65°C, 1 h),  $\diamond$  YFI\_BT(0.2 M, 85°C, 1 h),  $\triangle$ YFI\_BT(0.2 M, 105°C, 1 h).

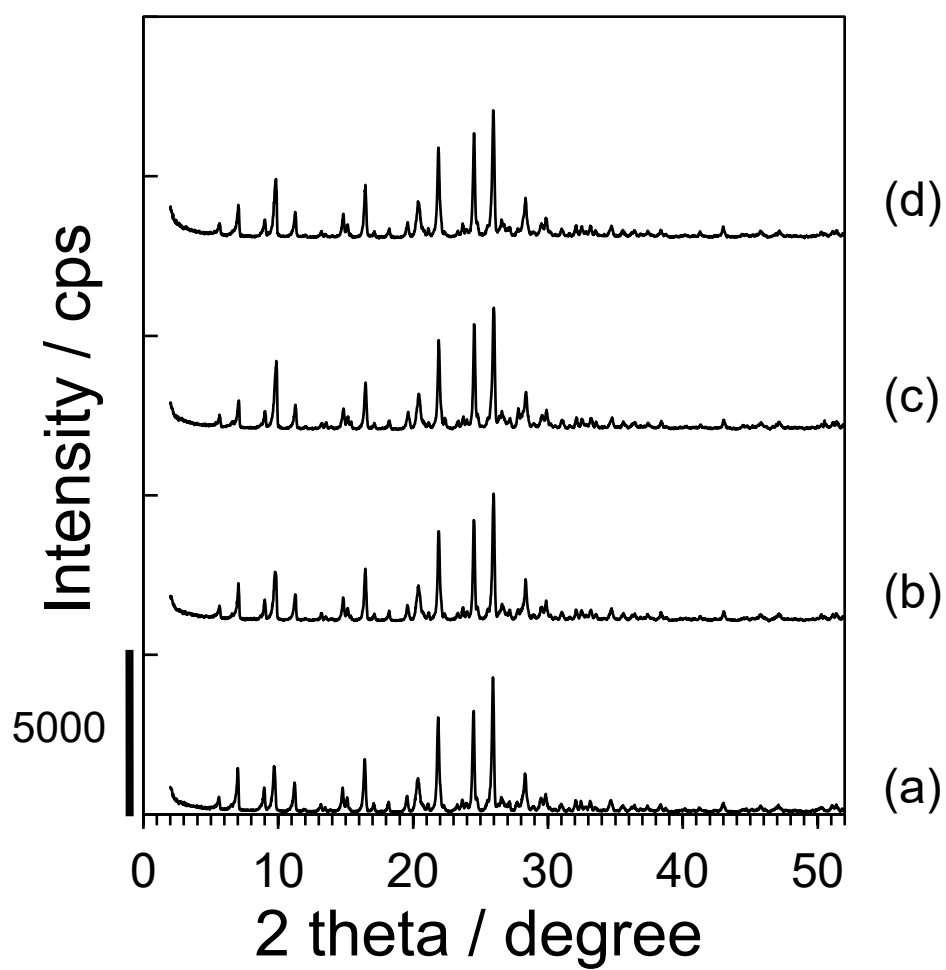


**Figure 4. 4.** XRD patterns of YNU-51 zeolite samples: (a) YFI\_cal, (b): YFI\_BT(0.02 M, 65°C, 0.5 h), (c) YFI\_BT(0.1 M, 65°C, 0.5 h), and (d) YFI\_BT(0.2 M, 65°C, 0.5 h).

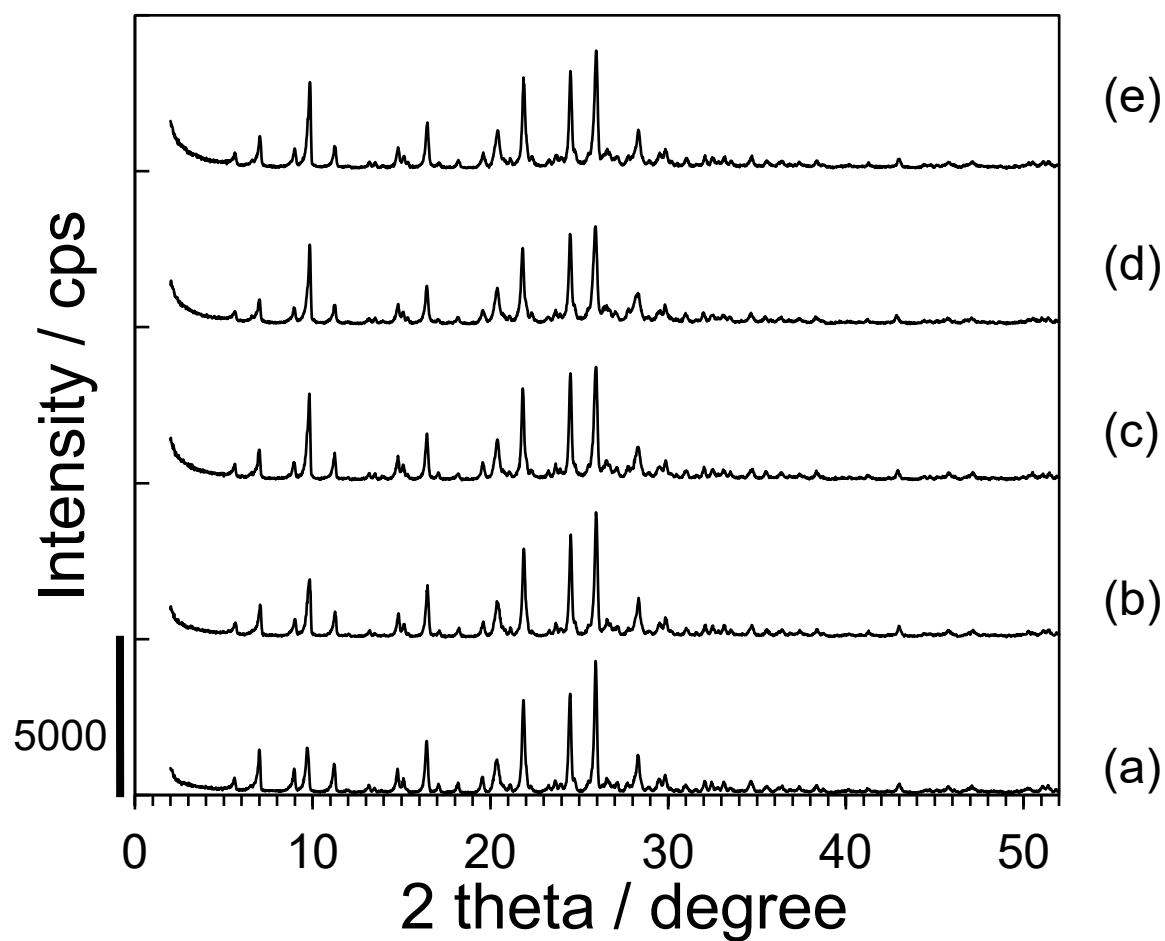


**Figure 4. 5.** XRD patterns of YNU-5l zeolite samples: (a) YFI\_cal, (b): YFI\_BT(0.2 M, 65°C, 0.5 h), (c) YFI\_BT(0.2 M, 65°C, 1 h), (d) YFI\_BT(0.2 M, 65°C, 2 h), and (e) YFI\_BT(0.2 M, 65°C, 1 h).



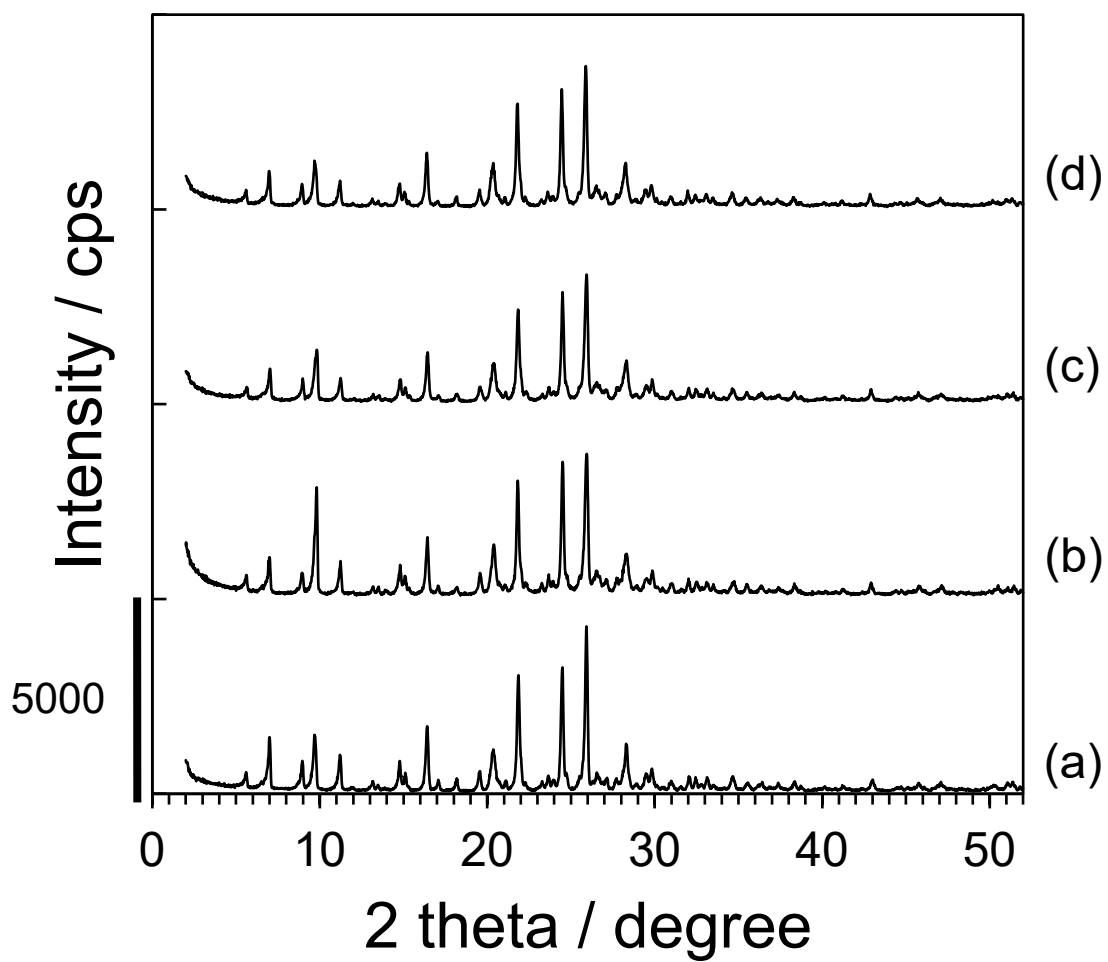


**Figure 4. 6.** XRD patterns of YNU-5I zeolite samples: (a) YFI\_cal, (b): YFI\_BT(0.2 M, 65°C, 1 h), (c) YFI\_BT(0.2 M, 85°C, 1 h), and (d) YFI\_BT(0.2 M, 105°C, 1 h).

Table 4.1 summarizes the relative crystallinity, the solid recovery yield, and textual properties of base-treated samples at different conditions. Base treatments leads to a maximum mesopore volume (Entry 9,  $0.34 \text{ cm}^3\text{g}^{-1}$ ) about 5 times in relation to that of parent calcined YNU-5 zeolite (Entry 1,  $0.06 \text{ cm}^3\text{g}^{-1}$ ) at a relative harsher treatment condition  $105^\circ\text{C}$  for 1 h. During desilication process, there is more or less degree of dissolution of framework and damage to crystalline structure. Relative crystallinity (R. C.) was used to evaluate the crystallinity of the resultant solids. In this work, R. C. is defined as the ratio of peak ( $24.5^\circ$ ,  $26.0^\circ$ ) intensity of XRD patterns in the below equation. As shown in Table 4.1, R.C. of base-treated samples at severe condition (Entry 5 and Entry 9) are still higher than 80%. All samples exhibited powder XRD patterns that were characteristic of a fully crystalline YFI structure (Figure 4.4–4.6).

$$\text{R. C.} = \frac{\text{peak intensity of treated sample}}{\text{peak intensity of parent sample}} \times 100\%$$

#### ***4.4.2. Dealumination of hierarchical YNU-5 zeolite***

Entry 9 in Table 4.1 exhibited high crystallinity (91.2%) and large mesopore volume ( $0.29 \text{ cm}^3\text{g}^{-1}$ ) at the same time. Therefore, it is the proper candidate used to examine effect of the hierarchy on the catalytic performance of YNU-5 zeolite. Base-treatment of calcined YNU-5 zeolite was carried out in a round-bottom flask, which was heated in oil bath at  $105^\circ\text{C}$ . To 60 mL of  $0.2 \text{ mol L}^{-1}$  NaOH aqueous solution, 1.0 g of calcined YNU-5 (denoted as YFI\_cal) was added and the suspension was stirred for 1 h. The whole mixture was cooled down using an ice-bath. After centrifuging, the residual solid was thoroughly washed with de-ionized water and dried at  $80^\circ\text{C}$  overnight. The resulting solid is designated as YFI-BT. The solid recovery was typically 68–70%. The YFI-BT samples were dealuminated with  $\text{HNO}_3$  solutions. The YFI-BT solid was suspended into  $0.35 \text{ mol L}^{-1}$  or  $2.0 \text{ mol L}^{-1}$  aqueous  $\text{HNO}_3$  with magnetic stirring and then heated in an oil bath at  $130^\circ\text{C}$  for 24 h. The resultant solid was collected by centrifugation, thoroughly washed with de-ionized water, and dried in a convection oven at  $80^\circ\text{C}$  overnight. The obtained solid is designated as deAl-[YFI-BT]( $x$ ). The value  $x$  in the oarentheses indicates Si/Al ratio of the sample determined by ICP-AES. To investigate the effect of structural hierarchy on the catalytic performance, non-hierarchical YNU-5 was also dealuminated under the same conditions, and the product is denoted as deAl-YFI( $x$ ). Zeolite samples obtained in this work exhibited typical XRD patterns of a fully crystalline YFI structure even after base and acid treatments (Figure 4.7).

**Table 4.1.** Textural properties of base-treated samples

Entry	Sample	R. C. / %	Yield / %	Molar Si/Al <sup>a</sup>	N <sub>2</sub> adsorption			
					S <sup>b</sup> /m <sup>2</sup> g <sup>-1</sup>	V <sub>micro</sub> <sup>b</sup> /cm <sup>3</sup> g <sup>-1</sup>	V <sub>meso</sub> <sup>c</sup> /cm <sup>3</sup> g <sup>-1</sup>	V <sub>p/p0=0.99</sub> /cm <sup>3</sup> g <sup>-1</sup>
1	YFI-cal	--	--	9.1	519	0.15	0.06	0.21
2	YFI-BT(0.2 M, 65°C, 0.5 h)	98.3	78.0	8.0	572	0.17	0.15	0.32
3	YFI-BT(0.2 M, 65°C, 1 h)	96.1	68.8	5.9	586	0.22	0.15	0.37
4	YFI-BT(0.2 M, 65°C, 2 h)	93.9	70.1	6.1	455	0.21	0.13	0.34
5	YFI-BT(0.2 M, 65°C, 3 h)	82.5	62.3	5.8	507	0.12	0.34	0.46
6	YFI-BT(0.02 M, 65°C, 0.5 h)	96.5	94.1	8.1	561	0.17	0.05	0.22
7	YFI-BT(0.1M, 65°C, 0.5 h)	96.0	86.9	7.9	588	0.17	0.12	0.29
8	YFI-BT(0.2 M, 85°C, 1 h)	90.5	70.9	6.6	480	0.19	0.12	0.31
9	YFI-BT(0.2 M, 105°C, 1 h)	91.2	69.7	6.3	553	0.12	0.29	0.41

<sup>a</sup> Molar ratios determined by ICP-AES.

<sup>b</sup> *t*-plot method applied to the N<sub>2</sub> isotherms.

<sup>c</sup>  $V_{\text{meso}} = V_{\text{total}} - V_{\text{micro}}$

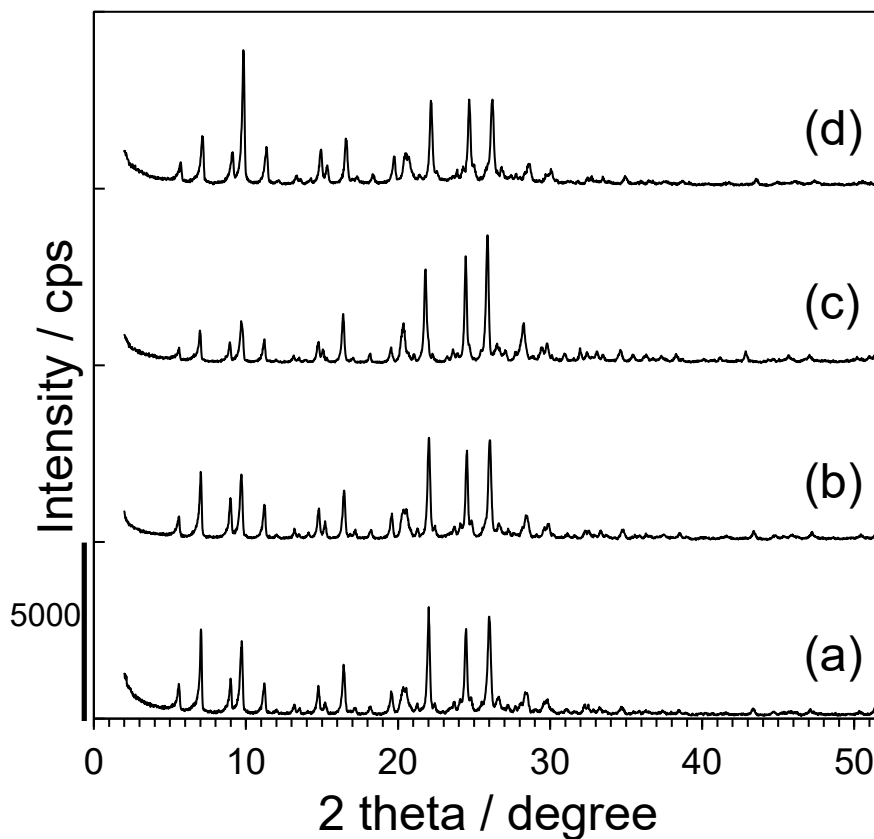


**Figure 4. 7.** XRD patterns of (a) YFI\_cal(9), (b) deAl-YFI(75), (c) YFI-BT(6), and (d) deAl-[YFI-BT](61).

Figure 4.8. shows representative FE-SEM images obtained of YFI\_cal and YFI\_BT. Highly pitted surface of YFI\_BT distinctly contrasts with conventional calcined YFI zeolite, YFI\_cal. It can be also seen that the crystal morphology and size remained mostly intact after base treatment, although the surface of the crystals became rougher. As shown in Figure 4.9., obvious signs of mesopores in cross sections of YFI\_BT samples were observed at high magnification.

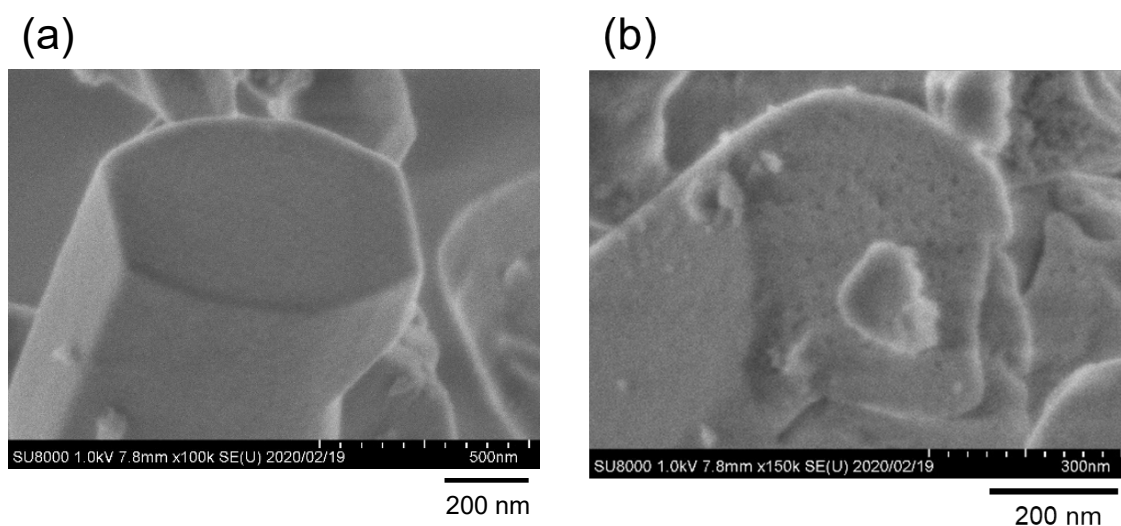


**Figure 4. 8.** FE-SEM images of (a) non-treated “YFI\_cal”, and (b) base-treated “YFI\_BT”. Abbreviations are explained in the text.

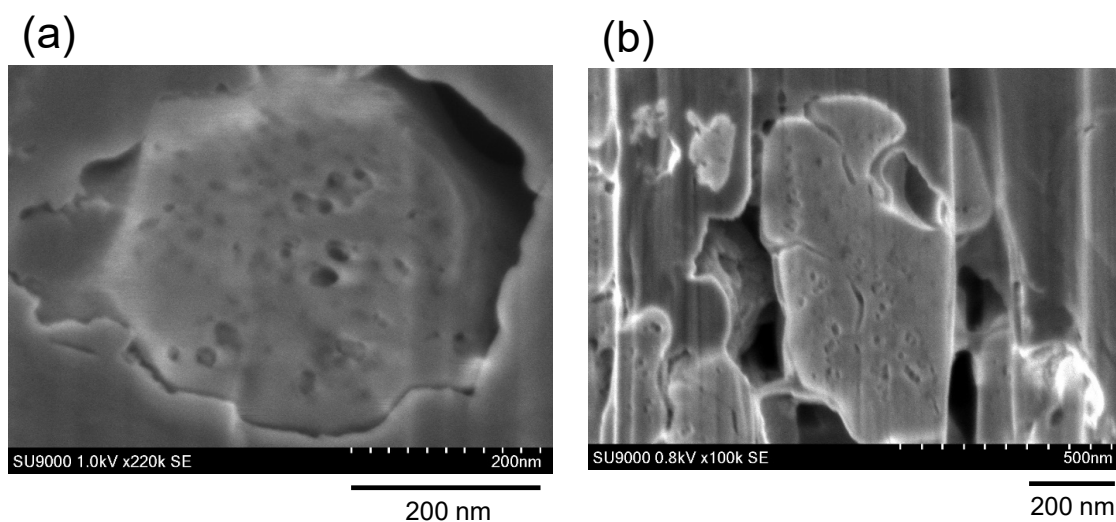


**Figure 4. 9.** FE-SEM images of YFI\_BT showing the cross-sectional structures: examples of mesopore channels approximately (a) vertical to and (b) parallel to cross-sections.

## 4.5 Physiochemical properties of treated samples

### 4.5.1 Textural properties of treated samples

Table 4.2. shows the textural properties based on N<sub>2</sub> adsorption-desorption isotherms. N<sub>2</sub> isotherms and pore-size distributions are shown in Figure 4.4. and 4.5. The significant hysteresis loops (Figure 4.4c and 4.4d) suggest the presences of mesopores. The YFI-BT sample has a much higher BET area<sup>16</sup> and a larger mesopore volume (317 m<sup>2</sup> g<sup>-1</sup> and 0.29 cm<sup>3</sup> g<sup>-1</sup>, respectively) compared to those of YFI\_cal (270 m<sup>2</sup> g<sup>-1</sup> and 0.09 cm<sup>3</sup> g<sup>-1</sup>, respectively). The presence of mesopores with a diameter of ca. 18 nm in YFI-BT and deAl-[YFI-BT] samples was confirmed by the BJH method.<sup>16</sup> After subsequent acid treatment, a slight increase in mesopore volume from 0.29 to 0.34 cm<sup>3</sup> g<sup>-1</sup> was observed, which is possibly due to the dissolution of Si debris accommodated in mesopores of YFI-BT into nitric acid.<sup>17,18</sup> As is often the case, there was at least some crystal damage by post-synthetic treatment.<sup>19,20</sup> The acid treatment under severe conditions found in the previous study for the framework stabilization of YNU-5 was also effective in this work.<sup>5,19</sup>

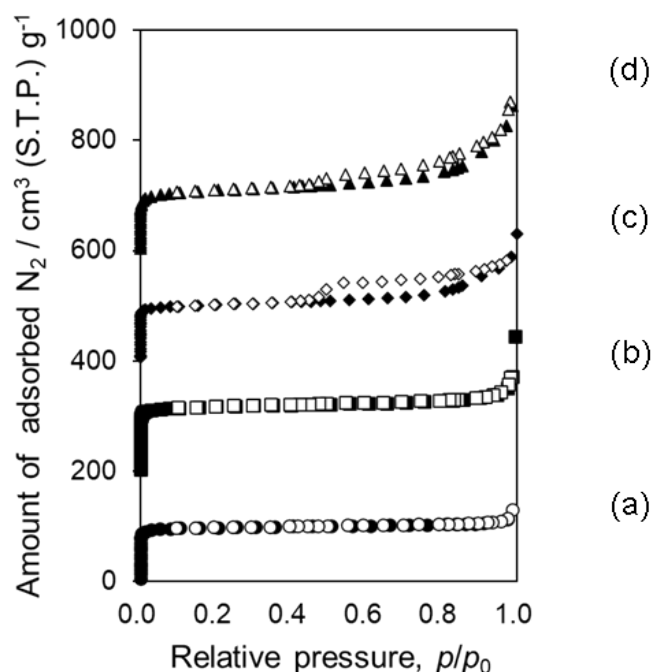


**Figure 4.10.** N<sub>2</sub> isotherms of the non-hierarchical and hierarchical zeolite samples: (a) YFI\_cal, (b) deAl-YFI, (c) YFI-BT, and (d) deAl-[YFI-BT]. The isotherms (b), (c) and (d) are offset vertically by 200, 400, and 600 cm<sup>3</sup> (S.T.P.) g<sup>-1</sup>, respectively. Filled and unfilled symbols indicate adsorption and desorption, respectively.

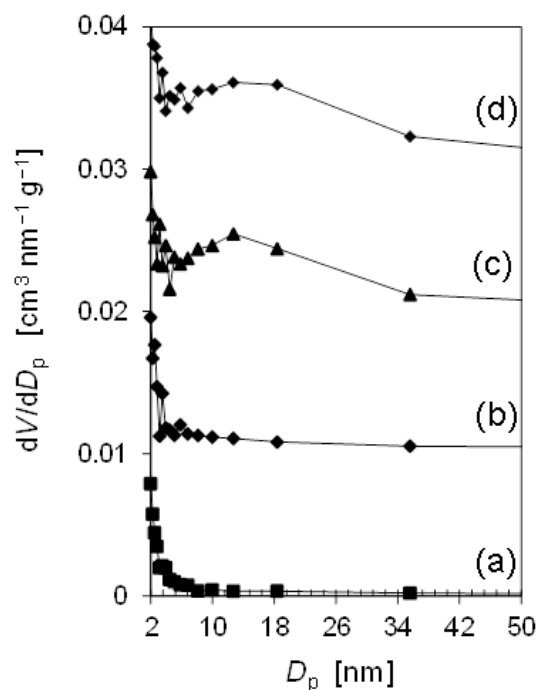


**Figure 4.11.** Pore size distributions for (a) YFI\_cal, (b) deAl-YFI, (c) YFI-BT, and (d) deAl-[YFI-BT], derived **from** nitrogen adsorption isotherms using the Barrett-Joyner-Halenda (BJH) method. The lines (b), (c) and (d) are offset vertically by 0.01, 0.02, and 0.03 cm<sup>3</sup> nm<sup>-1</sup> g<sup>-1</sup>, respectively.

**Table 4.2.** Textural properties of YNU-5 zeolite samples

Sample <sup>a</sup>	$S_{\text{BET}}^{\text{b}}$ /m <sup>2</sup> g <sup>-1</sup>	$V_{\text{micro}}^{\text{c}}$ /cm <sup>3</sup> g <sup>-1</sup>	$V_{\text{meso}}^{\text{d}}$ /m <sup>2</sup> g <sup>-1</sup>
YFI_cal(9)	270	0.13	0.09
deAl-YFI(75)	283	0.15	-
YFI-BT(6)	317	0.12	0.29
deAl-[YFI-BT](61)	369	0.11	0.34

a Values in parentheses are molar ratios determined by ICP-AES.

b Estimated by BET method<sup>16</sup> applied to the N<sub>2</sub> adsorption isotherms.

c Estimated by *t*-plot method applied to the N<sub>2</sub> adsorption isotherms.

d  $V_{\text{meso}} = V_{\text{total}} - V_{\text{micro}}$

### 4.5.2 Acidity of treated samples

The acidity of the base-treated YFI zeolite samples was investigated by  $\text{NH}_3$ -TPD. The profile of parent sample YFI\_cal gives two peaks, so-called *h*-peak and *l*-peak (Figure 4.6). The *l*-peak centered around 200°C is related to weakly adsorbed ammonia, and a larger *h*-peak observed at around 430°C is attributed to ammonia adsorbed on strong acid sites.<sup>21</sup> The parent  $\text{H}^+$ -YNU-5 has acid sites with strong acid strength and the adsorption heat of ammonia,  $\Delta H$ , was *ca.* 150 kJ mol<sup>-1</sup>.<sup>22</sup> The contents of acid sites decreased with the increase in  $\text{HNO}_3$  concentration from 0.35 to 2.0 mol L<sup>-1</sup>, and the decrease in acid sites was consistent with that in Al contents (Table 4.3). The existence of *h*-peak of deAl-[YFI-BT] samples similar to deAl-YFI samples (Figure 4.6) indicates that the acid sites of YNU-5 zeolite were preserved after base- and acid-treatments.

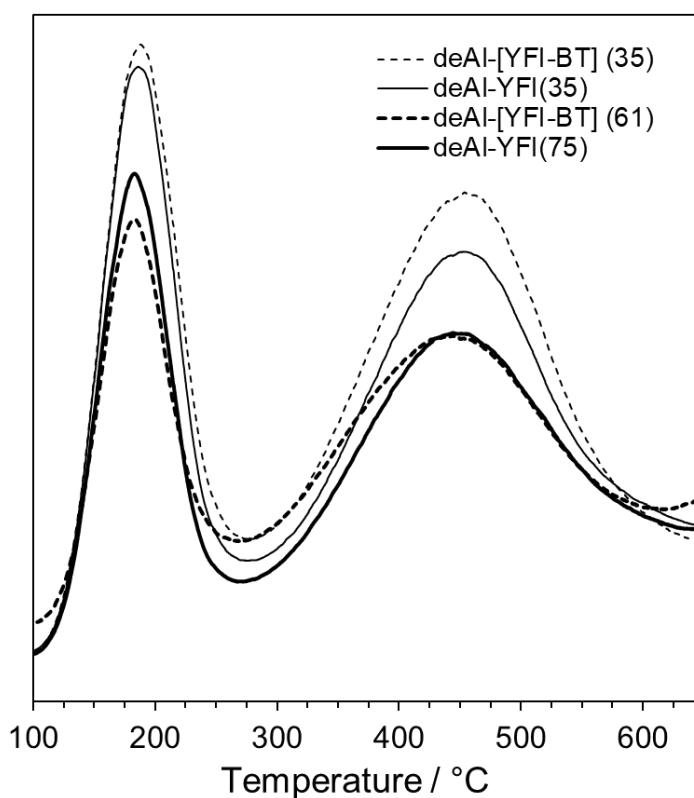


**Figure 4.12.**  $\text{NH}_3$ -TPD profiles of samples used as the catalysts.

**Table 4.3.** Acid amount and Al content of YNU-5 zeolite samples

Sample	Acid amount <sup>a</sup> /mmol g <sup>-1</sup>	Al content <sup>b</sup> /mmol g <sup>-1</sup>
deAl-YFI(35)	0.371	0.426
deAl-YFI(75)	0.224	0.258
deAl-[YFI-BT](35)	0.388	0.397
deAl-[YFI-BT](61)	0.301	0.315

a Acid amount was estimated by the *h*-peak in NH<sub>3</sub>-TPD profile.

b Al content was determined by ICP.

## 4.6 Catalytic test

The catalytic performance of the prepared materials for cracking of hexane was examined using a fixed-bed down-flow reactor. Figure 4.13. shows the variation over time in both hexane conversion and product distribution during the cracking of hexane at 550°C over H<sup>+</sup>-YNU-5 generated in situ from NH<sub>4</sub><sup>+</sup>-YNU-5 (Si/Al=10) as well as a dealuminated sample, deAl-YFI(22). The details of ion-exchange process and catalytic reaction are described in ESI. Although the conversion was 92% when the time on stream (TOS) was 5 min for the H<sup>+</sup>-YNU-5, it was quite rapidly decreased and was only 13% at the TOS of 55 min (Figure 4.13.a). This deactivation was likely caused by the large amount of coke (145 mg (g-catalyst)<sup>-1</sup> after 305 min of TOS) formed on the catalyst. The deactivation was comparatively suppressed in the case of deAl-YFI(22) as shown in Figure 4.13.b, in which the conversion was 83% and 41% at the TOS of 5 min and 55 min, respectively. This improvement was a typical effect of dealumination (i.e. high-silica composition) of the catalyst, especially the preferential removal of Al from external surface where heavy coking tends to take place. However, relatively large amount of coke (121 mg (g-catalyst)<sup>-1</sup> after 305 min of TOS) was yet formed on the deAl-YFI(22) catalyst, and the decrease in activity was still significant, indicating that further dealumination is needed to suppress the coke formation. Figure 4.14.a shows the result for deAl-YFI(35). Because of less amount of acid sites, the initial activity was lower accordingly (conversion at TOS = 5 min was 56%); however, the conversion maintained at the level of 26% when TOS was 305 min (Figure 4.14.a), along with the coke formation of 34.4 mg (g-catalyst)<sup>-1</sup> after 305 min of TOS. At the same Si/Al ratio of 35, remarkable effect of hierarchical structure was seen in Figure 4.14.b. The conversion was obviously increased in the case of deAl-[YFI-BT](35) than deAl-YFI(35), in which the conversion was 79% and 68% at the TOS of 5 min and 55 min, respectively (Figure 4.14b). The amount of coke formed on the catalysts after 305 min



of TOS was 74 mg (g-catalyst)<sup>-1</sup>. This does not mean that the coke formation is suppressed by the effect of hierarchical structure, but means deactivation is suppressed even when coking takes place by maintaining the mass transfer through the hierarchical structure.<sup>23</sup> The deactivations were similarly suppressed in the further dealuminated case of deAl-YFI(75) and deAl-[YFI-BT](61), regardless of the presence of hierarchical structure (Figure 4.14c and 4.14d). Even in this case, the hierarchical structure is considered to play a positive role for enhancing hexane conversion.

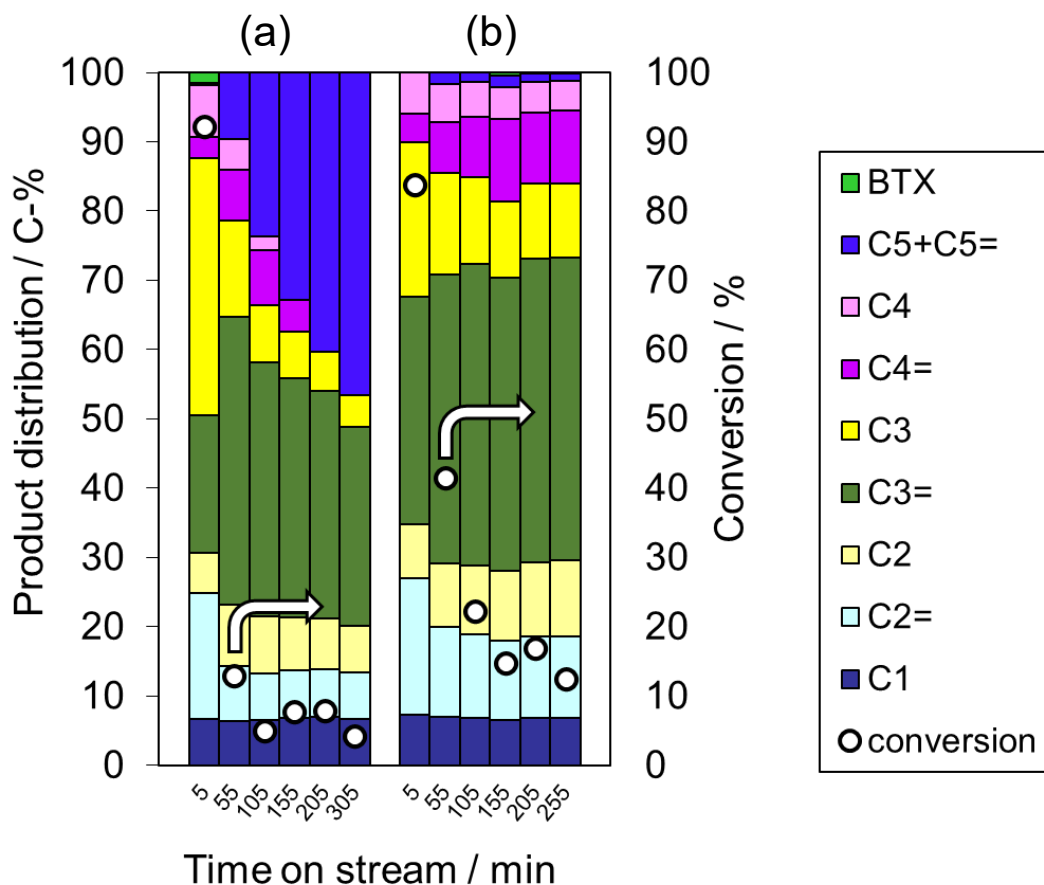


**Figure 4.13.** Product distribution and conversion of hexane over (a) H-YFI(10), generated in situ from NH<sub>4</sub>-YFI(10), and (b) deAl-YFI(22). The number in the parentheses is Si/Al ratios. Pre-treatment conditions: 550°C, 1 h under air flow (flow rate, 40 cm<sup>3</sup> (N.T.P.) min<sup>-1</sup>). Reaction conditions: catalyst, 100 mg; temperature, 550°C; W/F, 19.6 g-cat h (mol-hexane)<sup>-1</sup>; pellet size, 500–600 μm; He gas flow rate, 40 cm<sup>3</sup> (N.T.P.) min<sup>-1</sup>. Coke amounts on the spent catalysts are estimated to be 144.6 and 121.3 mg (g-catalyst)<sup>-1</sup> for (a) and (b), respectively.

Regarding the selectivity, the YNU-5 zeolite can be an efficient catalyst for propylene production. The propylene selectivity was enough high compared with those in the hexane cracking reactions over other high-silica zeolite catalysts such as MCM-68 and beta.<sup>24,25</sup> There is an obvious tendency for the YNU-5 with lower Si/Al ratio to slightly enhance the ethylene selectivity. This tendency could be related to the presence of strong Brønsted acid sites in the 8-rings.<sup>26</sup> The higher ethylene selectivity caused by strong Brønsted acid sites is typical for the same reaction over ZSM-5<sup>27</sup> that is a well-known 10-ring pore zeolite.

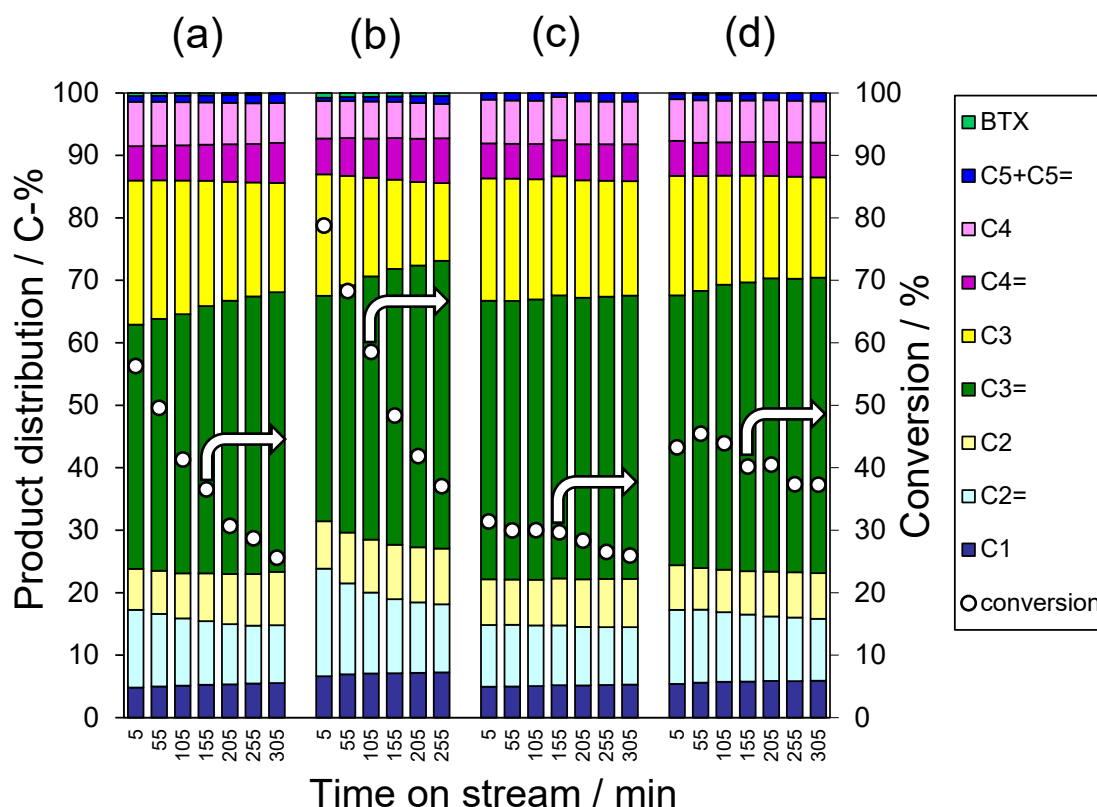


**Figure 4. 14.** Product distribution and conversion of hexane over (a) deAl-YFI(35), (b) deAl-[YFI-BT](35), (c) deAl-YFI(75) and (d) deAl-[YFI-BT](61). The number in the parentheses is Si/Al ratio. Reaction conditions: catalyst, 100 mg; temperature, 550°C; W/F, 19.6-cat h (mol-hexane)<sup>-1</sup>; He gas flow rate, 40 cm<sup>3</sup> (N.T.P.) min<sup>-1</sup>. Coke amounts on the spent catalysts are estimated to be 34.4, 74.3, 10.8 and 8.0 mg (g-catalyst)<sup>-1</sup> for (a), (b), (c), and (d), respectively.

## 4.7 Conclusions

In summary, hierarchical structure with effective acid sites was successfully introduced in YNU-5 zeolite for the first time, by means of base-treatment followed by acid-treatment. Dealumination of the non-hierarchical YNU-5 catalyst effectively suppressed the coke formation during hexane cracking process. Introducing the hierarchical structure further improved the catalytic performance of YNU-5 mainly by maintaining the mass transfer through the intra-particle mesopores. High selectivity to propylene as well as a potential to form ethylene was another advantage of YNU-5 zeolite catalyst with 12–12–8-ring framework. The achievement in this work opens up the possibility of YNU-5 for various catalytic applications, enhancing the industrial feasibility of this new zeolite as a stable solid-acid catalyst.

## 4.8 References

1. M. E. Davis, *Chem. Mater.*, **2014**, *26*, 239–245.
2. Ch. Baerlocher, L.B. McCusker, D.H. Olson, *Atlas of Zeolite Framework Types*, 6th ed., Elsevier, Amsterdam, 2007, see also: <http://www.iza-structure.org/databases>.
3. N. Nakazawa, T. Ikeda, N. Hiyoshi, Y. Yoshida, Q. Han, S. Inagaki, Y. Kubota, *J. Am. Chem. Soc.*, **2017**, *139*, 7989–7997.
4. N. Nakazawa, Y. Yoshida, S. Inagaki, Y. Kubota, *Microporous Mesoporous Mater.*, **2019**, *280*, 66–74.
5. Q. Liu, Y. Yoshida, N. Nakazawa, S. Inagaki, Y. Kubota, *Materials*, **2020**, *13*, 2030–2044.
6. H. Konno, T. Okamura, T. Kawahara, Y. Nakasaka, T. Tago, T. Masuda, *Chem. Eng. J.*, **2012**, *207*, 490–496.
7. S. Inagaki, S. Shinoda, S. Hayashi, T. Wakihara, H. Yamazaki, J.N. Kondo, Y. Kubota, *Catal. Sci. Technol.*, **2016**, *6*, 2598–2604.
8. S. Inagaki, K. Thomas, V. Ruaux, G. Clet, T. Wakihara, S. Shinoda, S. Okamura, Y. Kubota, V. Valtchev, *ACS Catal.*, **2014**, *4*, 2333–2341.
9. D. P. Serrano, J. M. Escola, P. Pizarro, *Chem. Soc. Rev.*, **2013**, *42*, 4004–4035.
10. N. D. Petkovich, A. Stein, *Chem. Soc. Rev.*, **2013**, *42*, 3721–3739.
11. D. Verboekend, J. Pérez-Ramírez, *Catal. Sci. Technol.*, **2011**, *1*, 879–890.
12. Y. Wei, T. E. Parmentier, K. P. de Jong, J. Zečević, *Chem. Soc. Rev.*, **2015**, *44*, 7234–7261.
13. J. Kim, M. Choi, R. Ryoo, *J. Catal.*, **2010**, *269*, 219–228.
14. M. Milina, S. Mitchell, P. Crivelli, D. Cooke, J. Pérez-Ramírez, *Nat. Commun.*, **2014**, *5*(1), 1–10.
15. J. Li, X. Li, G. Zhou, W. Wang, C. Wang, S. Komarneni, Y. Wang, *App. Catal, A: Gen.*, **2014**, *470*, 115–122.
16. M. Thommes, K. Kaneko, A. V. Neimark, J. P. Olivier, F. Rodriguez-Reinoso, J. Rouquerol, K. S. W. Sing, *Pure Appl. Chem.*, **2015**, *87*, 1051–1069 and references cited therein.
17. D. Verboekend, G. Vilé, J. Pérez-Ramírez, *Adv. Funct. Mater.*, **2012**, *22*, 916–928.
18. D. Verboekend, T. C. Keller, S. Mitchell, J. Pérez-Ramírez, *Adv. Funct. Mater.*, **2013**, *23*, 1923–1934.
19. Y. Wang, T. Yokoi, S. Namba, T. Tatsumi, *Catal.*, **2016**, *6*, 8.
20. T. Ikeda, Y. Yoshida, N. Nakazawa, S. Inagaki, Y. Kubota, *Microporous Mesoporous Mater.*, **2020**, *302*, 110197.
21. M. Niwa, N. Katada, *Catal. Surv. Jpn.*, **1997**, *1*, 215–226.
22. N. Katada, Private Communication.
23. H. Mochizuki, T. Yokoi, H. Imai, S. Namba, J. N. Kondo, T. Tatsumi, *App. Catal. A: Gen.*, **2012**, *449*, 188–197.
24. S. Inagaki, K. Takechi, Y. Kubota, *Chem. Commun.*, **2010**, *46*, 2662–2664.

25. Y. Kubota, K. Itabashi, S. Inagaki, Y. Nishita, R. Komatsu, Y. Tsuboi, S. Shinoda, T. Okubo, *Chem. Mater.*, **2014**, *26*, 1250–1259.
26. N. Katada, K. Suzuki, T. Noda, G. Sastre, M. Niwa, *J. Phys. Chem. C*, **2009**, *113*, 19208–19217.
27. S. Inagaki, S. Shinoda, Y. Kaneko, K. Takechi, R. Komatsu, Y. Tsuboi, H. Yamazaki, J. N. Kondo, Y. Kubota, *ACS Catal.*, **2013**, *3*, 74–78.

## Chapter Five

# Shape-selective alkylation of naphthalene over YNU-5 zeolite

*Shape-selective alkylation of naphthalene over conventional large-pore (12-ring) zeolites such as mordenite, beta and USY was first investigated prior to the catalytic use of YNU-5. YNU-5 zeolite is undoubtedly the candidate of the similar application because it has 12-ring channels. The shape-selective catalysis in the isopropylation of naphthalene (NP) over YNU-5 zeolites was discussed. In both cases of parent YNU-5 ( $H^+$ -form) and dealuminated YNU-5 zeolite, 1-isopropylnaphthalene (1-IPN) and 2-isopropylnaphthalene (2-IPN) were the principal products. As for the dialkylated naphthalene isomers, the selectivity to  $\beta,\beta$ -diisopropylnaphthalene ( $\beta,\beta$ -DIPN) was enhanced after dealumination, accompanying the decrease in the catalytic activity. Aluminum atoms on the external surface and near the pore-mouth of the 12–12–8-ring channel were preferentially removed by dealumination treatment with aqueous nitric acid, and the remaining internal acid sites played the important roles during the reaction. The high  $\beta,\beta$ -selectivity is attributed to restrict transition state mechanism inside the 12-ring channels. The reactant molecules are too bulky to access the acid sites inside 8-ring channel. This fact is consistent with the low conversion of naphthalene.*

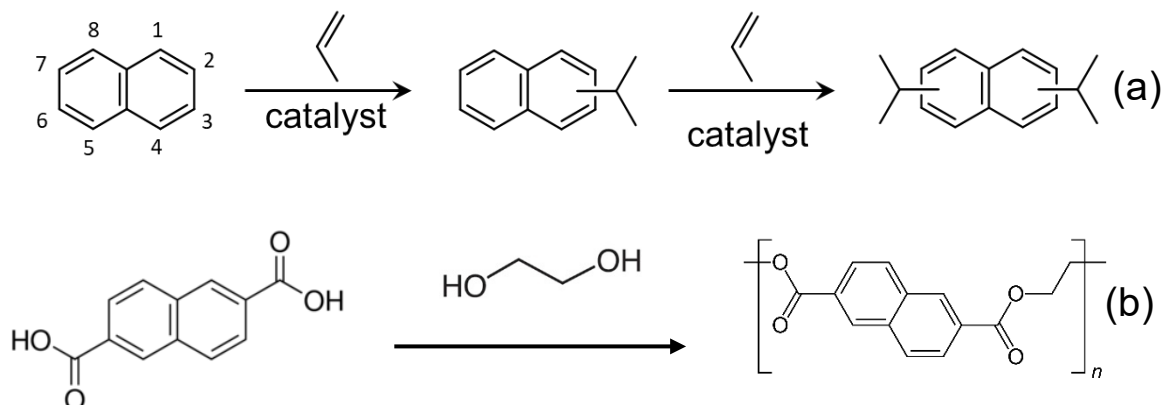
**Keywords:** YNU-5, isomerization of naphthalene

## 5.1 Introduction

2,6-diisopropylnaphthalene (2,6-DIPN) is a potentially useful raw material for production of polyethylene naphthalate (PEN) (Schem 5.1), polybutylene naphthalate (PBN) and liquid crystalline polymers (LCP) with superior properties.<sup>1–3</sup> The substrates are two very common chemical compounds: naphthalene(NP) and propylene. In 1991, Katayama<sup>4</sup> reported the isopropylation of naphthalene using various zeolite and detected 7 diisopropylnaphthalene(DIPN) isomers in bulk products. These isomers have different molecular size shown in Table 5.1. Therefore, the selectivity of DIPN directly depends on the channel shape of catalyst.

Due to their particularly ordered framework, zeolites have a special property- shape selectivity, attracting significant attention from researchers since from last century.

There are tremendous works about the investigation of the isopropylation of aromatic.<sup>5-10</sup> The mainly applied catalyst are USY, \*BEA, and MOR-type zeolites because of their large pore structure (12R) shown in Figure 5.1.



**Scheme 5.1.** The iospropylation of naphthalene (a) and the application of  $\beta,\beta$ -DIPN to produce PEN.

**Table 5.1.** Molecular sizes of DIPN isomers<sup>4</sup>

Molecule	1,3-DIPN	1,4-DIPN	1,5-DIPN	1,6-DIPN
Size, nm	0.88×1.04	0.73×1.07	0.71×1.16	0.71×1.18
Molecule	1,7-DIPN	2,6-DIPN	2,7-DIPN	
Size, nm	0.88×1.10	0.65×1.32	0.65×1.25	

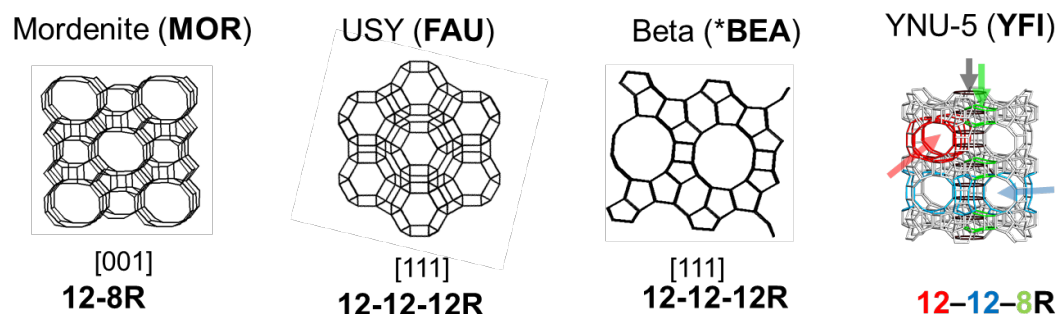


**Figure 5.1.** Channel structures of zeolites

These studies imply that zeolites with large pore channel system and strong Brønsted acidity are promising candidate for isopropylation of NP. YNU-5 is a new discovered zeolite with a novel framework of YFI (shown in Figure 5.1), containing a distinguishable three-dimensional channel system: 2-dimensional 12-ring ( $0.78\text{ nm} \times 0.59\text{ nm}$ ; large micropore) with channel intersection connected with 8-ring channel ( $0.44\text{ nm} \times 0.34\text{ nm}$ ; small micropore), thus forming a large space around  $7.97\text{ Å}$  that are accessible through 12-ring windows. The specific structure renders YNU-5 another promising candidate for hexane cracking reaction. Therefore, this chapter focused on the catalytic performance of YNU-5 zeolites in isopropylation of NP.

## 5.2 Synthesis of YNU-5 zeolite

The YNU-5 zeolite was typically synthesized as follows.<sup>19,21</sup> Initially, an aqueous  $\text{Me}_2\text{Pr}_2\text{N}^+\text{OH}^-$  solution ( $2.847\text{ mmol}\cdot\text{g}^{-1}$ ,  $11.94\text{ g}$ ,  $34.0\text{ mmol}$ ), aqueous NaOH solution ( $9.048\text{ mmol}\cdot\text{g}^{-1}$ ,  $3.32\text{ g}$ ,  $30.0\text{ mmol}$ ), aqueous KOH solution ( $6.075\text{ mmol}\cdot\text{g}^{-1}$ ,  $4.94\text{ g}$ ,  $30.0\text{ mmol}$ ), colloidal silica ( $21.59\text{ g}$ ; Ludox AS-40, DuPont de Nemours Inc., Wilmington, Delaware, USA,  $40.2\text{ wt\% SiO}_2$ ,  $8.68\text{ g SiO}_2$ ,  $144.4\text{ mmol SiO}_2$ ), and Milli-Q water ( $1.50\text{ g}$ ) were combined in a  $150\text{ mL}$  Teflon vessel. The vessel was tightly capped and the mixture stirred for  $3\text{ h}$  on a hot plate while maintaining a temperature of approximately  $60\text{ °C}$ . This procedure was essential to obtaining a clear solution. After cooling to room temperature, a FAU-type zeolite (Tosoh Co., Tokyo, Japan, HSZ-350HUA,  $5.03\text{ g}$ ;  $\text{Si/Al} = 5.5$ ) was added and the resulting suspension was stirred for  $10\text{ min}$  at room temperature. It should be noted that the synthesis results were found to be sensitive to the FAU-type zeolite manufacturer's lot that was employed, and so the starting gel composition had to be slightly tuned depending on the lot number. For a typical example in this work, the molar composition of the starting gel was  $0.265\text{SiO}_2$  (from FAU) –  $0.735\text{SiO}_2$  (from colloidal silica) –  $0.025\text{Al}_2\text{O}_3$  (from FAU) –  $0.17\text{Me}_2\text{Pr}_2\text{N}^+\text{OH}^-$  –  $0.15\text{NaOH}$  –  $0.15\text{KOH}$  –  $7.5\text{H}_2\text{O}$ . This mixture was transferred to a  $125\text{ mL}$  Teflon-lined stainless-steel autoclave that was subsequently sealed and allowed to stand statically for  $4\text{ days}$  in a convection oven at  $160\text{ °C}$ . After cooling the autoclave to room temperature, the resulting solid was separated by filtration, washed several times with de-ionized water, and dried overnight. The as-synthesized YNU-5 zeolite was obtained as a white powder ( $6.72\text{ g}$ ) and was calcined at  $550\text{ °C}$  for  $6\text{ h}$  to remove occluded organics to give the final product ( $6.31\text{ g}$ ) as a white powder ( $\text{Si/Al} = 9.1$ ).



### 5.3 Ion-exchange of YNU-5 zeolite

Ion exchange of the calcined samples to the  $\text{NH}_4^+$ -form was performed using an  $\text{NH}_4\text{NO}_3$  solution as follows.  $\text{NH}_4\text{NO}_3$  (2.0 g) and the calcined sample (1.0 g) were suspended in  $\text{H}_2\text{O}$  (50 mL pure water) in a 250 mL polypropylene bottle. The bottle was capped tightly and allowed to stand at  $80^\circ\text{C}$  for 24 h with occasional release of pressure and careful shaking. After cooling, the sample was separated by filtration and washed with de-ionized water. This process was repeated twice, after which the sample was dried overnight at room temperature. The resulting zeolite was again calcined in a muffle furnace, during which the temperature was raised from ambient to  $550^\circ\text{C}$  over a period of 6 h, and kept at the same temperature for 6 h to give the sample in  $\text{H}^+$  form.

### 5.4 Dealumination of YNU-5 zeolite

The calcined YNU-5 samples were converted to protonated dealuminated analogues using various acid treatments. Direct dealumination of the calcined YNU-5 (typically 1.0 g) was accomplished by refluxing with  $2.0 \text{ mol L}^{-1}$   $\text{HNO}_3$  solutions ( $60 \text{ mL (g-sample)}^{-1}$ ) in a 200 mL round bottom flask at  $130^\circ\text{C}$  in an oil bath for 24 h. These conditions also stabilized the framework of the material due to Si migration. The dealuminated versions of YFI are referred to herein as deAl-YFI ( $n$ ), respectively, where  $n$  indicates the Si/Al ratio.

### 5.5 Characterization

Powder X-ray diffraction (XRD; Ultima-IV, Rigaku, Akishima, Tokyo, Japan) data were collected using  $\text{Cu K}\alpha$  radiation and operating at 40 kV and 20 mA to examine the crystallinity and phase purity of the zeolite catalysts. The Si/Al molar ratios in the bulk materials were determined by inductively coupled plasma—atomic emission spectrometry (ICP-AES; ICPE-9000, Shimadzu Ltd., Kyoto, Japan). In preparation for these analyses, a catalyst sample (20 mg) was suspended in Milli-Q (Merck KGaA, Darmstadt, Germany) water (5 g) within a Teflon beaker followed by the addition of 47% HF (120 mg) at room temperature, ultrasonication for 2 min to provide dissolution, and dilution with Milli-Q water (90 g).

## 5.6 Isopropylation of naphthalene

### 5.6.1 *Experiment procedures*

Illustration of setups of isopropylation of naphthalene (NP) is shown in Figure 5.2. A typical isopropylation reaction is as follow:

1. Clean the washers with air flow.
2. Input substrates NP 3.2 g and 0.1 g Catalyst.
3. Close the autoclave. Lubricate the washers and lubricate the screws firstly.

Firstly, do screwing by hands, not so tightly. Then, check that the distance between the lid and autoclave are consistent. If not, do some adjustment. Afterwards, close the autoclave tightly with the wrench.

4. The autoclave is purged with N<sub>2</sub>; for 3 times. The pressure should be >2 Mpa for leak test. 5. Leak test. Method I: Put the autoclave in the water to see whether there are bubbles. If there are, do step 3 again. Method II: Make the autoclave bandaged and leave a small hole. Check with soap water. After leak test, release the N<sub>2</sub> in autoclave and dry the autoclave including the deep hole which is very important.

6. Purge the gas-line with propylene for 3 times.
7. Connect the autoclave, gas-line and cylinder, leak test with soap water.
8. Close all the valves in autoclave. Then start heating to desired temperature.
9. Input propylene, start stirring and reaction starts

10. When it finishes, cool the autoclave in water immediately. Transfer the product with acetone completely into sample tube (15 mL). The product is analyzed by GC after centrifuging.

11. Wash the autoclave with dish cleaning liquid first. Then with water, Dry with air flow. Wash with acetone and dry with air flow, do this step for 3 times. Then purge the remaining water in autoclave with air flow for 30 min and dry in the 100 °C oven for 1 hour and last 30 min-air flow.

### 5.6.2 *GC analysis*

Instrument: Claros 580

Column: InertCap 17

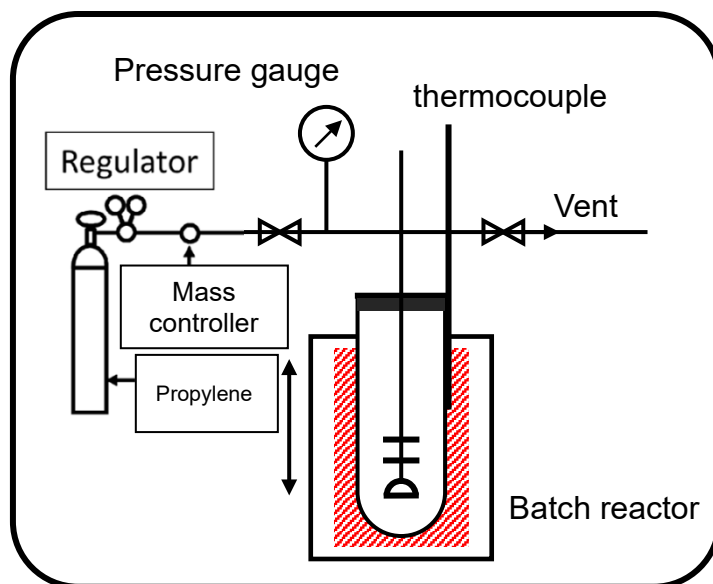
(50% Diphenyl-50% Dimethylpolysiloxane)

Injector Temp (°C) : 280; Carrier Flow: 1.00 mL/min He

Detector Temp (°C) : 300;

Detector Flow (mL/min): Air 450; H<sub>2</sub> 45; He 30.

The temperature program and assignment of products are shown in Table 5.1 and 5.2, respectively.

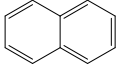
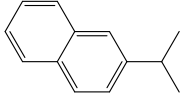
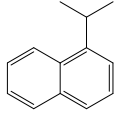
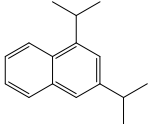
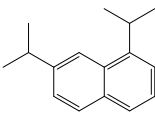
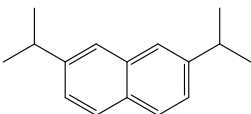
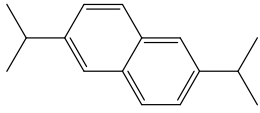
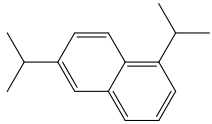
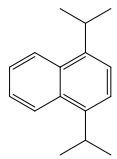
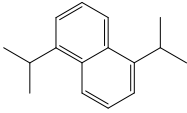


**Figure 5.2.** Illustration of the setups of isopropylation reaction.

**Table 5.2.** Temperature program of GC analysis

Program	Ramp Rate (°C/min)	Setpoint (°C)	Hold Time (min)
Initial:		120.00	5.00
Step 1:	2.50	250.00	0.00
Step 2:	10.00	280.00	5.00

**Table 5.3.** Assignment of compounds

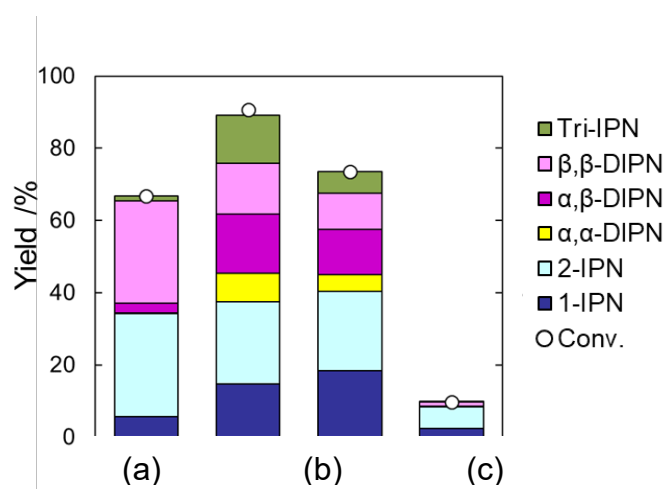
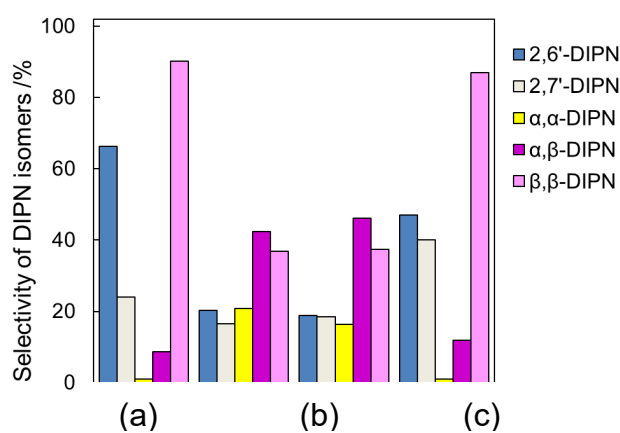
Retention time /min	Compound	Structure	Abbreviation
17.5	Naphthalene		NP
28.4	2- isopropylnaphthalene		2-IPN
29.3	1- isopropylnaphthalene		1-IPN
37.0	1,3- diisopropylnaphthalene		1,3-DIPN
37.4	1,7- diisopropylnaphthalene		1,7-DIPN
38.7	2,7- diisopropylnaphthalene		2,7-DIPN
38.9	2,6- diisopropylnaphthalene		2,6-DIPN
39.5	1,6- diisopropylnaphthalene		1,6-DIPN
40.2	1,4- diisopropylnaphthalene		1,4-DIPN
40.8	1,5- diisopropylnaphthalene		1,5-DIPN

## 5.7 Results and Discussion

To investigate the intrinsic catalytic characteristics, various zeolites (MOR, USY, \*BEA, and YFI) were used in isopropylation of NP. Reaction conditions are shown in Table 5.4. The results are shown in Figure 5.3 and 5.4. Here, I didn't focus on the yield of triisopropylnaphthalene isomers because of its small amount in the bulk product, mainly discussing IPN and DIPN. IPN are 1-IPN and 2-IPN. 7 kinds of DIPN (Table 5.3) isomers are divided into  $\alpha,\alpha$ -DIPN,  $\alpha,\beta$ -DIPN,  $\beta,\beta$ -DIPN. The most desired product is 2,6-DIPN. Generally, the selectivity of  $\beta,\beta$ -DIPN(2,6-, 2,7-DIPN) in the isopropylation reaction is used to evaluate the shape-selectivity of the catalyst. As same to the previous report,<sup>7</sup> MOR(Figure 5.3a) exhibits good performance, with the primary products of 2-IPN and  $\beta,\beta$ -DIPN. Compared to MOR(220), Y(80) and \*BEA(300) present obviously different product distributions, a larger amount of triisopropylnaphthalene isomers and more  $\alpha,\beta$ -DIPN. Even with high Al content, deAl-YFI(56) gave a much lower conversion of NP (around 10%). A possible reason is the acid sites in 8-ring channel did not work because of the inaccessibility. Fortunately, deAl-YFI(56) gave high selectivity of  $\alpha,\beta$ -DIPN isomers (Figure 5.4d). The comparison between H-YFI(10) and deAl-YFI(56) was also discussed. As expected, H-YFI(10)(Figure 5.5a) has conversion of NP than deAl-YFI(56) due to higher acid amount. However, as depicted in Figure 5.6, dealuminated YNU-5 zeolite has an obvious enhancement on selectivity of  $\beta,\beta$ -DIPN(87%) with respect to the one of H-YFI(10) sample(45%).

**Table 5.4.** Reaction conditions of isopropylation of NP

No.	Temp. (°C)	Pressure (MPa)	Period (h)	Cat.	Cat Details	Weight (g)	Reactant (mmol)
(a)	250	0.80	2	M-220	MOR (220)	0.1	25
(b)	250	0.80	2	FAU80	Y (80)	0.1	25
(c)	250	0.80	2	BEA300	BEA (300)	0.1	25
(d)	250	0.80	2	de-Al YFI	deAl-YFI(56)	0.05	10

**Figure 5.3.** Reaction results of isopropylation of NP using (a) MOR(220), (b)Y(80), (c)\*BEA(300), and (d) YFI(50). Reaction conditions: 250°C, 2 h. Propylene pressure: 0.8 MPa. The number in the parentheses is the molar Si/Al ratio.**Figure 5.4.** Selectivity of DIPN during isopropylation of NP using (a) MOR(220), (b)Y(80), (c)\*BEA(300), and (d) YFI(50). Reaction conditions: 250°C, 2 h. Propylene pressure: 0.8 MPa

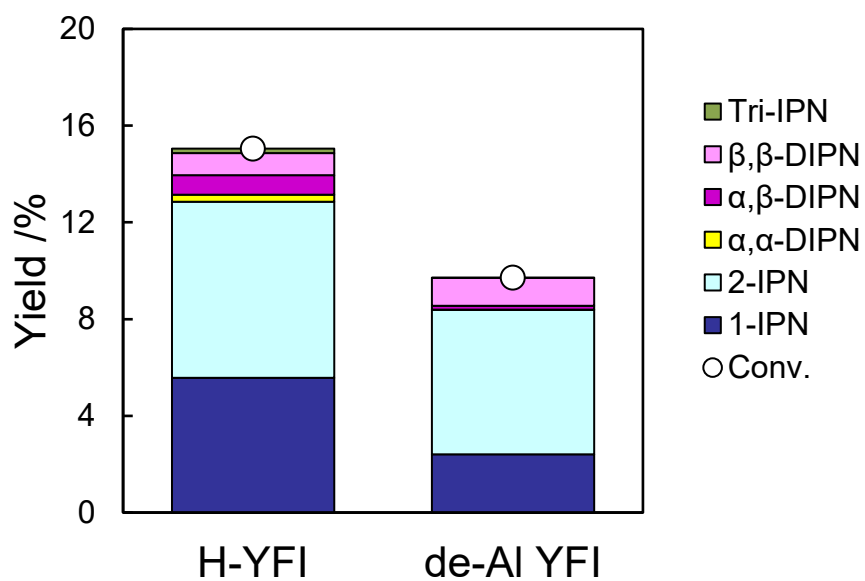


**Figure 5.5.** Yield of IPN and DIPN during isopropylation of NP using (a) H-YFI(10), (b)deAl-YFI(50), Reaction conditions: 250°C, 2 h.

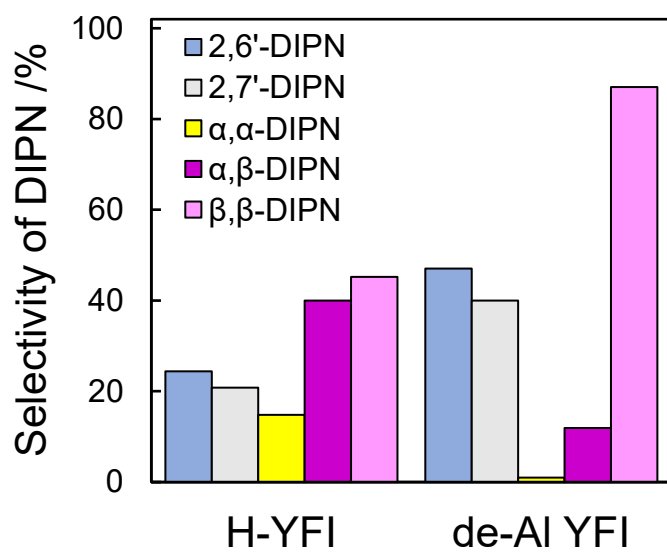


**Figure 5.6.** Selectivity of DIPN during isopropylation of NP using (a) H-YFI(10), (b)deAl-YFI(50), Reaction conditions: 250°C, 2 h.

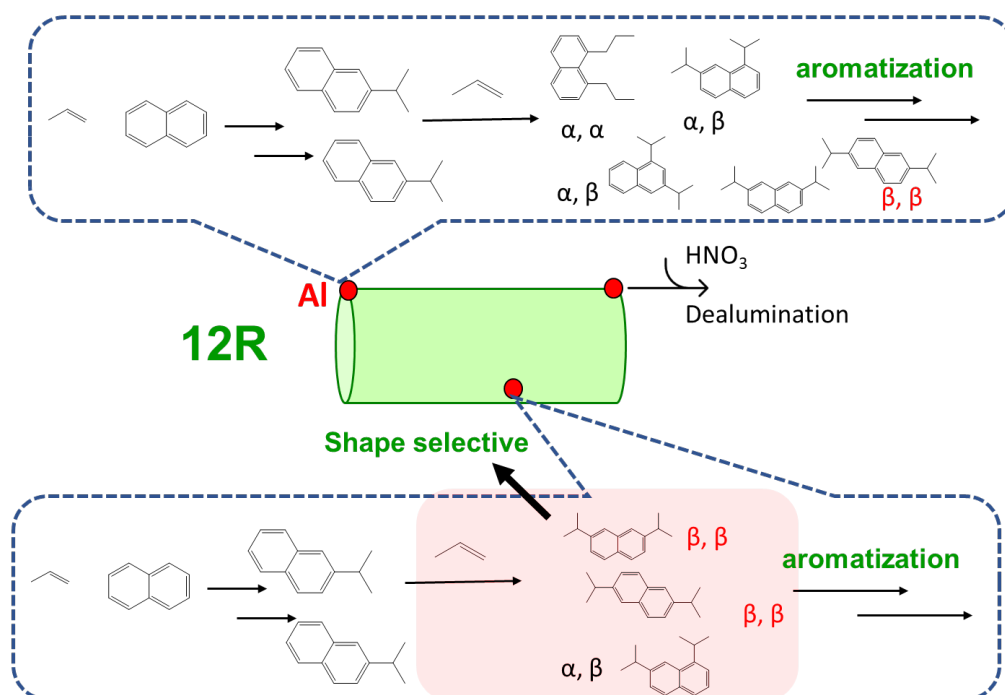


**Figure 5.7.** Possible scheme of isopropylation of NP using YNU-5 zeolite



## 5.8 Conclusions

In summary, on low SiO<sub>2</sub>/Al<sub>2</sub>O<sub>3</sub> YNU-5, β,β-DIPN is both isomerized and further alkylated by propylene on the non-selective external surface of the catalyst. However, the shape selectivity of β,β-DIPN was obviously enhanced by removal of Al atoms at the external surface and pore mouth of 12 channels which are easily accessible. The possible scheme in isopropylation of NP using YNU-5 zeolite is shown in Figure 5.7. The acid sites accommodated inside the 12 channels favor the selectivity of β,β-DIPN isomers.

## 5.9 References

1. C. Song, H.H. Schobert, *Am. Chem. Soc. Div. Fuel Chem. Prepr.*, **1992**, 37(2), 524.
2. C. Song, H.H. Schobert, *Fuel Process. Technol.*, **1993**, 34, 157.
3. C. Song, H.H. Schobert, *Am. Chem. Soc. Div. Fuel Chem. Prepr.*, **1995**, 40(2), 249.
4. A. Katayama, M. Toba, G. Takeuchi, F. Mizukami, S. I. Niwa, S. Mitamura, *J. Chem. Soc., Chem. Commun.*, **1991**, 1, 39–40.
5. Y. Sugi, M. Toba, *Catal. Today*, **1994**, 19, 187–211.
6. Y. Sugi, Y. Kubota, J.J. Spivey, *Royal Soc. Chem.*, **1997**, 13 13–55.
7. Y. Sugi, *J. Chin. Chem. Soc.*, **2010**, 57, 1–13.
8. J. H. Kim, Y. Sugi, T. Matsuzaki, T. Hanaoka, Y. Kubota, X. Tu, M. Matsumoto, *Microporous Mesoporous Mater.*, **1995**, 5, 113–121.
9. Y. Sugi, H. Maekawa, H. Naiki, K. Komura, Y. Kubota, *Bull. Chem. Soc. Jpn.*, **2008**, 81, 897–905.
10. R. Brzozowski, W. Skupiński, *J. Catal.*, **2003**, 220, 13–22.

## *Chapter six*

### *Conclusions and outlook*

**Conclusions:** This thesis targeted an improved understanding of the novel YNU-5 zeolite with YFI framework in three aspects: the preferable synthetic conditions, introducing of mesopores, and evaluation of its catalytic performance over various reaction systems. YNU-5 zeolites were synthesized, characterized, and applied to various catalytic reactions, DTO reaction, alkane cracking, and alkylation. During the synthesis investigation, it was found that a very slight amount of an impurity phase tended to be formed along with the desired product YNU-5. This minor phase was very often MFI. The presence of this nanoparticle contaminant phase evidently improved the performance of the catalytic system during the DTO reaction. Based on the product distribution obtained using highly dealuminated, very pure YNU-5 as a solid acid catalyst, this material behaves more like a 12-ring zeolite. The highly dealuminated YNU-5 also shows increased selectivity for high value C3 and C4 olefins, which suggests potential practical applications. Properly dealuminated YNU-5 catalyst exhibits high resistance to coking and good catalytic stability even at high temperature of 650°C. More importantly, it also has high selectivity of light olefins C3= and C2=. Based on these results, YNU-5 is a useful cracking catalyst. For further improvement of catalytic properties, there are two methods: (a) synthesis of nanosized YNU-5 zeolites; (b) introducing mesopores system to YNU-5 framework. The former strategy is difficult to realize. However, hierarchical YNU-5 zeolites were successfully obtained by base treatment. Additionally, I found that introducing the hierarchical structure further improved the catalytic performance of YNU-5 mainly by maintaining the mass transfer through the intra-particle mesopores. In the isopropylation reaction, dealuminated YNU-5 zeolites shows high shape selectivity of  $\beta,\beta$ -DIPN. The achievements in this work open up the possibility of YNU-5 for various catalytic applications, enhancing the industrial feasibility of this new zeolite as a stable solid-acid catalyst.

YNU-5 zeolite, as a new-discovered zeolite, is a potential solid acid catalyst with many advantages: like large micropore channel systems, high thermal stability, and tunable Al contents. However, there is still plenty of work and efforts needing to be carried to know more about properties of YNU-5 zeolite. Additionally, the modification of YNU zeolite is also a priority. For example, the introduction of hierarchy into the framework using soft template and the metal modification to prepare multi-functional catalyst. In this work, hierarchical YNU-5 was successfully prepared with post-

synthetic treatment, while this route inevitably leads to the loss of crystallinity and the limitation of the order of mesopores. An alternative is to put the focus on the synthesis method using quaternary ammonium-type cationic organosilane surfactant as mesopore-generating agent composing of a long hydrophobic alkyl tail and a hydrophilic quaternary ammonium head group. Typical examples are 3-[(trimethoxysilyl)propyl]hexadecyldimethylammonium chloride ( $[(\text{CH}_3\text{O})_3\text{SiC}_3\text{H}_6\text{N}^+(\text{CH}_3)_2\text{C}_{16}\text{H}_{33}]$ ) and their structural analogues. The soft surfactant template has the advantage of facile control of structure through the molecular manipulation of functional groups. Hierarchical structure and strong acidity make YNU-5 zeolite as a potential acid catalyst. Hierarchical zeolite also can be used in host-guest chemistries for designing multi-functional materials owing to a large amount of silanol groups.

## *Acknowledgment*

I wish to express my most sincere appreciation to my supervisor, Prof. Yoshihoro Kubota. He showed an ideal image of a professor to me. I always admired his creativity and hard work. In academic research, his advice and patience for my various difficulties were incredibly helpful. Thank you for your tolerant attitude to my mistakes. Prof. Kubota also offered me many opportunities to communicate with other researchers in this field and the chance to learn knowledge from all over the world. Thank Prof. Yoshihiro Sugi for instructing me the isopropylation experiments.

I would like to thank Prof. Satoshi Inagaki. The discussions with him were always cheerful and helpful. He patiently explained the very fundamental but extremely significant information to me. I thank Dr. Yuko Nishi for her kind and helpful advice in my seminars. In addition, I also thank the members of the jury: Prof. Ken Motokura, Prof. Hideaki Yoshitake, and Prof. Izuru Kawamura. Thank you for having accepted to evaluate this work.

All members in Kubota-Inagaki lab made me the work in the lab interesting and enjoyable. I felt the warmth and friendness from all the members. I know how fortunate I was to have such good people as coworkers. My thanks are honestly expressed to Kai Asanuma, Ryota Sugimoto, Shota Odagawa, Yuki Orui, Kanako, Suyama, Kazuya, Ohuchi, Tae Okuda, Takuto, Kishida, Yasumitsu Shimura, Yusuke Ban, Takuto Miyatani, and Shengxiang Zhang for their encouragement, support and wonderful atmosphere in the lab throughout the years of my PhD. I also want to thank my seniors Dr. Naoto Nakazawa and Dr. Qiao Han. I wish them good luck, health, and profound success.